MIXING IN COMPLEX COASTAL HYDROGEOLOGIC SYSTEMS

A Thesis
Presented to
The Academic Faculty

By

Chunhui Lu

In Partial Fulfillment
of the Requirements for the Degree Doctor of Philosophy in
the School of Civil and Environmental Engineering

Georgia Institute of Technology

May 2011

MIXING IN COMPLEX COASTAL HYDROGEOLOGIC SYSTEMS

Approved by:

Dr. Jian Luo, Advisor
School of Civil and Environmental Engineering
Georgia Institute of Technology

Dr. Aris P. Georgakakos
School of Civil and Environmental Engineering
Georgia Institute of Technology

Dr. Philip J. Roberts
School of Civil and Environmental Engineering
Georgia Institute of Technology

Dr. Peter K. Kitanidis
Department of Civil and Environmental Engineering
Stanford University

Dr. Jiawen Yang
School of City and Regional Planning
Georgia Institute of Technology

Date Approved: April 1, 2011

DEDICATION

To my wife, Jing Shi,

ACKNOWLEDGMENTS

I would like to express my sincerest gratitude and appreciation to my supervisor, Dr. Jian Luo for his invaluable guidance, continuous support, and high standard that have led me throughout all the stages of my Ph.D. Without his help, this dissertation could have never come to an end.

I would also like to thank my committee members: Dr. Aris P. Georgakakos, Dr. Philip J. Roberts, Dr. Peter K. Kitanidis, and Dr. Jiawen Yang for their constructive comments, suggestions, and salient advice to help complete this dissertation.

I would like to gratefully acknowledge the group members of Environmental Fluid Mechanics and Water Resources (EFM&WR) for their comments and critiques. I would like to especially acknowledge my officemates Mr. Yinming Chen and Ms. Rulan Gong for their help and support in my study and research.

Finally, my sincere warmherarted gratitude goes to my wife, Jing Shi, and our parents, Yanan Jiang, Wangao Lu, Hongxia Shen, and Tao Shi, for their endless love, understanding, and patience not only to complete this dissertation but also to take a journey of my life this far and to the rest of my life.

TABLE OF CONTENTS

LIST OF TABLES

LIST OF FIGURES

LIST OF SYMBOLS

C_m	dissolved solute concentration in the mobile domain [ML^{-3}]
C_{im}	dissolved solute concentration in the immobile domain [ML^{-3}]
D	hydrodynamic dispersion coefficient tensor [L^2T^{-1}]
R	dimensionless radial distance from the well [-]
R_0	dimensionless well radius [-]
R_0^+	point with an infinitesimally small distance to the well boundary [-]
K_f	equivalent freshwater hydraulic conductivity [LT^{-1}]
T_i	dimensionless injection duration [-]
T_s	dimensionless storage duration [-]
T_e	dimensionless recovery duration [-]
T_f	water level fluctuation period
T_{crit}	dimensionless critical value of injection duration [-]
W	width of the mixing zone under the coupled effect of mass transfer and water-level fluctuation [L]
W_{ss}	mixing-zone width under steady-state condition [L]
V_r	volume of recovered water [L^3]
V_i	total volume of injected water [L^3]
c_m	dissolved solute concentration in the mobile domain [ML^{-3}]
c_{im}	dissolved solute concentration in the immobile domain [ML^{-3}]
c_m^*	dimensionless concentration in the mobile domain [-]
c_{im}^*	dimensionless concentration in the immobile domain [-]
c_{m0}^*	dimensionless concentration in the mobile domain at the beginning of the storage [-]
c_{im0}^*	dimensionless concentration in the immobile domain at the beginning of the storage [-]
$c_{m,n-1}^*$	dimensionless mobile concentration during the (n-1)th ASR cycle [-]
$c_{im,n-1}^*$	dimensionless immobile concentration during the (n-1)th ASR cycle [-]
$c_{im0,n-1}^*$	dimensionless initial immobile concentration of the nth ASR cycle [-]
c_0	initial concentration after first injection [ML^{-3}]
q	specific pumping rate [L^2T]
q_s	flow rate per unit volume of aquifer of the source/sink [T^{-1}]
r	radial distance from the well [L]
r_w	well radius [L]
t	time [T]
t_i	injection duration [T]
t_s	storage duration [T]
t_e	recovery duration [T]
v	pore fluid velocity [LT^{-1}]
$\boldsymbol{v}$	pore water velocity vector [LT^{-1}]
$\|v\|$	absolute magnitude of pore fluid velocity
z	vertical coordinate directed upward [L]

α_L	longitudinal dispersivity [L]
α_T	transverse dispersivity [L]
β	capacity ratio [-]
ε	dimensionless constant with a value of 0.7143 for salt concentrations [-]
ϕ	dimensionless pumping rate
θ_m	mobile region porosity [L^3L^{-3}]
θ_{im}	immobile region porosity [L^3L^{-3}]
θ_e	effective porosity [L^3L^{-3}]
ρ	fluid density [ML^{-3}]
ρ_f	freshwater density [ML^{-3}]
ρ_s	seawater density [ML^{-3}]
ξ	first-order mass transfer rate coefficient [T^{-1}]
τ	dimensionless time
τ_{im}	mass transfer timescale [T]

SUMMARY

The mixing zone developed at the freshwater-seawater interface is one of the most important features in complex coastal hydrogeologic systems, which controls subsurface flow and reactive transport dynamics in coastal subsurface environments. In the face of growing water scarcity and deteriorating water quality and offshore ecological environments, scientists, engineers and policy makers must take urgent actions altogether to understand the interactive, dynamic physical, chemical and biological processes in coastal aquifers, and to review, develop and test effective strategies and techniques for sustainable development of coastal groundwater resources and near-shore environment. This research focuses on two important topics in costal subsurface systems: one is the freshwater-seawater mixing-zone development and the other is the application of aquifer storage and recovery (ASR). The first one aims to improve scientific understandings about the key mechanisms controlling the growth and decay of the freshwater and seawater interface, and the latter aims to improve engineering solutions for sustainable management of coastal groundwater resources.

Freshwater-seawater mixing-zone development is influenced by many physical and chemical processes such as the characteristics of geologic formation, hydrodynamic fluctuations of groundwater and seawater levels, fluid-rock interactions, and others. Wide mixing zones have been found in many coastal aquifers all over the world. However, the mechanisms responsible for wide mixing zones are not well understood. In this thesis, two hypotheses are proposed to explain wide mixing zones in coastal aquifers:

(1) kinetic mass transfer coupled with transient conditions, which create the movement of the mixing zone, may widen mixing zones; and (2) aquifer stratification may widen the mixing zone.

The hypotheses were tested by both multiscale numerical simulations and laboratory experiments. Numerical simulations were based on a variable-density groundwater model by varying mass transfer parameters, including immobile porosity, mobile porosity and mass transfer coefficient, and the hydraulic conductivity contrast between aquifer layers. Laboratory experiments were conducted in a quasi-two-dimensional tank, where real beach sands were installed and foodstuff dyes were used to visualize the development of freshwater-seawater mixing zone. The major conclusions included (1) the mixing zone can be significantly widened when the mass transfer timescale and the period of transient boundary is comparable due to the nonequilibrium mass transfer effects; and (2) a thick mixing zone occurs in low-permeability layer when it overlays upon a fast flow layer. These results not only improve the understanding of the dynamics of mixing-zone development and its associated geochemical processes in coastal aquifers, but also identify hydrogeologic conditions for the model of sharp-interface approximation to be valid.

In addition to better understanding the mechanisms and dynamics of mixing zone, this thesis also investigates the cost-effective management of coastal groundwater management. To protect and conserve limited water recourses in coastal regions, interest in aquifer storage and recovery (ASR) has been growing in recent years. ASR is a promising strategy for water resources management and has been widely used in many

contaminated and saline aquifers. However, its performance may be significantly constrained by mass transfer effects due to the mobilization of solutes initially residing in immobile domains. Better understanding of kinetic mass transfer effects on ASR is needed in order to aid the decision-making process. A numerical model is developed to simulate ASR performance by combining the convergent and divergent dispersion models with a first-order mass transfer model. By analyzing the concentration history at the pumping well, simple and effective relationships were derived for investigating ASR efficiency under various mass transfer parameters, including capacity ratio and mass transfer timescales, and operational parameters. Based on such relationships, one can conveniently determine whether a site with mass transfer limitations is appropriate or not for ASR and how many ASR cycles are required for achieving a positive recovery efficiency.

CHAPTER 1

INTRODUCTION

Groundwater serves as a major source for freshwater supply in many countries all over the world, particularly in arid and semi-arid regions. In the United States, the usage of groundwater is up to about 50% of all drinking water and it may be up to eighty percent in some rural areas [OTA, 1984]. Particularly, groundwater resources are vital for highly populated coastal areas. However, sustainable use of groundwater resources is being compromised by a multitude of threats such as declining groundwater levels, pollution, and saltwater intrusion. Flow and transport in coastal hydrogeologic systems is more complicated than that in inland freshwater aquifer systems due to the presence of the ocean. Interaction between groundwater and coastal seawater results in a transition zone in coastal aquifers between groundwater environments and ocean environments, referred as subsurface estuary. Both human activities and natural processes exert substantial pressures on groundwater resources and eco-environments in subsurface estuaries: (1) excessive groundwater withdrawals have upset the long-established balance between freshwater and seawater potentials, causing encroachment of salty seawater into freshwater aquifers, resulting in the worldwide seawater intrusion problem; (2) excessive chemical loading, particularly nutrient-enriched groundwater due to rapid urban and/or intensive agricultural development, through submarine groundwater discharge (SGD) across land/sea margins, result in increasing negative impacts on fragile estuary ecosystems; and (3) regional and global climate change, such as extreme

precipitation/drought events and seawater-level rise, exacerbates the issues and complicates management strategies for sustainable estuary ecosystems. In the face of growing water scarcity and deteriorating water quality and offshore ecological environments, scientists, engineers and policy makers must take urgent actions altogether to understand the interactive, dynamic physical, chemical and biological processes in subsurface estuary, and to review, develop and test effective strategies and techniques for sustainable development of coastal groundwater resources and offshore environments.

The main goal of this thesis is to improve our scientific understanding of subsurface mixing in complex coastal hydrogeologic systems and to facilitate the design of effective engineering strategies for sustainable management of groundwater resources under mixing limitations. Two specific topics explored in this research include (i) behaviour and dynamics of freshwater-seawater mixing-zone development; and (ii) recovery efficiency of aquifer storage and recovery (ASR) systems for optimal groundwater management. For the first topic, we are particularly interested in the mechanisms responsible for wide mixing zones, a topic that has been investigated for many years without conclusive findings. For the second topic, we aim to understand the performance of ASR installed in aquifers with mass transfer limitations and to improve engineering design.

1.1 Freshwater-Seawater Mixing-Zone Development

Due to the presence of saltwater in the aquifer formation, a mixing zone (also called transition zone, zone of diffusion, and zone of dispersion) is formed between lighter freshwater flowing to the sea and the denser underlying seawater [Bear, 1972]. Figure 1.1 shows a typical cross-section of a coastal aquifer with a freshwater-seawater interface, which delineates a freshwater zone and a seawater zone. The location, shape, and extent of this freshwater-seawater mixing zone depend not only on the hydrogeologic characteristics of the aquifer, but also on the hydrodynamic fluctuations of the groundwater and seawater levels. This mixing zone is of particular interest in practice because (1) the location and size of the mixing zone directly reflect the impact area during seawater intrusion; (2) the movement of the mixing-zone manifests changes in the flow regime and could be a potentially important driver for saline water exchange; (3) a wide mixing zone indicates stronger mixing, and consequently enhances reactive transport processes in coastal aquifers; and (4) as a complementary process of seawater intrusion, submarine groundwater discharge (SGD) occurs near the mixing zone, which is now widely recognized as a major chemical pathway for contaminants entering coastal waters and considerable negative impact on the marine ecosystem [Johannes, 1980; Simmons, 1992, Church, 1996, Moore, 1996].

In this topic, we are particularly interested in the width or thickness of the mixing zone (as shown in Figure 1.1) because the mixing-zone width is a direct indicator of the mixing extent in the subsurface and has important implications in upconing, SGD and reactive transport processes. Wide mixing zones have been observed in many coastal

aquifers (reviewed in the next Chapter). However, the mechanisms responsible for wide mixing zones remain unknown.

1.2 Recovery Efficiency of ASR Systems

ASR is a powerful engineering technology for water resources management and environmental protection. ASR serves to store freshwater deep underground when excessive water is available for recovery later when needed to meet urban, agriculture, ecosystem, industrial, recreational, emergency and other water uses. The main benefits of ASR systems are (i) substantial amounts of water can be stored deep underground, greatly reducing the need to construct large and expensive surface reservoirs, (ii) ASR may store and expand the function of an aquifer that has experienced long-term declination in water levels due to heavy pumping to meet growing urban and agriculture water needs, and (iii) the development of environmentally friendly ASR systems can alleviate land subsidence and act as a hydraulic barrier against saltwater intrusion.

The performance of an ASR system is generally quantified by a recovery efficiency (RE) defined as the quantity of stored water that can be recovered without further treatment divided by the total quantity stored [Kimbler et al., 1975]. RE is properly measured on an individual operation cycle basis, with the recognition that a large volume of water must first be injected in a system to flush out native waters. RE may be significantly less than one, when an ASR system is placed in a contaminated aquifer or in a costal aquifer filled with brackish or saline water. The storage of freshwater in brackish or saline aquifers is a miscible displacement process in which a fluid with one

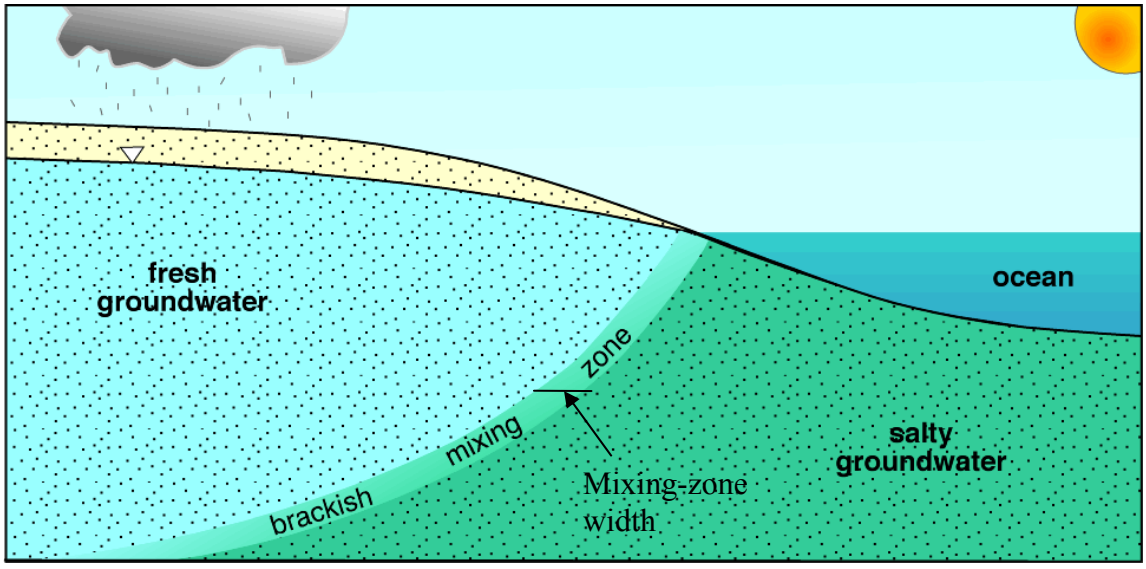

Figure 1.1 A typical cross-section of a coastal aquifer. (Source: http://myweb.cwpost.liu.edu/vdivener/notes/groundwater.htm)

density displaces another with different density within a porous medium [Kumar et al., 1970]. Density-induced tilting of the unstable interface, mixing at the interface, and ambient groundwater displacement due to a background hydraulic gradient are regarded as main factors controlling RE of ASR [Moulder, 1970; Merritt, 1986; Kumar and Kimbler, 1970; Maliva et al., 2006; Ward et al., 2007, 2008 and 2009].

1.3 Research Motivation, Objectives, and Approach

1.3.1 Research Motivation

Wide mixing zones have been observed in many aquifers all over the world [Xue et al. 1993; Wu et al., 1993; Price et al., 2003; Cherry, 2006]. Many studies have been conducted to understand the mechanisms responsible for wide mixing zones, but could not reach an agreement. The first topic of this research is to answer the scientific question: what are the possible mechanisms responsible for wide mixing zones?

Two hypotheses are proposed:

1. Kinetic mass transfer between mobile and immobile solutions coupled with the movement of the mixing zone may significantly enhance solute mixing and cause wide freshwater-seawater mixing zones.

2. Aquifer stratification may create wide mixing zone, even in steady-state flow systems.

The motivation of the first hypothesis is based on two facts. First, the mixing zone in reality is not stationary but moving. The moving mixing zones, which can be resulted by long-term freshwater level fluctuations, have been observed in many coastal aquifers [Michael et al., 2005]. On the other hand, kinetic mass transfer always occurs in subsurface environments. Field experiments have found the mass transfer behavior of saltwater [Culkin et al., 2008].

The motivation of studying aquifer stratification is because aquifer stratification is very common in coastal aquifers and aquifer stratification may have significant effects on a moving mixing zone due to unsynchronized movement of the mixing zone in different layers.

ASR provides an effective solution for optimal management of water resources to meet existing and future freshwater demands. Despite the fact that many studies have been reported to investigate various factors influencing the RE of ASR, significant knowledge gaps exist in terms of guidelines for optimal design of ASR operations and selecting appropriate ASR sites. The second topic of this research is to investigate the performance of ASR under kinetic mass transfer limitations. Specifically, we aim to develop simple but effective guidance that can facilitate the design of efficient ASR operations and the selection of ASR sites. The motivation of investigating kinetic mass transfer effects on recovery efficiency of an ASR system because this effect has been observed in the field condition. In the field experiment of an ASR system in SC, salinity rebound occurs during the storage period, which indicates that some salts are initially storaged in immobile zone of the aquifer and thus mass transfer effects exist.

1.3.2 Specific Objectives

Specific objectives are to:

1. numerically analyze the coupled effects of kinetic mass transfer and freshwater level fluctuations on dynamic mixing-zone development;
2. numerically evaluate the effects of aquifer stratification on mixing-zone development under both steady state and transient flow conditions;
3. experimentally visualize the mixing zones developed in stratified porous media;
4. investigate the RE of an ASR in aquifers with mass transfer limitations;
5. propose strategies which can improve the RE of ASR.

1.3.3 Approaches

The approaches used in studies involves numerical, analytical and laboratory experimental methods. Specifically, numerical method is employed to study coupled effects of kinetic mass transfer and transient flow conditions on the mixing-zone development. Both numerical and laboratory experiment methods are used to investigate mixing-zone development in stratified aquifers. For the topic of ASR, both numerical and analytical methods are used. Detailed model development and laboratory setup will be described in the following chapters.

1.4 Organization of the Thesis

The thesis consists of nine chapters. A brief introduction is provided in this chapter. A comprehensive literature review is given in Chapter 2. The study of effects of kinetic

mass transfer coupled with the movement of mixing zones on widening mixing zones is presented in Chapter 3. Chapter 4 continues the topic in Chapter 3, which further investigates the dynamic responses of seawater-freshwater mixing zone in coastal aquifers with kinetic mass transfer. Chapter 5 presents the effects of aquifer stratification on mixing-zone development. In Chapter 6, recovery efficiency of aquifer storage and recovery systems with mass transfer limitations is investigated. Chapter 7 provides conclusions of studied topics. Chapter 8 discusses the limitations and implications of the studies. Further recommended studies are given in Chapter 9.

CHAPTER 2

LITERATURE REVIEW

This chapter summarizes the comprehensive scientific literature relating to the following three topics: (i) seawater intrusion, (ii) recovery efficiency of aquifer storage and recovery systems, and (iii) kinetic mass transfer. For seawater intrusion, we focus on the mixing-zone development, which is one of two primary topics in this thesis.

2.1 Seawater Intrusion

Seawater intrusion is the movement of seawater into freshwater aquifers, characterized by the heavier seawater flowing below the lighter freshwater in the geologic formation. Seawater intrusion has a significant impact on water resources, especially in populated coastal areas where vital groundwater is vulnerable to salinization. Salty water is detrimental to most plants and relatively a small portion of seawater (about 1%) is sufficient to make freshwater fail secondary drinking-water standards (250 mg/l for chloride). Seawater intrusion may be caused either by long-term processes, such as land subsidence or climate change resulting in seawater rise, or by short-term human activities, such as groundwater withdrawal lowering groundwater levels and allowing salty water to seep into the fresh water supply. Once a coastal aquifer has been salinated, restoration of water quality to pre-intrusion levels is difficult and costly.

The impact of seawater intrusion on groundwater resources has long been recognized as a worldwide problem [Kafri and Arad, 1979; Pauc, 1989; Kashgarian and Tanaka, 1991; Largier and Taljaard, 1991; Santiago, 1991; Xue et al., 1993; Zubari et al., 1994; Simmons and Narayan, 1998; Ergil, 2000; Neilson-Welch and Smith, 2001; Fakir et al., 2002; Foyle et al., 2002] In the United States, many coastal aquifers have been contaminated by salt water [e.g., Bond and Bredehoeft, 1987; Lam et al., 1994; Segovia-Zavala et al., 1998; Foyle et al., 2002; Beuhler, 2003]. In the coastal area of Georgia (GA), South Carolina (SC), and Florida (FL), increased groundwater pumpage due to population growth and sustained industrial activity has increased stresses on the coastal groundwater system since the 1980s [Payne et al., 2006]. The Upper Floridian aquifer, the principal source of water in the coastal area, has been used extensively, resulting in substantial water-level decline near Savannah, GA, and seawater intrusion at the northern end of Hilton Head Island, SC, and at Brunswick, GA, which constrains the future development of the Upper Floridian aquifer [Cherry, 2006; Payne et al., 2006].

2.1.1 Freshwater-Seawater Mixing Zone

Seawater intrusion involves the displacement of freshwater by seawater and mixing of seawater and mixing of seawater with freshwater, and is ultimately controlled by the flow field and site-specific transport mechanisms in coastal aquifers. A major characteristic is variable-density flow and convection-driven mixing caused by density gradient. Even a low-density difference can affect flow and transport significantly [Simmons et al., 2005]. Across the interface between salt water and fresh groundwater, seawater intrusion develops a mixing zone, where significant convection caused by a

density gradient occurs [Henry, 1964; Galeati et al., 1992]. Seawater intrusion can thus be described by growth and decay of the mixing zone. Specifically, wide mixing zones are observed in many coastal aquifers. For example, in the Upper Floridian aquifer downtown Brunswick, GA, the mixing zone of saltwater and freshwater has been detected across an area of increasing size [Cherry, 2006]. However, the controlling mechanism in the mixing zone is still not well understood.

The diagram in Figure 2.1 illustrates the problem of seawater intrusion. The shallow unconfined aquifer contains two fluids (freshwater and saltwater) with differing densities that are separated by a mixing zone. For steady-state groundwater gradient and seawater level, the mixing zone may be at equilibrium state due to pressure balance (Figure 2.1a). Decreases in groundwater levels inland or increases in seawater levels may reduce or even reverse the groundwater gradient and destruct the equilibrium state, allowing salt water to displace freshwater (Figure 2.1b).

2.1.2 Numerical Modeling

Two approaches are available to describe seawater intrusion. By utilizing the approximation of interface flow, i.e., the mixing zone is approximated by a sharp interface, potential-flow theories can be applied to describe the interface propagation [e.g., Bear and Dagan, 1964; Ozturk, 1970; Collins and Gelhar, 1971; Huppert and Woods, 1995; Ramesh et al., 1995; Xue et al., 1995; Dagan and Zeitoun, 1998; Naji et al., 1998; Sakr, 1999; Kacimov and Obnosov, 2001; Cartwright et al., 2004; Bakker, 2006; Kacimov and Sherif, 2006].

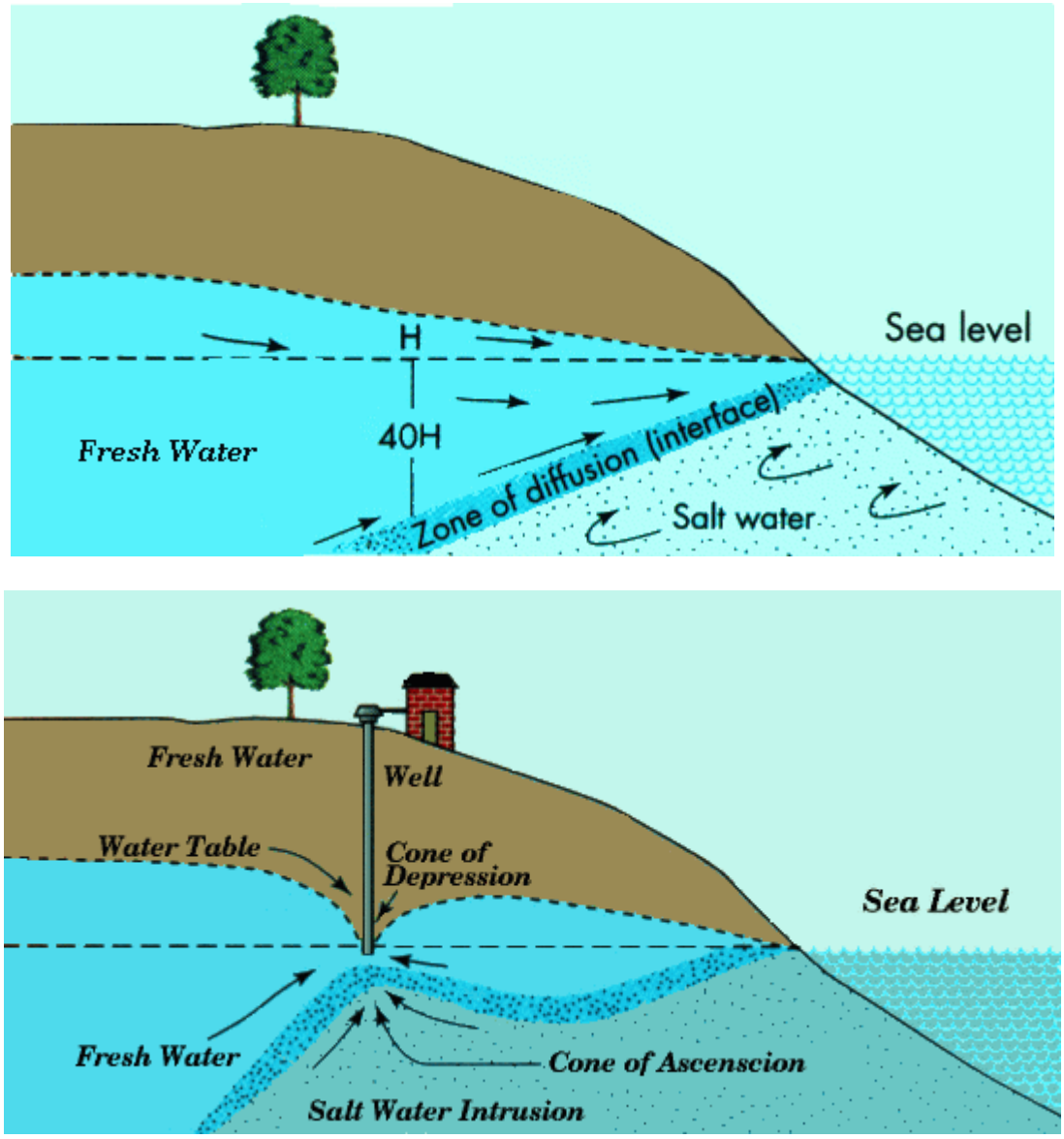

Figure 2.1 Conceptual diagrams of seawater intrusion. (a) natural environment; (b) groundwater withdrawal (Source: http://www.lenntech.com/groundwater/seawater-intrusions.htm).

However, it is now computationally feasible to adopt a more realistic model of the mixing zone through a system of variable density flow equations and the advection-dispersion equation [e.g., Henry 1964; Fan and Kahawita, 1994; Croucher and O'Sullivan, 1995; Kolditz et al., 1998; Ackerer et al., 1999; Paniconi et al., 2001; Diersch and Kolditz, 2002; Gotovac et al., 2003; Simpson and Clement, 2003; Simmons, 2005; Langevin and Guo, 2006; Dentz et al., 2006]. In this context, a wide mixing zone, rather than a sharp interface, can be simulated, which is more consistent with field observations in many coastal aquifers [e.g., Xue et al., 1993; Price et al., 2003; Cherry 2006; Kim et al., 2006]. For example, groundwater salinity measurements in the Everglades National Park, in Southern Florida, USA, indicated the presence of a wide (6–28 km) seawater mixing zone [Price et al., 2003]; in the Floridian aquifer near downtown Brunswick, GA, USA, the mixing zone of seawater and freshwater has been detected across an area of increasing size [Cherry, 2006]; Xue et al. [1993] reported a wide mixing zone of 1.5-6.0 km in the coastal area of Laizhou Bay, China, and also found that the increasing extension of the salt water intrusion is a major concern in this area [Wu et al., 1993]; Barlow [2003] summarized groundwater conditions in freshwater-saltwater environments of the Atlantic Coast, in which wide mixing zones were observed in many coastal aquifers, e.g., the Biscayne aquifer near Miami (see Figure 2.2), Florida, the upper Potomac aquifer in Virginia's Inland Wedge, the Floridian aquifer system in South Carolina, Georgia, and Florida, and the lower Tamiami aquifer in south-western Florida.

2.1.3 Wide Mixing Zone

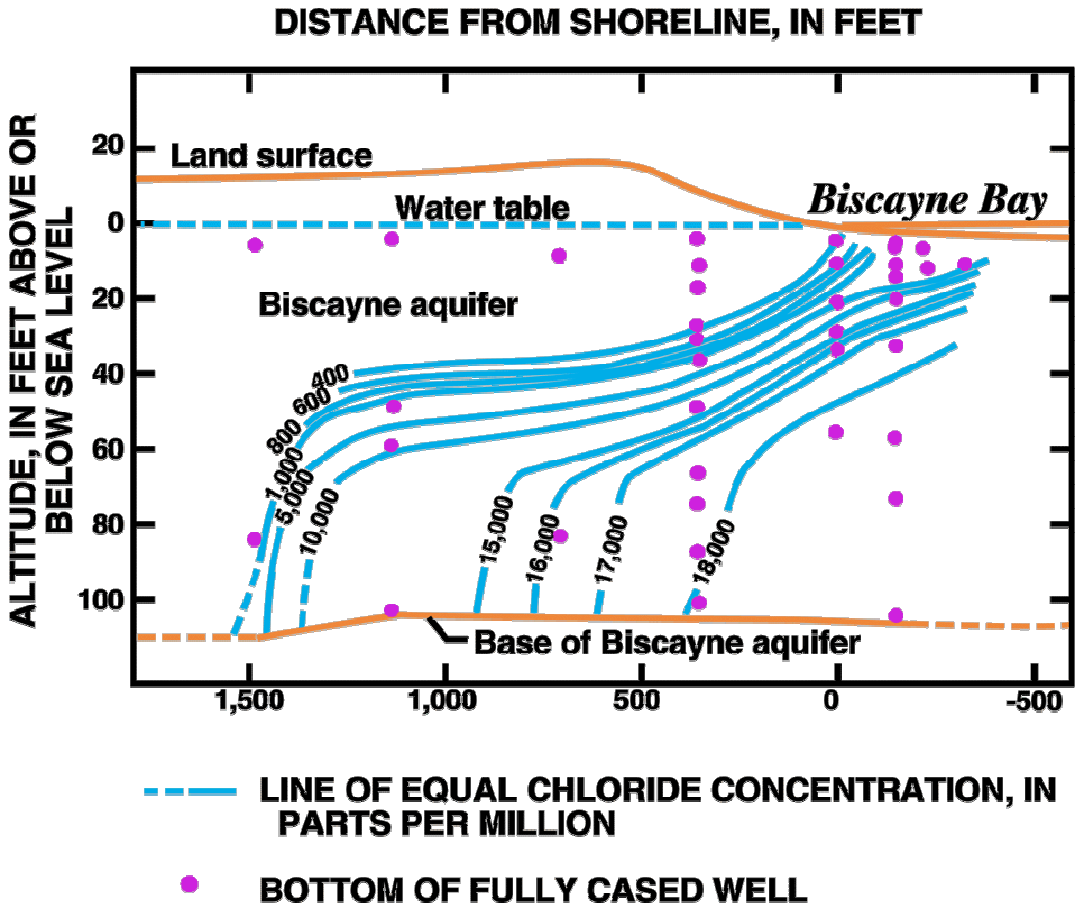

Figure 2.2 Mixing zone in the Biscayne aquifer near Miami, Florida. (Source: water.usgs.gov/ogw/gwrp/saltwater/fig3.html).

In past decades, a number of numerical studies targeted at simulating the mixing zone have been conducted in an attempt to gain better understanding of the factors controlling the width of the mixing zone. For example, Volker and Rushton [1982] systematically studied a variety of parameters which may have an effect on the mixing-zone width and found that a larger dispersion coefficient or a lower freshwater discharge gradient would make an important contribution to a wider steady mixing zone, while the relative density of seawater does not have much effect on its width. Transverse dispersivity has now widely been recognized as a leading factor for explaining the width of a steady mixing zone [Dagan, 2006]. An increasing transverse dispersivity would have a shear effect, bring the steady mixing zone seaward at the bottom and landward at the top and finally creating a broader mixing zone [Abarca, 2006]. However, in the field scale, transverse pore-scale dispersion only causes the presence of a thin mixing zone. In practice, investigators present numerical solutions by assuming a large, perhaps unwarranted, value of transverse dispersivity [Huyakorn et al., 1987; Essink, 2003]. In other words, a large value of transverse dispersivity only provides a convenient way to reproduce the wide mixing zone in reality, but usually seems to be unreasonable and holds a poor physical meaning.

The mechanism responsible for the wide mixing zone still remains debatable. In general, factors affecting flow and mixing in the mixing zone are regarded to include: (1) hydraulic heterogeneity, (2) dispersion/diffusion, and (3) transient flow conditions. Heterogeneity in the hydraulic conductivity of the formation is well known to significantly affect groundwater flow and solute transport. In variable density flow

systems, heterogeneity can perturb flow over various length scales and lead to a spatially varying specific-discharge field and thus to nonuniform advection. As a result, the mixing zone becomes increasingly irregular in sharp, enhancing mixing caused by diffusion across its interface. Classical stochastic subsurface theory has analyzed the spatial moments of extended plumes and matched them with macrodispersion equations, which are Fickian in the large-time limit [Dagan, 1989; Gelhar, 1993; Rubin, 2003]. Homogenization techniques have been employed to derive effective macroscopic transport parameters for transport in heterogeneous media. However, heterogeneity has not been well studied for variable density flow systems, especially for mixing in mixing zones. Only recently has heterogeneity been considered in the study of the mixing zone [e.g., Voss and Souza, 1989; Schincariol and Schwartz, 1990; Welty and Gelhar, 1991, 1992; Schincariol et al., 1994; DeWit and Homsy, 1997a, 1997b; Welty et al., 2003; Graf and Therrien, 2005; Held et al., 2005; Reinelt, 2005; Simmons, 2005]. However, the theoretical analyses by Held et al. [2005] indicated that the use of macroscopic dispersion coefficients is inappropriate and the effective dispersion coefficients are more close to the local-scale coefficients. Abarca et al. [2006] showed that the effects of moderate heterogeneity on increasing the width of the mixing zone are small. Thus, the widening of the mixing zone width may not simply be attributed to heterogeneity of the formation.

In the past, diffusion and local dispersion is mainly responsible for the development of a wide mixing zone [e.g., Henry, 1964]. The effect of local longitudinal dispersion on macroscopic transport in heterogeneous domains is of minor importance. Local

transverse dispersion, by contrast, significantly contributes to solute mixing in heterogeneous formations. It may lead to macroscopically longitudinal mixing of two solute clouds, which is stronger than the mixing caused by local longitudinal dispersion, although the local transverse dispersivities are typically assumed to be about an order of magnitude smaller than the longitudinal counterparts. However, large values of dispersion coefficients must be employed to describe a wide mixing zone, even for a heterogeneous formation. Karasaki et al. [2006] found a thin mixing zone in a homogeneous formation, which cannot be explained by the solution to the Henry's problem which shows a wide mixing zone, but are better described by potential-flow theories which completely neglect the transverse dispersion. Hence, to generate a wide mixing zone, either large values of local dispersivities or highly heterogeneous formations need to be assumed, both of which may be unrealistic. Smith [2004] demonstrated a strong dependence of convective overturn on the aquifer dispersivities, suggesting that it is more appropriate to apply a scale-dependent dispersion coefficient. Henry [1964] attributed the large dispersion to the transient effects introduced by tidal effects. However, Karasaki et al. [2006] failed to reproduce a wide mixing zone by imposing a time-varying sinusoidal boundary condition without using a large dispersion coefficient. Laboratory experiments have also been conducted to study mixing mechanisms in variable density flow systems [e.g., Schincariol and Schwartz, 1990; Simmons et al., 2002].

Furthermore, the role of tidal fluctuations on the width of the mixing zone has been investigated by Ataie-Ashtiani et al. [1999]. Numerical results obtained from SUTRA

indicated that the tidal activity creates a thicker interface than would occur without tidal effects. Nevertheless, the portion of the width increased by tidal effects is limited. Moreover, the same authors have found that the configuration of the interface is radically changed when the tidal fluctuations are included. Karasaki et al. [2006] failed to reproduce a wide mixing zone by imposing a time-varying sinusoidal boundary condition without using a large dispersion coefficient.

Overall, no convincing explanation has been given for a wide mixing zone, and few researches have been done to identify the relative importance of the mechanisms mentioned above. In addition, the studies summarized above do not provide a solid foundation for the assessment of groundwater resources in coastal areas subject to both natural processes and human activities, such as groundwater withdrawal. Finally, most studies on impacts of climate change at the regional scale are focused on precipitation change and temperature increase [e.g., Arnell, 1998; Loaiciga et al., 2000], but little attention has been paid directly to seawater intrusion, particularly the mixing-zone development [Sherif and Singh, 1999; Bobba, 2002].

2.2 Recovery Efficiency of ASR

ASR involves injecting water into an aquifer through wells and then pumping it out when needed. The aquifer essentially functions as a water bank. Deposits are made in time of surplus, typically during the rainy season, and withdrawals occur when available water falls short of demand. The major attraction of ASR is that it can potentially provide very large volumes of storage, at a much lower cost than other options. ASR has

been widely used in many countries including United States, United Kingdom, and Australia. Currently, about 95 ASR sites are in operation around the United States, ranging from a single well to 30 wells with recovery capacities ranging from 0.5 MGD from single wells to 100 MGD from well fields.

The most important parameter used to assess ASR performance is recovery efficiency (RE). RE is defined as the percentage of water injected into a system in an ASR site that meets the predefined water quality criteria when recovered [Kimbler et al., 1975]. The ideal ASR system would substitute subsurface storage for a surface water tank and recover 100% of the injected fresh water. However, multiple mechanisms including physical, chemical, and biologic processes can degrade water quality and finally control ASR efficiency (e.g., Ma and Spalding, 1996; Mirecki et a., 1998; Parkurst and Petkewich, 2001; Gaus et al., 2002; Vanderzalm et al., 2002; Petkewich et al., 2004; Herczeg et al., 2004; Le Gal La Salle et al. 2005; Ward et al., 2007, 2008 and 2009). It is therefore not surprising that RE may be significantly less than 100%, particularly for an ASR system placed in an aquifer filled with brackish or contaminated water.

The density effects on ASR's performance in brackish aquifers have been broadly studied [e.g. Esmail and Kimbler, 1967; Kumar and Kimbler, 1970; Bakker et al., 2004; Brown, 2005; Pavelic et al., 2006; Ward et al., 2007]. Figure 2.3 shows the schematic illustration of density effects on ASR. The vertical interface between injected freshwater and ambient saltwater is inherently unstable due to the density difference between two fluids. Brown [2005] and Pavelic et al. [2006] suggested that the density difference

between injected and ambient water is simply a controlling factor used to determine whether or not density effects are significant on RE. According to theoretical mixed-convection analysis, however, Ward et al. [2007] concluded that the density contrast alone is to determine whether density effects are negligible, but density effects in ASR also depend on the relative influences of the density difference, hydraulic conductivity, pumping rates, injected radius, storage duration, and dispersivity. More detailed review of density effects in ASR can be found in Ward et al. [2007]. An integrated assessment of lateral flow, density effects and dispersion in ASR was given by Ward et al. [2009].

The importance of anisotropy and layered heterogeneity of the brackish aquifers in ASR was theoretically examined by Ward et al. [2008]. Their simulation results indicated that higher RE may be expected in highly anisotropic cases because the density induced tilting effect is retarded by the smaller vertical hydraulic conductivity. On the other hand, a similar sensitivity was found when heterogeneity represented by alternating horizontally infinite isotropic bands of high and low hydraulic conductivity was found, showing that highly heterogeneous cases also correspond to higher REs.

Numerical studies of three ASR field sites in Wisconsin showed that dispersive mixing was the most important process affecting the value of RE [Lowry, 2004; Lowry and Anderson, 2006]. With a large longitudinal dispersivity, RE would be highly decreased [Lowry and Anderson, 2006; Ward et al., 2007]. Culkin et al. [2008] developed a 3D model to evaluate the impact of dual domain mass transfer processes on ASR efficiency based on the data from a pilot-scale ASR study in Charleston, South

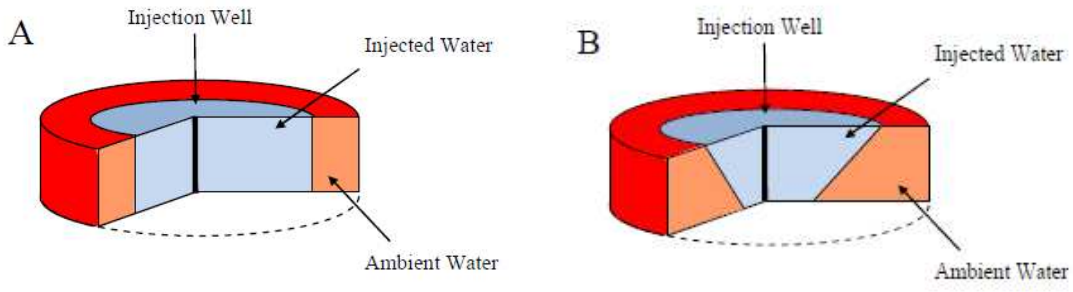

Figure 2.3 Schematic illustration of density effects on ASR- (A) without density effects; (B) with density effects.

Carolina. The modeling results show that rate-limited mass transfer can explain a rebound in salinity during fresh water storage in a brackish aquifer.

2.3 Kinetic Mass Transfer

Transport models with mass transfer descriptions usually conceptualize a porous or fractured medium as consisting of two overlapping continuous media: a mobile domain, where advective-dispersive transport occurs, and an immobile one with a continuous withdrawal and return of solute mass [Coats and Smith, 1964; van Genuchten and Wierenga, 1976]. Mass transfer models have received increasing attentions in recent years because: (1) they are capable of characterizing various pore-scale diffusion processes between relative mobile and immobile domains, in which the latter may consist of sorption sites, dead-end pores, porous particles, aggregates, fractures, or macropores [e.g., Chen and Wagenet, 1995; Haggerty and Gorelick, 1995, 1998; Carrea et al., 1998; Salamon et al., 2006]; and (2) in the absence of sufficient aquifer characterization, mass transfer models may be used with macroscopic advective-dispersive models to describe extreme asymmetric concentration profiles in anomalous transport caused by aquifer heterogeneities [e.g., Berkowitz and Scher, 1997, 1998; Harvey and Gorelick, 2000; Dentz and Berkowitz, 2003; Zinn et al., 2004; Berkowitz et al., 2006].

Mass transfer occurs in almost all fractured and porous heterogeneous media over various scales ranging from pore scale to field scale. Mass transfer between the mobile and immobile domains is kinetically controlled. As the simplest approximation, first-

order models are often used to describe the kinetic mass transfer processes. Other mass transfer models are also available for describing various asymmetric transport behaviours. Haggerty and Gorelick [1995] proposed a multirate model by superimposing a distribution of first-order mass transfer rates to characterize incomplete mixing in the immobile domain and various diffusion processes. Based on the same belief of the pore-scale heterogeneities, Carrera et al. [1998] developed a more versatile model of linear mass transfer, in which mass transfer are described by a convolution product of concentrations in the mobile domain and a memory function rather than predefining the mass transfer model. By choosing appropriate memory functions, the model can reproduce the first order, multirate, sphere, layer or cylinder diffusive models [e.g., Carrera et al., Haggerty et al., 2000].

The first order mass transfer models are commonly employed in theoretical and practical studies due to its simplicity. This model involves three parameters including mobile θ_{im} and immobile porosity θ_m, and mass transfer rate coefficient ξ which controls how quickly mass transfer occurs between two domains. For cases with very low ξ, transport models that incorporate dual domain collapse to single domain models with the effective porosity being θ_m since the immobile zone is almost nullified. For cases with very high ξ, there is instantaneous transport between the mobile and immobile regions. Therefore, transport models that incorporate dual domain also collapse to single domain models with an effective porosity being θ_{im}, accompanying a retardation factor R given by $1+\theta_{im}/\theta_m$ [Neville, 2006].

CHAPTER 3

EFFECTS OF KINETIC MASS TRANSFER COULPED WITH THE MOVEMENT OF MIXING ZONES ON WIDING MIXING ZONES IN COASTAL AQUIFERS

3.1 Introduction

Interaction between groundwater and coastal seawater results in two complementary processes: seawater intrusion and submarine groundwater discharge (SGD). Understanding these processes meets the urgent needs for preserving vital fresh groundwater resources in coastal and offshore environments in highly populated coastal areas worldwide. The mixing zone developed at the freshwater-seawater interface is one of the most important features in complex coastal hydrogeologic systems. As the cumulative effect of many processes and mechanisms, such as periodic tidal activities, seasonal water-table change, groundwater withdrawal, transport processes driven by density gradient, diffusion and dispersion, and properties of geological formations, etc., the growth and decay of the mixing zone can (1) directly reflect the extent of mixing in coastal aquifers; and (2) provide extremely useful information to serve as an indicator of and measure for effective management of groundwater resources and sustainable stewardship of coastal and offshore environments. For example, upconing of the mixing zone generally indicates the occurrence of seawater intrusion subject to excessive groundwater withdrawal [Bear, 1972]; and the movement of the mixing zone due to seasonal water-table fluctuation is often associated with the seasonal variations of SGD [Michael et al., 2005]. Thus, gaining a better grasp of mixing-zone development in

coastal aquifers within various hydrogeologic settings is a milestone in our efforts to significantly improve our understandings of flow and transport in complex coastal hydrogeologic systems.

In general, two types of mathematical models have been used to describe the mixing-zone development: sharp-interface approximation and miscible-fluid model. In the sharp-interface approximation, it is assumed that there is a stationary and abrupt interface between freshwater and intruding seawater, implying that no mixing takes place between freshwater and seawater. This approach is a major simplification and may allow one to use potential-flow theory for describing interface propagation, and provides a useful tool for developing a variety of analytical solutions [e.g., Bear and Dagan, 1964; Strack, 1976; Huppert and Woods 1995, Naji et al., 1998]. The second approach, based on the density-dependent miscible saltwater-freshwater systems, accounts for the presence of a variable-density mixing zone. The latter model is of particular interest in practical applications where one desires to evaluate salt and other species concentrations in coastal aquifers. In this work, we will focus on this model. Due to its practical significance, several numerical models based on miscible-fluid physics have been developed to describe and study the problem of seawater intrusion over the past 20 years [Voss and Souza, 1987; Ataie-Ashtiani et al., 1999; Paniconi et al., 2001; Zhang et al., 2004; Paster et al., 2006; Qahman and Larabi, 2006]. Analytical solutions for seawater intrusion based on miscible-fluid systems are only available for steady-state, simplified cases [Dentz et al., 2006; Bolster et al., 2007].

Both narrow and wide mixing zones have been observed in numerical, laboratory, and field studies. With a fine discretization and small dispersion, numerical simulations produced narrow mixing zones [e.g., Benson et al., 1998; Karasaki et al. 2006]. Laboratory experiments also demonstrated narrow mixing zones in homogeneous media [e.g., Zhang et al., 2001; Goswami and Clement, 2007; Abarca and Clement, 2009]. However, many field measurements found wide mixing zones, ranging from hundreds of feet to miles. This finding cannot be simply explained by upscaling small-scale laboratory data. For example, groundwater salinity measurements in the Everglades National Park, in Southern Florida, USA, indicated the presence of a wide (6–28 km) seawater mixing zone [Price et al., 2003]. In the Floridian aquifer near downtown Brunswick, GA, USA, the mixing zone of seawater and freshwater has been detected across an area of increasing size [Cherry, 2006]. Xue et al. [1993] reported a wide mixing zone of 1.5-6.0 km in the coastal area of LaiZhou Bay, China, and also found that the increasing extension of the salt water intrusion is a major concern in this area [Wu et al., 1993]. Barlow [2003] summarized groundwater in freshwater-saltwater environments of the Atlantic Coast, in which wide mixing zones were observed in many coastal aquifers, e.g., the Biscayne aquifer near Miami, Florida, the upper Potomac aquifer in Virginia's Inland Wedge, the Floridian aquifer system in South Carolina, Georgia, and Florida, and the lower Tamiami aquifer in south-western Florida, etc.

The mechanisms responsible for a wide mixing zone still remain the subject of debate. Local dispersion has been considered as a primary mechanism responsible for the occurrence of the mixing zone. During the movement of the seawater front in either

the landward or the seaward direction, elements of each fluid are transferred into the opposite environment by the convection component of dispersion, wherein to a large extent they become inseparably blended with other fluid by mixing and molecular diffusion [Cooper, 1959]. Dagan [2006] pointed out that transverse dispersion is the main mechanism creating mixing in the seawater-freshwater interface, but the presumed small transverse pore-scale dispersion can only create a narrow mixing layer at the interface. The extent of mixing is also influenced by hydrodynamic fluctuations of the groundwater and seawater levels. Volker and Rushton [1982] compared a variety of aquifer parameters and the influence of the flow conditions on the configuration and location of the interface. They concluded that a decrease in the dispersion coefficient leads to the contraction of the dispersion zone for a constant freshwater discharge, while the interface becomes more diffuse as the freshwater discharge decreases provided that the dispersion coefficient keeps invariant. Ataie-Ashtiani et al. [1999] numerically examined the effects of tidal fluctuations on seawater intrusion in an unconfined aquifer, and found that the tidal activity created a thicker interface than would occur without tidal effects. However, Karasaki et al. [2006] failed to reproduce a wide mixing zone by imposing a time-varying sinusoidal boundary condition without using a large dispersion coefficient. Heterogeneity in the hydraulic conductivity of the formation also contributes to the mixing enhancement. Heterogeneous hydraulic conductivities lead to spatially varying specific-discharge fields and thus to nonuniform advection. As a result, the mixing zone becomes increasingly irregular in shape, enhancing mixing caused by diffusion across its surface. However, Abarca et al. [2006] showed that the effects of moderate heterogeneity on increasing the width of mixing zone are small. Thus, the

widening of the mixing zone may not simply be attributed to heterogeneity of the formation.

In this research, we provide an alternative plausible explanation for wide mixing zones observed in coastal aquifers. The hypothesis is that the movement of the mixing zone combined with kinetic mass transfer effects may significantly widen the mixing zone. Transport simulations with mass transfer usually conceptualize a porous or fractured heterogeneous medium as consisting of two overlapping continuous media: a moving domain, where advective-dispersive transport occurs, and an immobile one with a continuous withdrawal and return of solute mass [Coats and Smith, 1964; van Genuchten and Wierenga, 1976]. This study is motivated by the facts that (1) the mixing zone, in reality, seldom remains stationary, and (2) mass transfer processes, occurring in almost all fractured and porous heterogeneous media over various scales ranging from pore scale to field scale, can significantly enhance solute mixing [Michalak and Kitanidis, 2000]. Previous investigations of the mixing-zone width are mostly based on the steady state or tidal conditions. Under these conditions, the mixing zone is nearly stationary [Volker and Rushton. 1982; Ataie-Ashtiani et al., 1999; Robinson et al., 2007]. In reality, however, mixing zones seldom remain stationary. Large scale recharge into the aquifer as well as withdrawals from it leads to the movement of mixing zone from one position to another. It is now recognized that seasonal oscillations of inland recharge appear to be widespread, clearly indicating that a seasonal mixing-zone movement occurs in coastal aquifers [Michael et al., 2005]. On the other hand, the movement of mixing zone can also be caused by the seaward boundary. Cartwright and Nielsen

[2003], based on field experiments, indicated that the mixing zone movement can be caused by coastal waves. It is worth noting that the movement of mixing zone has been also observed in many other coastal areas [Wu et al., 1993; Cherry, 2006]. To the best of our knowledge, no study focusing on the mixing-zone development has considered the combined effect of mass transfer processes and transient conditions. Langevin et al. [2003] conducted a simulation of variable-density flow coupled with dual-domain transport for the Henry problem. Without the consideration of mixing-zone movement, they found that the steady-state salinity distribution was roughly the same as the salinity distribution for the classical Henry problem.

3.2 Numerical Model

The proposed hypothesis will be tested by conducting two-dimensional (vertical cross-section) numerical simulations based on the variable-density flow and transport equations for a scaled-tank model and a field-scale model. Transient effects will be introduced by imposing periodic water levels at the seaward and landward boundary. A dual domain transport model with first-order mass transfer will be applied to describe transport processes with kinetic mass transfer between mobile and immobile domains. The numerical model is solved by the density-dependent groundwater flow code SEAWAT-2000 implemented in a graphic user interface software Groundwater Vista 5.20 developed for 3D groundwater flow and transport modeling. SEAWAT-2000 itself was developed by combining MODFLOW and MT3DMS into a single program solving the coupled flow and solute-transport equations. MT3DMS is implemented with an optional, dual-domain formulation for modeling mass transport.

3.2.1 Governing Equations

The governing equation for saturated variable-density groundwater flow in terms of freshwater head is described by [Langevin and Guo, 2006]:

$$\nabla \cdot \left[\rho K_f \left(\nabla \cdot h_f + \frac{\rho - \rho_f}{\rho_f} \cdot \nabla z \right) \right] = \rho S_f \frac{\partial h_f}{\partial t} + \theta_e \frac{\partial \rho}{\partial t} - \rho_s q_s \tag{3.1}$$

where z [L] is the vertical coordinate directed upward; K_f [LT^{-1}] is the equivalent freshwater hydraulic conductivity; h_f [L] is the equivalent freshwater head; ρ [ML^{-3}] is the fluid density; ρ_f [ML^{-3}] is the freshwater density; S_f [L^{-1}] is the equivalent freshwater storage coefficient; t [T] is the time; θ_e is the effective porosity; and ρ_s [ML^{-3}] and q_s [T^{-1}] are the density and flow rate per unit volume of aquifer of the source/sink, respectively [Langevin et al., 2003].

The dual-domain transport model involving advection, molecular diffusion, mechanical dispersion, and first-order mass transfer is described by:

$$\theta_m \frac{\partial C_m}{\partial t} + \theta_{im} \frac{\partial C_{im}}{\partial t} = \nabla \cdot \left(\theta_m \mathrm{D} \nabla C_m \right) - \nabla \cdot \left(\theta_m \mathrm{v} C_m \right) \tag{3.2a}$$

$$\theta_{im} \frac{\partial C_{im}}{\partial t} = \xi \left(C_m - C_{im} \right) \tag{3.2b}$$

where θ_m is porosity of the mobile domain and is equal to θ_e; θ_{im} is porosity of the immobile domain; C_m [ML^{-3}] is dissolved concentration in the mobile; C_{im} [ML^{-3}] is

dissolved concentration in the immobile domain; ξ [T^{-1}] is first-order mass transfer rate between the mobile and immobile domain; **D** [L^2T^{-1}] is the hydrodynamic dispersion coefficient tensor; and **v** [LT^{-1}] is the pore water velocity vector.

The relationship between the fluid density and salt concentration is represented by the linear function of state:

$$\rho = \rho_f + \varepsilon C_m \tag{3.3}$$

where ε is a dimensionless constant with a value of 0.7143 for salt concentrations ranging from zero to 35 kg m^{-3}, a typical concentration value for seawater [Langevin et al., 2003]; and ρ is expressed in kg m^{-3}.

3.2.2 A Scaled Tank Model and Numerical Implementation

A scaled tank model is designed to simulate the mixing-zone development under the considerations of transient conditions and mass transfer effects. Zhang et al. [2002] presented an experimental study of a dense contaminant plume in an idealized coastal aquifer based on a tank model, which was numerically studied by Brovelli et al. [2007]. Due to its high computational efficiency, this scaled tank model is used here to carry out investigate mass transfer effects on the development of the mixing zone and sensitivity analysis. A schematic representation of the seawater intrusion problem is shown in Figure 3.1. The tank is 1.650m long, 0.6m high, and 0.1m wide with a beach slope (vertical/horizontal ratio) 1:6.12. A homogeneous, isotropic hydraulic conductivity of 4×10^{-3} m s^{-1} is assigned to the domain. The mean local longitudinal and transverse

dispersivities are measured to be 6.49×10^{-4} m and 1×10^{-4} m, respectively. The total porosity is 0.37. The mean seawater level and the constant freshwater level are 0.439 m and 0.463 m, respectively. The seawater and freshwater densities are 1025 kgm^{-3} and 1000 kgm^{-3}, respectively, which represent a salt concentration of 35 kgm^{-3} for seawater. The parameters for the scaled tank model are summarized in Table 3.1.

Rather than only tidal conditions used by Zhang et al. [2002] and Brovelli et al. [2007], periodic water-level fluctuations are imposed respectively at the seaward and landward boundaries to create the movement of the mixing zone. First, a triangular, periodic function with a period of 40 minutes (see Figure 3.2) is imposed at the seawater boundary to simulate the periodic tidal-like motion, while a constant freshwater level of 0.463 m is defined at the landward boundary. The linear variation of water level can be directly implemented based on the variable head boundary condition in SEAWAT by specifying two values of hydraulic head at the beginning and at the end of the stress period, respectively. The software linearly interpolates between the two values according to a defined time step. The use of the triangular function instead of a sinusoid function is intended to minimize the computational effort because much more pressure periods will be needed to reproduce the sinusoidal function. Then, another triangular, periodic function with a period of 80 minutes and amplitude of 0.04 m is defined at the landward boundary to simulate the water-table fluctuations, while the seawater level is kept constant at 0.439 m. In reality, the period of the freshwater-table fluctuations may be much greater than that of the tidal motion. Sensitivity analysis will be conducted later to investigate the effects of both periods. A constant salt concentration of 35 kgm^{-3} is

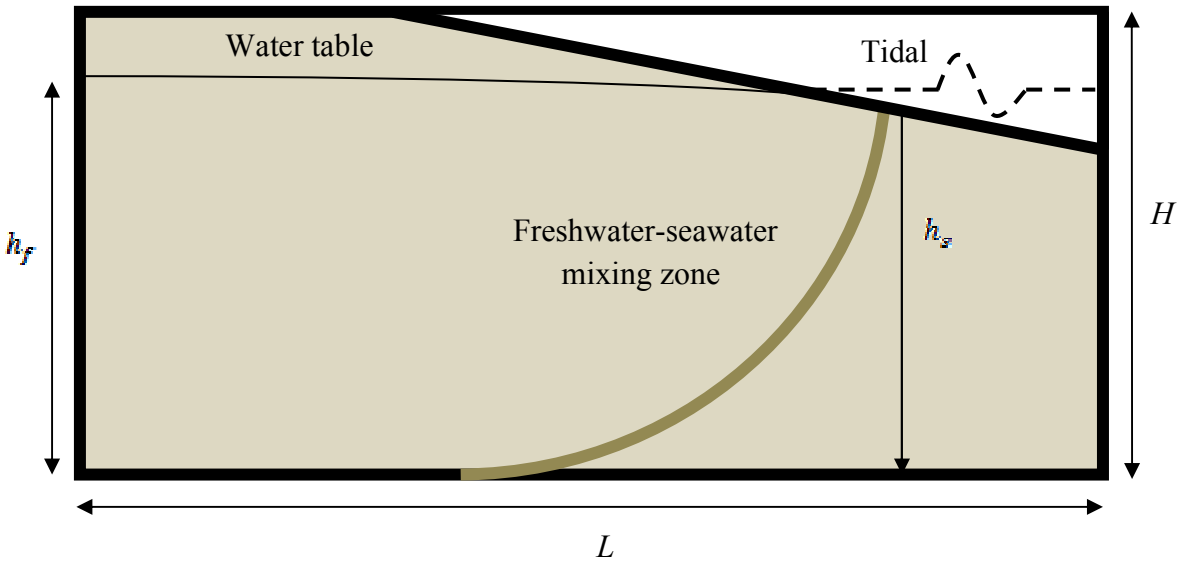

Figure 3.1 Schematic representation of the seawater intrusion problem.

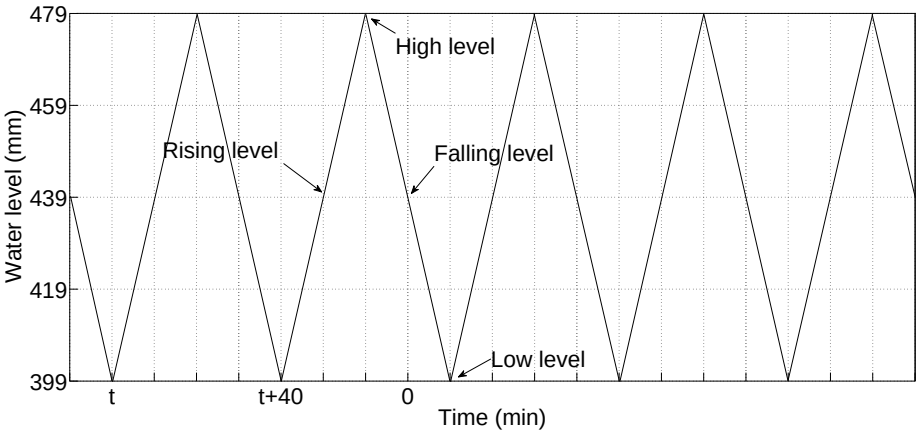

Figure 3.2 Transient water levels caused by fluctuations. The fluctuation period is 40 minutes. The arrows indicate different water level stages.

Table 3.1. Geometry, hydrogeological, and transport parameters used in the experimental study of Zhang et al. [2002].

Parameter	Variable	Value
Domain length, m	L	1.650
Domain height, m	H	0.6
Domain width, m	W	0.1
Beach slope	φ	1 : 6.12
Horizontal saturated hydraulic conductivity, m s-1	K_h	4×10^{-3}
Vertical saturated hydraulic conductivity, m s-1	K_v	4×10^{-3}
Longitudinal dispersivity, m	α_L	6.49×10^{-4}
Transverse dispersivity, m	α_T	1×10^{-4}
Total effective porosity	θ_e	0.37
Mean seawater level, m	h_s	0.463
Constant freshwater level, m	h_f	0.439
Seawater density, kg m^{-3}	ρ_s	1025
Freshwater density, kg m^{-3}	ρ_f	1000
Salt concentration, kg m^{-3}	C_s	35

enforced at the seaward boundary.

The simulation domain is discretized into 9900 cells in order to satisfy the accuracy and convergence requirement for grid spacing in terms of the local Péclet number [Voss and Souza, 1987; Zhang et al., 2001; Volker et al., 2002; Brovelli et al., 2007]. The entire model domain is divided into two zones: a surface water zone and an aquifer zone. To simplify the numerical simulation, a large hydraulic conductivity of $0.4ms^{-1}$, i.e., 100 times of the saturated aquifer hydraulic conductivity, a constant porosity of 1, and a constant saltwater concentration of 35 kg m^{-3} are assigned to all the cells in free seawater area [Winter, 1976; Anderson et al., 2002; Mao et al., 2006; Brovelli et al., 2007; Robinson et al., 2007]. In addition, to reproduce the flat surface of the sea, a horizontal strip of cells with a variable-head boundary condition is added onto the seawater surface [Brovelli et al., 2007]. Simulations start from steady-state conditions generated by using the mean seawater level and the mean freshwater level. The simulation duration for each case is fifty periods of the corresponding triangular functions, a sufficiently long period for the scaled tank models to reach a dynamic equilibrium state of the concentration distribution, i.e., the tolerance of the maximum concentration variation is satisfied when doubling the computation periods.

3.2.3 A Field Scale Model and Numerical Implementation

For the field-scale case, we consider a 2D model domain that is 200m long and 35m high with a beach slope 1: 10. The aquifer was assumed to be isotropic and homogeneous with K_f = $20md^{-1}$, $n_e = 0.4$, longitudinal dispersivity α_L = 0.5m and

transverse dispersivity α_T = 0.05m. Hydraulic conductivity of 1000md^{-1}, $n_e = 1$ and constant salt concentration of 35kgm^{-3} are assigned to the cells in free seawater area so that the entire domain can be solved by SEAWAT. The mean seawater level and the mean freshwater level are 28 m and 29 m, respectively. For field-scale applications, transient effects introduced by periodic tidal motion on the movement of the mixing zone may not be as effective as those introduced by the freshwater-table fluctuations because (1) tidal motion has a much shorter period than freshwater-table fluctuations; (2) the amplitude of freshwater-table fluctuations can be much larger than that of tidal motion because of seasonal precipitation and temperature patterns; and (3) the effects of the freshwater-table change may be enlarged to 40 times on the freshwater-seawater interface according to the Ghyben-Herzberg law based on potential equilibrium [Bear, 1972]. In this research, we impose a triangular, periodic head variation with a period of one year and an amplitude of 1 m at the landward boundary, while a constant seawater level of 28 m is specified at the seaward boundary. For the numerical simulation, a mesh resolution of 0.5 m was adopted, yielding 28000 cells. This discretization results in a satisfactory Pe of 1. The dynamic equilibrium state of the concentration distribution is found after 100 periods, i.e., 100 years.

3.3 Results of the Tank Model

3.3.1 Steady-State Condition

Steady-state cases are first simulated to serve as control cases, which neglect both mass transfer and transient conditions introduced by tidal motion and freshwater-table

fluctuations. By assuming a constant seawater level of 0.439 m and a constant freshwater level of 0.463 m, a SEAWAT simulation was first run for steady-state conditions without considering the mass transfer effect. Figure 3.3 shows the mixing zone, where the contour lines delineate the normalized concentrations 0.1, 0.5, and 0.9. Rather than a sharp interface, a narrow mixing zone is formed due to density gradient and local dispersion. The salinity distribution simulated in our study matches well experimental [Zhang et al., 2002] and numerical results [Zhang et al., 2001; Brovelli et al., 2007] previously obtained based on the same scaled tank model. We also evaluate the mixing zone by including mass transfer but still neglecting transient effects. Similar to the observation by Langevin et al. [2003], the resulting mixing zone is almost the same as the one neglecting mass transfer. Thus, for steady-state analyses, mass transfer does not make significant contributions in altering salinity distributions. In fact, by forcing the transient terms in Eq. (3.2) to be zero, the transport model reduces to the case without mass transfer. That is, the steady-state salinity distributions will become identical for cases with and without mass transfer, although the timescales to reach the steady state may be different.

3.3.2 Transient and Mass Transfer Effects

Figure 3.4 shows the mixing zones with the consideration of seawater level oscillations but neglecting mass transfer. A wider mixing zone, particularly at the toe, is observed compared with the mixing zone shown in Figure 3.3. Furthermore, due to the seawater level oscillations the interface is pushed seaward. This phenomenon is

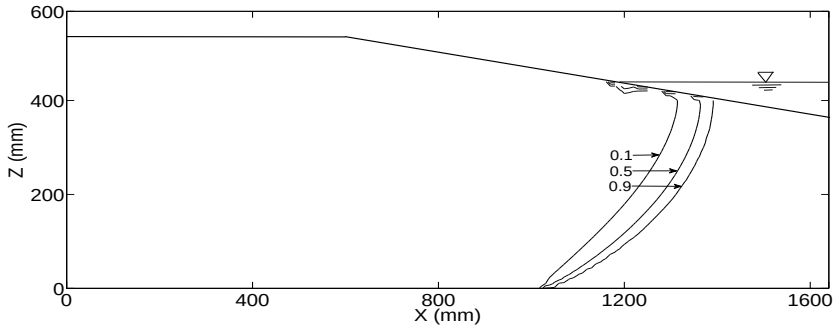

Figure 3.3 The variable-density mixing zone between the freshwater and seawater for steady-state conditions in the absence of water level fluctuation and kinetic mass transfer (tank scale model). The solid lines are the contour lines of normalized salt concentrations.

consistent with the simulation results obtained by Robinson et al. [2007], who conducted a numerical study on a field-scale domain to investigate the effect of tidal forcing on a subterranean estuary. In addition, their results show that the interface is pushed more seaward with a larger amplitude tide. Seawater-level fluctuation forces the seawater back and forth and, thus, the equilibrium state shown in Figure 3.3 is disturbed, yielding a transient velocity field and a fluctuated concentration distribution, which result in enhanced mixing and a wider mixing zone due to hydrodynamic dispersion. This phenomenon has been demonstrated by the laboratory experiment of Zhang et al. [2002]. Ataie-Ashtiani et al. [1999], however, observed the exact opposite effects that that a larger tidal amplitude may force the seawater to intrude further inland. The difference may be resulted from the assumption of an unsaturated zone above the groundwater table given in Ataie-Ashtiani et al.'s analysis.

However, previous studies including numerical work conducted by Robinson et al. [2006, 2007] and Ataie-Ashtiani et al. [1999] and field experiments by Cartwright et al. [2004] indicate that the mixing zone of the saltwater wedge does not fluctuate over the course of a tidal cycle because the forcing timescale is too short. Hence, the movement of the mixing zone in our study can be attributed to the small tank scale and relatively large timescale of seawater level fluctuation. In reality, however, the mixing zone may be forced landward by a combination of increasing tidal range, wave height and infiltration of wave run-up [Cartwright and Nielsen, 2001a,b]. Once the wave forcing is decreased the contour gradually moved seaward [Cartwright and Nielsen, 2003]. Therefore, the movement of the mixing zone of our scaled tank model may be

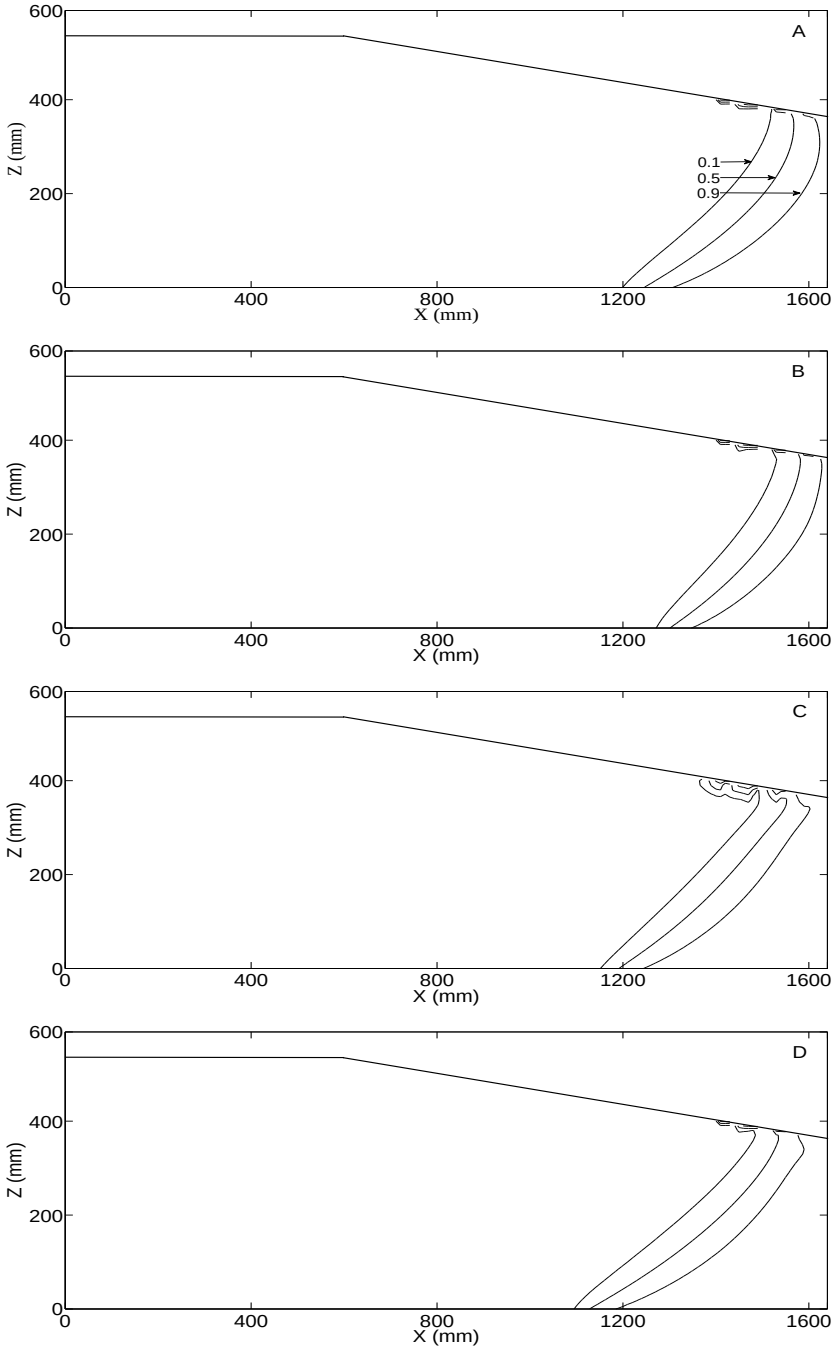

Figure 3.4 Mixing zones at different seawater level stages within a fluctuation period with the consideration of seawater level fluctuation alone (tank scale model). (A) low level, (B) rising level, (C) high level, and (D) falling level.

regarded as a result of complex effects from the seaward boundary.

Figure 3.4 also shows that the position of the mixing zone varies at different seawater level stages, i.e., the hydraulic gradient determines the position of the mixing zone. Thus, we can only define a dynamic-equilibrium state instead of a steady state for the transient case. As mentioned before, dynamic equilibrium is defined as the state where the mixing-zone position has no significant variations by doubling the simulation duration. In addition, although the position of the mixing zone varies, the width does not change noticeably over the course of one periodic cycle.

Figure 3.5 shows the mixing zones with the consideration of both mass transfer effects and seawater level oscillations, where both mobile porosity and immobile porosity are set to be 0.185 and the first-order mass transfer rate coefficient is 0.025 min^{-1}. Figure 3.5 clearly shows that the mass transfer effect leads to significantly wider mixing zones at all stages of the seawater level compared with those shown in Figure 3.4. In particular, it is more pronounced at the low and falling water level stages. As already mentioned, in the absence of seawater level oscillations, i.e., the mixing zone is stationary, mass transfer has no effect on the steady-state salinity distribution because there is no concentration gradient between the mobile and immobile domains and Eq. (3.2) can be simplified to the classical advection-dispersion equation, although the timescale to reach the steady state may be changed. However, in transient cases, the mixing zone is pushed back and forth by complex effects from the seaward boundary, resulting in non-equilibrium in the salt concentrations in the mobile and immobile domains and an enhanced mass exchange between them. The immobile domain here

essentially acts as a sink or source for solutes in the mobile zone, determined by the direction of concentration gradient between the two domains. Specifically, salts in the mobile domain diffuse into the immobile domain as the mixing zone is dragged inland, while salts are released from the immobile domain to the mobile domain driven by reversed concentration gradients when the mixing zone is towed toward the sea. The disturbed concentration and density gradient field leads to enhanced mixing and a wider mixing zone than would occur in the absence of mass transfer. Moreover, Figure 3.5 shows that the combination of mass transfer and seawater level fluctuations has greater influences on the high concentration contour lines (see the contour lines of normalized concentration 0.9), which become closer to the seaward boundary. Certainly, if an increasing amplitude of seawater level fluctuation is considered, which means a broader movement of the transition zone is obtained, one may expect to observe an expanding transition zone.

Freshwater-level fluctuation is observed in many areas, which has been found as a main reason leading to the movement of the mixing zone [Michael et al., 2005]. Figure 3.6 shows the mixing zones under periodic oscillations of the freshwater level without mass transfer effects. Like the effect from seawater level fluctuations shown above, the mixing zone is pushed seaward, and wider mixing zones are formed. However, the mixing zone moves within a broader range due to a larger period of the freshwater-level fluctuation. The width of the mixing zone caused by freshwater variation is expected to increase when the mass transfer effect is taken into account. Figure 3.7 exhibits the mixing zones with the consideration of both mass transfer and freshwater-level

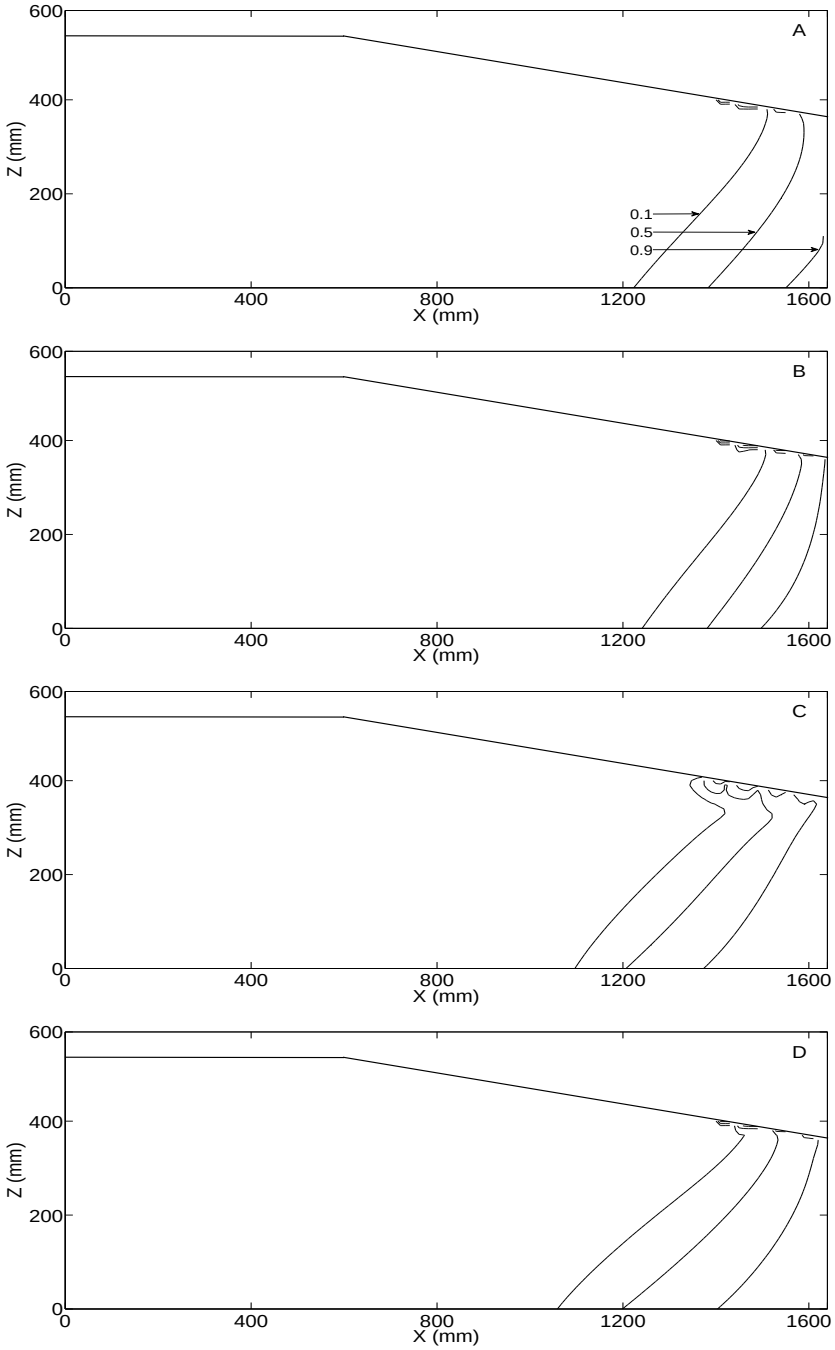

Figure 3.5 Mixing zones at different seawater level stages within a fluctuation period with the consideration of both seawater level fluctuation and kinetic mass transfer (tank scale model). (A) low level, (B) rising level, (C) high level, and (D) falling level.

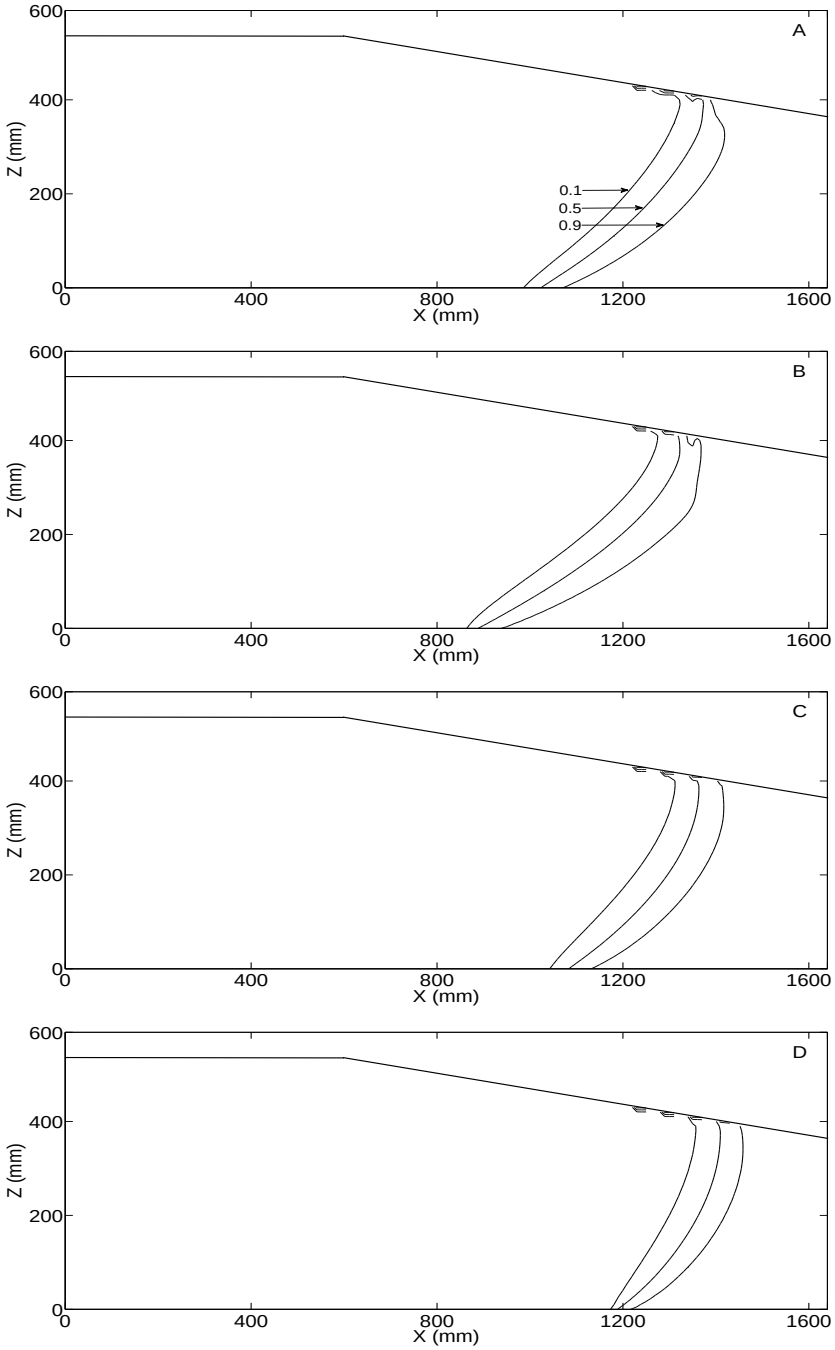

Figure 3.6 Mixing zones at different freshwater level stages within a fluctuation period with the consideration of freshwater level fluctuation alone (tank scale model). (A) low level, (B) rising level, (C) high level, and (D) falling level.

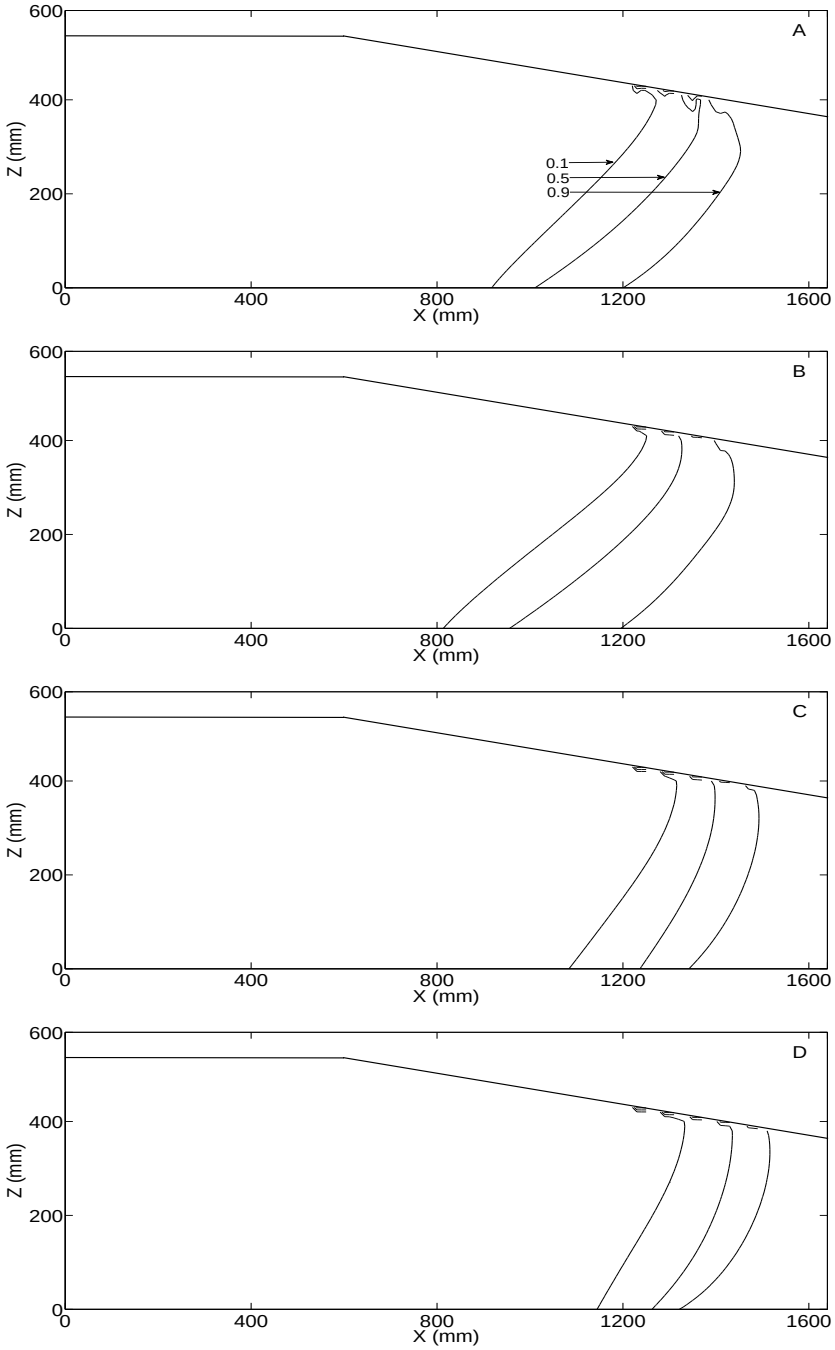

Figure 3.7 Mixing zones at different freshwater level stages within a fluctuation period with the consideration of both freshwater level fluctuation and kinetic mass transfer (tank scale model). (A) low level, (B) rising level, (C) high level, and (D) falling level.

oscillations, where both mobile and immobile porosities are set to be 0.185 and the first-order mass transfer rate coefficient is 0.0125 min^{-1}. Likewise, the introduced mass transfer effect significantly increases the width of the mixing zone, especially at the rising level stages. Similarly, one may expect that a larger fluctuation amplitude will lead to a wider mixing zone.

3.3.3 Sensitivity Analysis

Parameters of kinetic mass transfer, including mobile and immobile porosity and the first-order rate constant, will be varied in order to investigate the effects of kinetic mass transfer. In order to interpret the results concisely and produce a meaningful generalization, the following dimensionless variables are defined:

$$\tau = \xi^{-1} / T_f \tag{3.4}$$

$$\beta = \theta_{im} / \theta_m \tag{3.5}$$

$$w = W / W_{ss} \tag{3.6}$$

where T_f is the water level fluctuation period; ξ^{-1} represents a characteristic mass transfer time in the immobile domain; β is known as the capacity ratio; W_{ss} is the mixing-zone width under steady-state condition; and W is the width of the mixing zone under the coupled effect of mass transfer and water-level fluctuation. For simplicity, W is represented by the horizontal distance between concentration contour lines of 0.1 and 0.9. Here, we choose the width of the mixing zone at the height of 200 mm at the rising

tidal moment to calculate W. Similar results will be obtained for the width of the mixing zone at other heights and tidal moments. By assuming a constant total porosity for the mobile and immobile domain, the effects of mass transfer parameters and water level fluctuations on the dimensionless width of the mixing zone, *w*, can be investigated by varying the dimensionless variables, τ and β.

Figure 3.8 shows the simulated results for the sensitivity analysis for the tank model. The width of the mixing zones formed by varying the freshwater level is somewhat wider than that by seawater-level fluctuation since the period of the former is assumed larger than the latter. For both cases, with a given mean retention time, i.e., a constant first-order mass transfer rate coefficient, the width of the mixing zone increases with the capacity ratio, indicating that a larger immobile domain may cause a wider mixing zone. With a given capacity ratio, i.e., a constant porosity of the immobile domain, the width of the mixing zone is maximized when the retention timescale of the mass transfer and the period of the water-level fluctuation become comparable, i.e., at the same order of magnitude. In such cases, the effects of the capacity ratio will also be maximized. In addition, the left and right tails of the curves shown in Figure 3.8 (a) and (b) indicate that the mass transfer may not have significant impacts on widening the mixing zone when there is a several orders of magnitude difference between the retention timescale and the water-level fluctuation period. In fact, both the limiting cases of very small and large mass transfer rate coefficients can be simplified to a classical advective-dispersive transport problem. For a small mass transfer rate coefficient, it is equivalent to the transport problem in a medium with a smaller total porosity, i.e.,

practically no mass transfer occurs within a period. For a large mass transfer rate coefficient, the kinetic mass transfer may be considered as an instantaneous process, which simplifies the two-domain model into a one-domain model with a retardation factor, $1+\beta$. Thus, for both limiting cases, the width of the mixing zone will approach the dynamic equilibrium state in the absence of mass transfer. In our tank model, the mixing zone is significantly widened for τ between 0.1 and 100, and the width reaches maximum for τ to be about 1, i.e., ξ^{-1} is equal to T_f. For example, the width of the mixing zone is approximately 3.7 times as wide as that under steady state condition for the freshwater-level fluctuation case with $\beta = 1$ and $\tau = 1$ (see Figure 3.8(b)). If other parameters are kept constant, we may expect that the width of the mixing zone will become much larger for a higher β.

3.4 Field Scale Modeling Results

The field-scale model described in section 2 corroborates the results obtained based on the tank model. Figure 3.9 shows the mixing zone under steady-state condition, where a narrow mixing zone is generated. With the introduction of freshwater-level fluctuations, the steady-state system is disturbed and the mixing zone is slightly widen (see Figure 3.10). Mass transfer effect is then introduced, where mobile and immobile porosities both are set to be 0.2, namely, $\beta = 1$. Three mass transfer coefficients including 0.027 d^{-1}, 0.0027 $d^{-1}$and 0.00027 $d^{-1}$are employed, which correspond to dimensionless variable τ as 0.1, 1, and 10, respectively. The corresponding mixing zones at the rising water level stage for these three cases are exhibited in Figure 3.11,

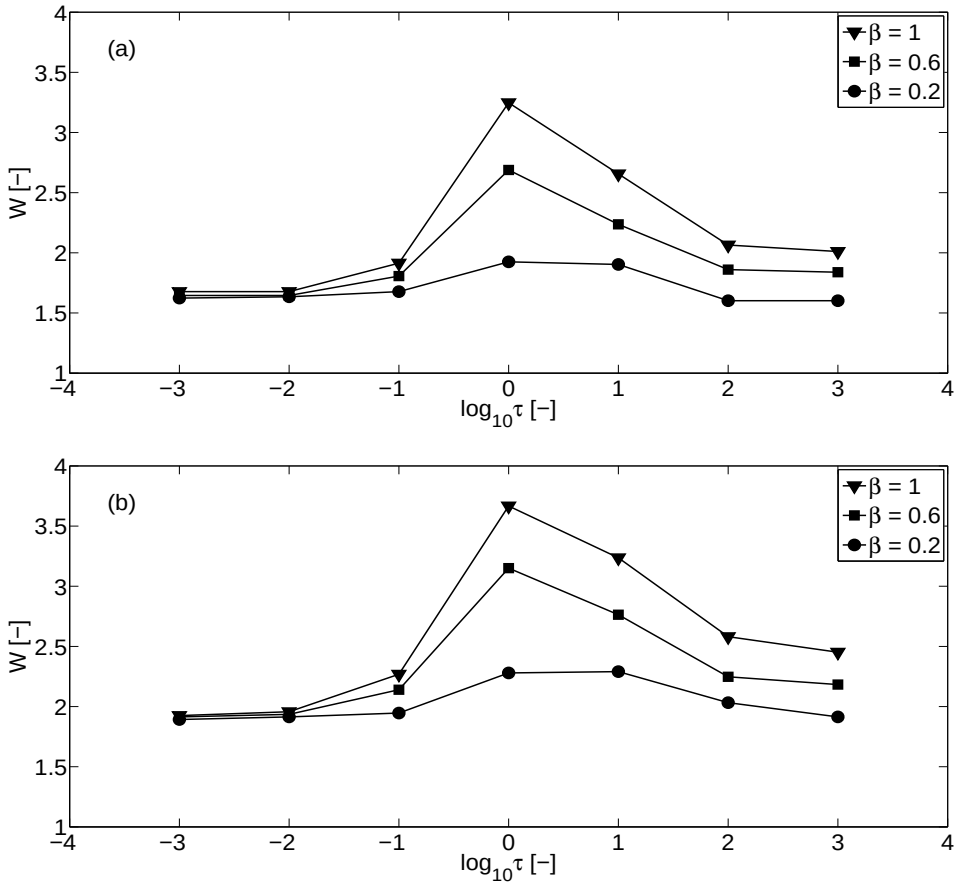

Figure 3.8 Sensitivity analysis for the effects of combining mass transfer and movement of the mixing zone which is caused by (a) seawater level fluctuation and (b) freshwater level fluctuation.

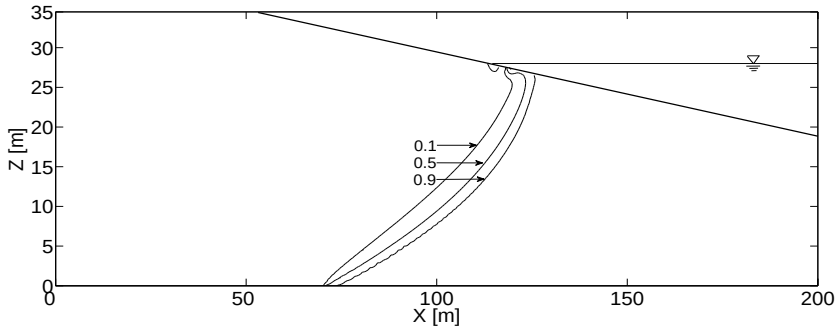

Figure 3.9 The variable-density mixing zone between the freshwater and seawater for steady-state conditions in the absence of water level fluctuation and kinetic mass transfer (field scale model). The solid lines are the contour lines of normalized salt concentrations.

which clearly shows wider mixing zones than those shown in Figure 3.10. In particular, the mixing-zone width in the case with $\tau = 1$ is maximal, consistent to the result found in the tank model.

In the absence of mass transfer, dispersivities, particularly transverse dispersivity, is considered to be the primary factor affecting the width of the mixing zone [Ataie-Ashtiani et al., 1999; Dagan, 2006]. In order to reproduce a wide mixing zone in a real case, the common method is to assume a large, perhaps unwarranted, value of dispersivities [Dagan, 2006]. In this section, we briefly compare the effects of dispersivities and mass transfer on the mixing-zone width. In addition to the dispersivities assumed in the cases discussed above, two more groups of longitudinal and transverse dispersitivies are adopted in the field-scale model: α_L = 2.5 m and α_T = 0.25 m, and α_L = 0.1 m and α_T = 0.01 m.

Figure 3.12 shows the mixing zones at the rising freshwater level stage with the consideration of the freshwater-level fluctuation alone. It is obvious that larger dispersivities yield a wider mixing zone. However, the maximum mixing zone shown in Figure 3.12(C) is still not as wide as that in Figure 3.11(B), although both longitudinal and transverse dispersivities are twenty-five times of those in the previous case. Thus, in order to generate a wider mixing zone, larger dispersivities must be accepted.

Figure 3.13 shows the results by further introducing mass transfer with $\beta = 1$ and $\tau = 1$ into the three cases with different dispersivities. It is shown that all mixing zones are significantly widened compared with those shown in Figure 3.12. Furthermore, with

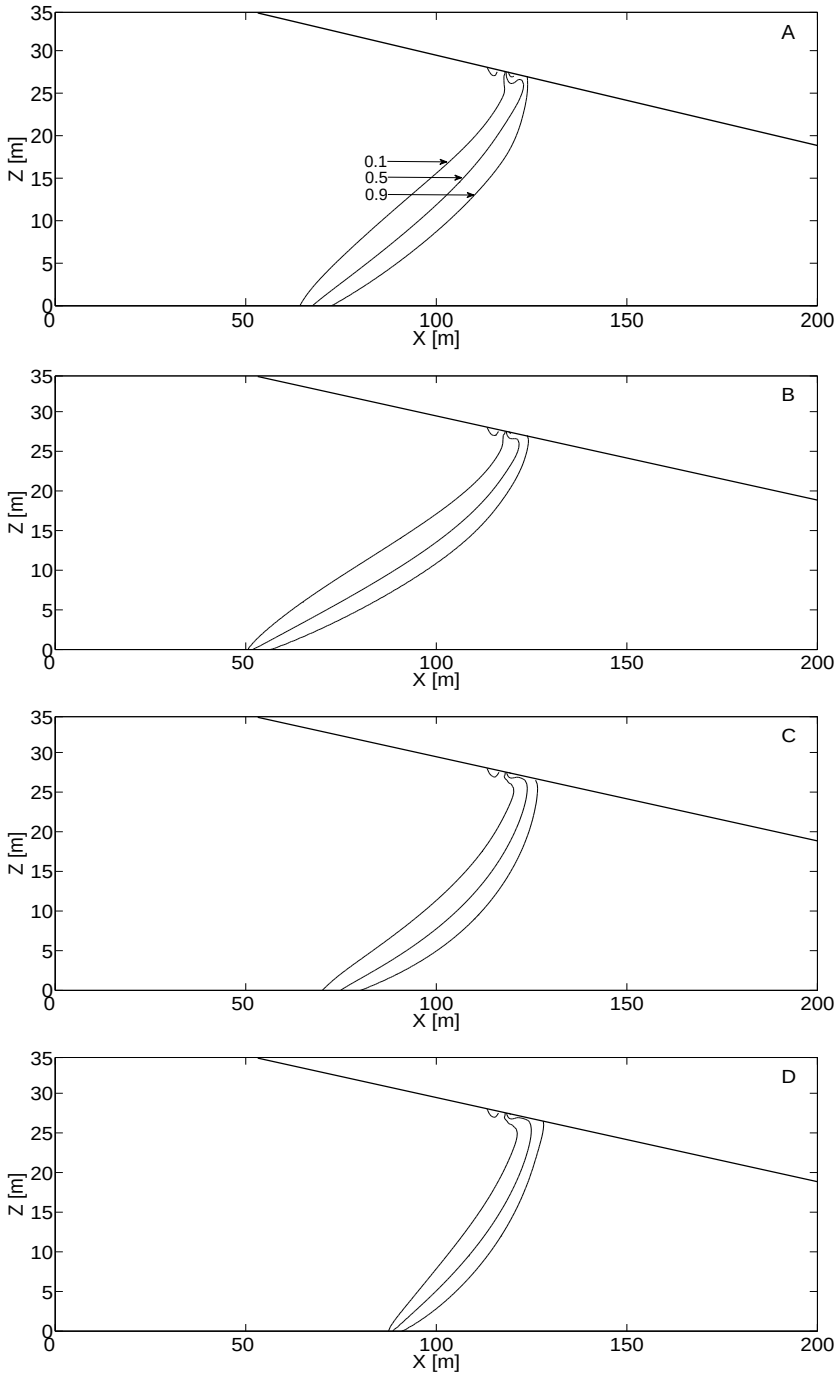

Figure 3.10 Mixing zones at different freshwater level stages within a fluctuation period with the consideration of freshwater level fluctuation alone (field scale model). (A) low level, (B) rising level, (C) high level, and (D) falling level.

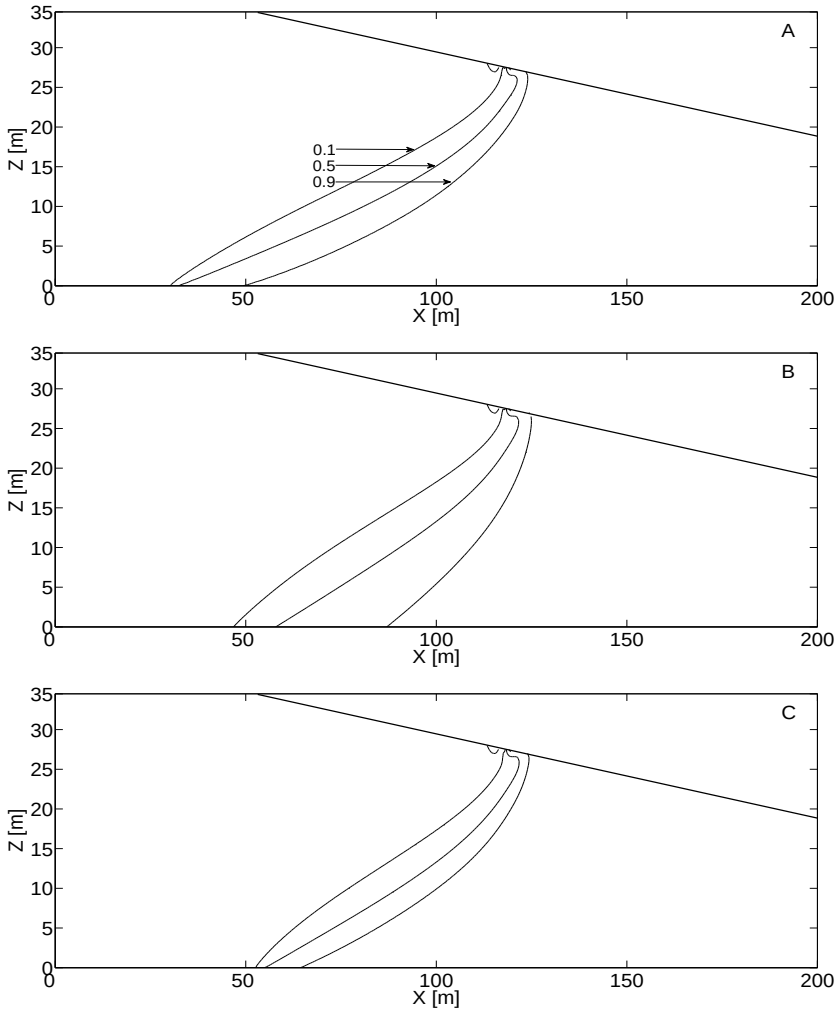

Figure 3.11 Mixing zones at the rising freshwater level stage with the consideration of both freshwater level fluctuation and kinetic mass transfer (field scale model), in which (A) $\tau = 10$, (B) $\tau = 1$, and (C) $\tau = 0.1$.

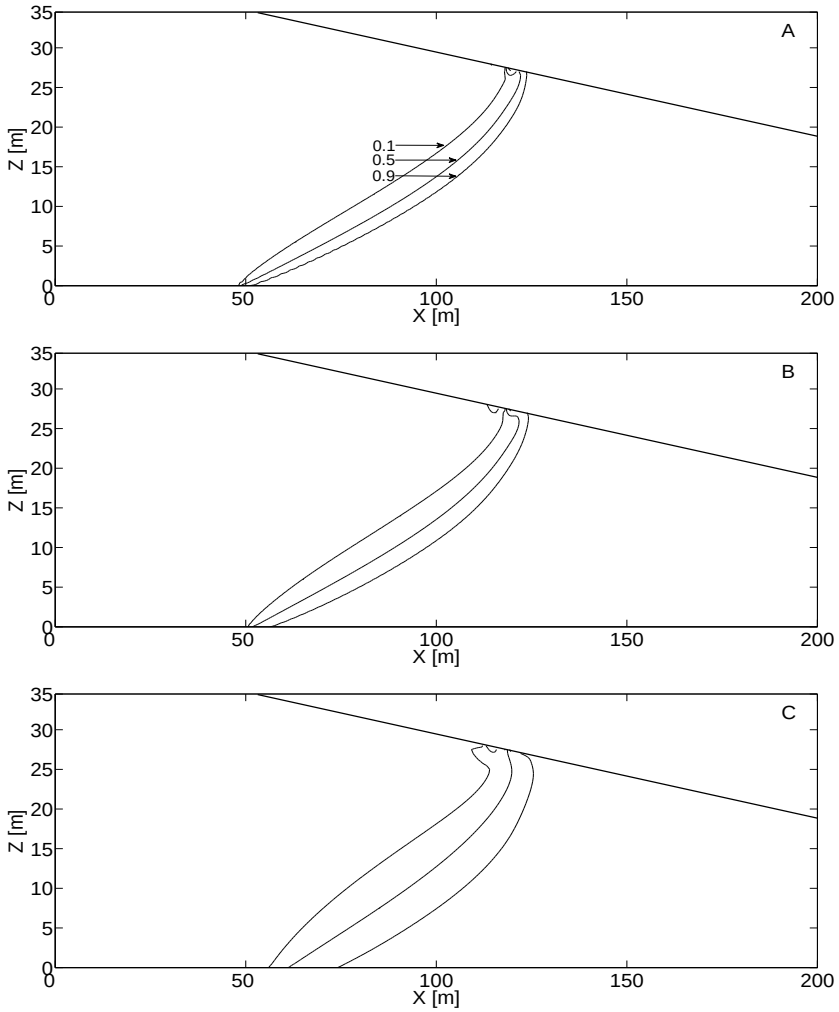

Figure 3.12 Mixing zones at the rising freshwater level stage with the consideration of the freshwater level fluctuation alone (field scale model), in which (A) α_L = 0.1 m and α_T = 0.01 m, (B) α_L = 0.5 m and α_T = 0.05 m, and (C) α_L = 2.5 m and α_T = 0.25 m.

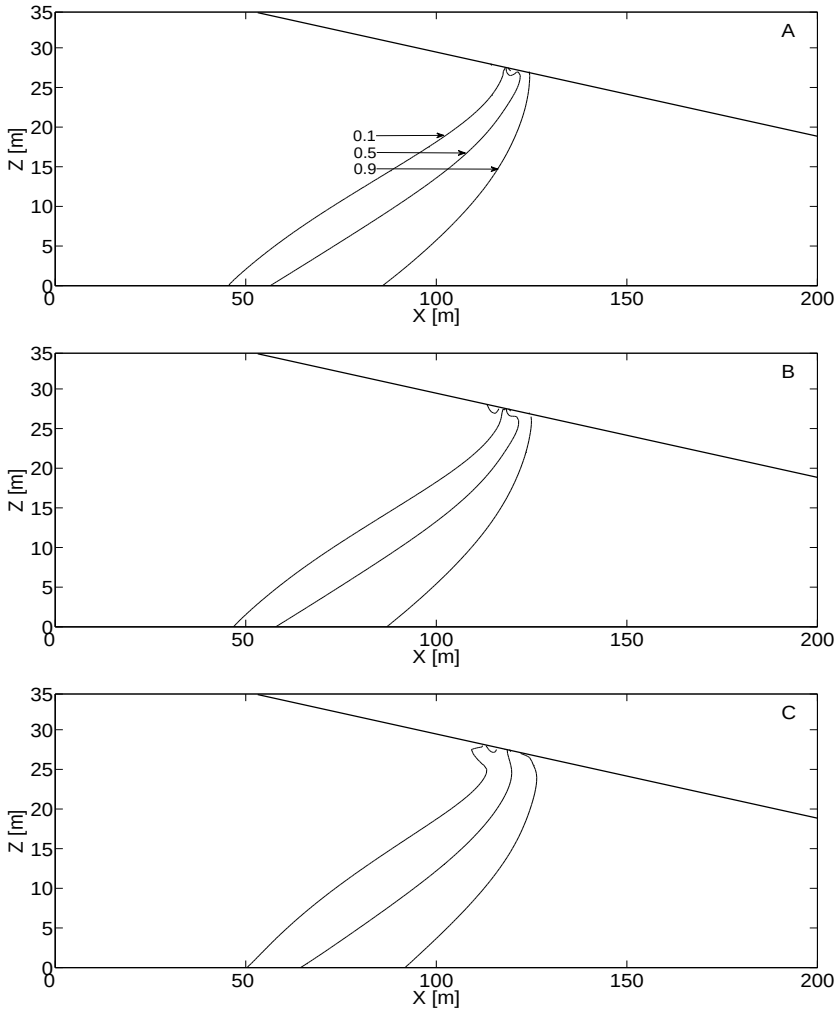

Figure 3.13 Mixing zones at the rising freshwater level stage with the consideration of both freshwater level fluctuation and kinetic mass transfer (field scale model), in which (A) α_L = 0.1 m and α_T = 0.01 m, (B) α_L = 0.5 m and α_T = 0.05 m, and (C) α_L = 2.5 m and α_T = 0.25 m.

the mass transfer effect, all the mixing-zone widths become similar, although different dispersivities are used. The mass transfer effect dominates the mixing-zone width change. Therefore, in our cases, the effect of kinetic mass transfer is more pronounced than the dispersivities on widening the mixing zone.

3.5 Conclusions

Wide mixing zones have been observed in many aquifers all over the world. However, no agreement has been reached in terms of the responsible mechanisms. In the present work, we propose the hypothesis that kinetic mass transfer combined with movement of mixing zones may significantly widen mixing zones in coastal aquifers. The hypothesis is tested by conducting numerical simulations based on the variable-density groundwater model for both a scaled-tank model and a field-scale model. The movement of the mixing zone may be caused by complex effects from both the seaward boundary (e.g., wave run-up) and the landward boundary (e.g., seasonal fluctuation of fresh groundwater head). In our simulations, the movement of the mixing zone is created by assuming triangular, periodic functions for water-level oscillations at the seawater and landward boundaries, respectively. In the absence of kinetic mass transfer, the created transient effects slightly widen the mixing zone compared with that in steady state. With the introduction of kinetic mass transfer, mixing zones are significantly widened at all stages within the period.

Furthermore, sensitivity analyses of dimensionless variables based on the tank model yield the following observations: (1) the mixing zone may be significantly

widened by the mass transfer effect regardless of which boundary causes the movement of the mixing zone; and (2) a larger capacity ratio of mass transfer leads to a wider mixing zone, and the maximum width may be reached when the mean retention timescale in the immobile domain and the water-level fluctuation period become comparable. Our simulations also investigate the effects of dispersivities on the mixing-zone development. Larger dispersivities always yield wider mixing zones. However, dispersivities may not be as effective as kinetic mass transfer on widening the mixing zone in our cases. More importantly, larger dispersitivies and mass transfer are based on different physical interpretations of the transport processes and formation properties. Large, perhaps unwarranted dispersitivities are often considered as the misrepresentation of aquifer heterogeneities [Dagan, 2006]. On the other hand, as is well-known, no natural geological media are truly homogenous, and mass transfer occurs in almost all fractured and porous heterogeneous media over various scales ranging from pore scale to field scale. Our findings provide a plausible explanation for wide mixing zones in coastal aquifers which may consist of low-permeability zones, dead-end pores, porous particles, aggregates, and rock matrix between fractures. In such aquifers, the effects of kinetic mass transfer and the movement of mixing zone caused by tidal motion, freshwater-table fluctuations, groundwater withdrawal, etc., must be considered to evaluate the growth and decay of the variable-density mixing zone. Certainly, other parameters, such as the amplitude of the periodic stimulation, the hydraulic conductivity, the rate of freshwater flow, the heterogeneity of the geological formations, may influence the growth and decay of the mixing zone. Research of these mechanisms on mixing-zone development is continuing.

CHAPTER 4

DYNAMICS OF FRESHWATER-SEAWATER MIXING-ZONE DEVELOPMENT IN DUAL-DOMAIN FORMATIONS

4.1 Introduction

The mixing zone developed at the freshwater-seawater interface is one of the most important features in complex coastal hydrogeologic systems [e.g., Cooper et al., 1964, Robinson et al., 2007a]. Across the mixing zone, the salt concentration and fluid density vary between those of freshwater and seawater. The density gradient within the mixing zone causes the rise of diluted saltwater, overlaying seawater, and results in flow circulation as the seawater moves towards the mixing zone to replace the diluted saltwater. Understanding the dynamics of mixing-zone development under various hydrogeologic conditions is essential for designing effective and sustainable management strategies of groundwater resources in coastal and offshore environments.

The present research aims to numerically investigate the dynamic process of mixing-zone development in a dual-domain subsurface medium. Our previous study has found that kinetic mass transfer between relatively mobile fluids and fluids in stagnant pores combined with periodic movement of the mixing zone may significantly enhance mixing and result in a much thicker mixing zone, as shown in Figure 4.1 [Lu et al., 2009]. Kinetic mass transfer occurs in almost all fractured and porous media over various scales ranging from pore scale to field scale, and has significant implications for

coastal groundwater management. For example, the aquifer storage and recovery (ASR) strategy may have a low freshwater recovery ratio in a dual-domain coastal aquifer due to the mobilization of solutes initially residing in immobile domains [Eastwood and Stanfield, 2001; Culkin et al., 2008]. Prior to this research, thick mixing zones were usually characterized by large dispersion coefficients or assuming highly heterogeneous hydraulic conductivity fields, both of which may not be realistic [Dagan, 2003]. In addition, our previous numerical results have shown that the recharge and tidal fluctuations may only slightly increase the thickness of the mixing zone in the absence of kinetic mass transfer [Lu et al., 2009]. In this chapter, we conduct numerical experiments to illustrate the dynamic process of mixing-zone enhancement for a periodically moving mixing zone in the presence of kinetic mass transfer. With the consideration of mass transfer and freshwater level fluctuations, the thickness of the mixing zone may vary significantly within a period, which may have important implications for coastal geochemical processes. Specifically, the major questions considered here are: How does the spatial and temporal distribution of a mixing zone vary in response to variations of hydrogeologic conditions and how are such variations different from those by assuming large dispersion coefficients?

4.2 Numerical Method

A typical two-dimensional domain (see Figure 4.1) is set up to represent a cross-shore transect of an unconfined coastal aquifer with a length of 200m, a thickness of 35m, and a beach slope of 0.1, similar to previously reported numerical experiments [Michael et al., 2005; Robinson et al., 2006, 2007b; Lu et al., 2009]. For this domain, a

base model is first built by defining the following hydrogeologic conditions. The aquifer is isotropic and homogeneous with both mobile and immobile porosities being 0.2, representing a unitary capacity ratio of mass transfer, i.e., the ratio between the immobile and mobile porosity. The value of the hydraulic conductivity K is 30 m/d. The longitudinal and transverse dispersivity are 0.5 m and 0.05 m, respectively. Seasonal freshwater level fluctuations are imposed at the landward vertical boundary by defining a triangular, periodic hydraulic head variation with the amplitude A = 1m and the period T = 360 d. The use of the triangular function instead of a sinusoid function is to minimize the pressure periods required to reproduce the periodic function [Zhang et al., 2001; Brovelli et al., 2007]. The first-order mass transfer rate coefficient is assumed to be 0.0028 d^{-1}, which implies a retention time scale in the immobile domain, defined as the reciprocal of the first-order mass transfer rate coefficient, equal to the period of freshwater fluctuations. At the seaward vertical boundary, constant hydraulic head and salt concentration are assigned because tidal activities have a much shorter period and may hardly cause the movement of the mixing zone in a large-scale simulation [Cartwright et al., 2004; Michael et al., 2005]. The mean hydraulic gradient between the landward boundary and coastline is 0.0067. The upper boundary in the aquifer is phreatic surface with negligible groundwater recharge, and the bottom is a no-flow boundary.

A miscible fluid model with coupled flow and transport processes is applied to simulate the mixing-zone development in a dual-domain coastal aquifer. Transport

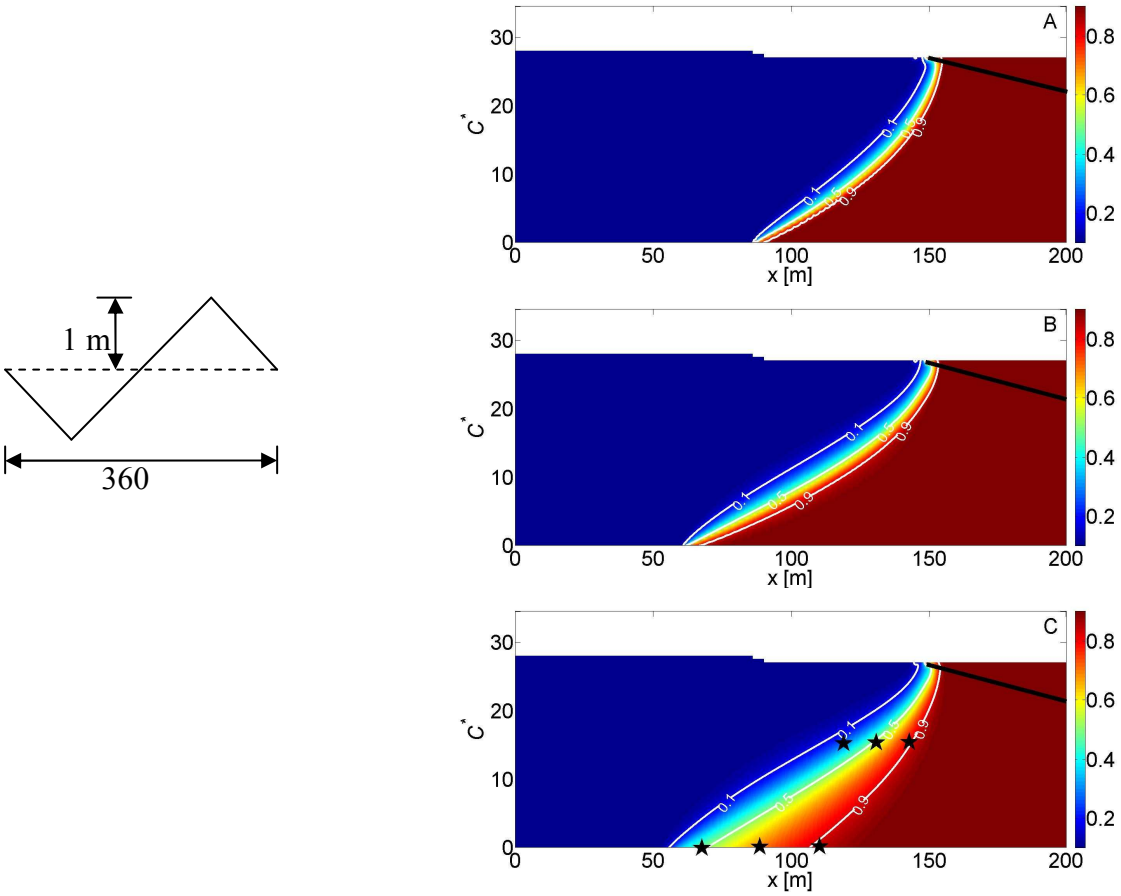

Figure 4.1 A numerical simulation of freshwater-seawater mixing zone in an unconfined aquifer. (A) steady-state normalized concentration distribution in the absence of kinetic mass transfer; (B) normalized concentration distribution of a transient simulation without kinetic mass transfer; and (C) normalized concentration distribution of a transient simulation with kinetic mass transfer at the time event when the freshwater boundary (left boundary) equal the mean freshwater head. The thick black lines represent the coastal beach with a slope of 0.1. The mixing zones are characterized by three concentration contour lines normalized by the seawater salt concentration: 0.1, 0.5 and 0.9. The stars in (C) represent six observation points at the depths of z = 0 and 15 m.

processes include advection, dispersion, and a first-order kinetic mass transfer between the mobile and immobile domain. Flow and transport is coupled by a linear relationship between density and concentration in the mobile domain. The density-dependent groundwater flow code SEAWAT-2000 [Langevin et al., 2003] is used to simulate the groundwater flow and salt transport problem described above. The entire domain is divided into two zones: an ocean zone and an aquifer zone, which are separated by the slanted beach. A high hydraulic conductivity (10^3 m/d), an effective porosity $n_e = 1$, and a constant saltwater concentration of 35 kg/m^3 are assigned to the ocean zone. Furthermore, a horizontal strip of cells with the same boundary conditions at the seaward vertical boundary are added on the top of the ocean surface to reproduce the flat surface of the ocean [Brovelli et al., 2007; Robinson et al., 2007b]. The entire domain is discretized into a uniform grid with a cell size of 0.5 m$\times$0.5 m, yielding 28000 cells in total. This grid spacing corresponds to a local Peclet number of 1.

The following numerical experiments are conducted: (1) steady-state simulations for the base model with and without mass transfer; (2) transient simulations for the base model with periodic freshwater level fluctuations; and (3) transient simulations by varying a series of parameters, including hydraulic conductivity, dispersion coefficients, amplitude of freshwater fluctuations, and mass transfer coefficients. All transient simulations start from steady-state simulations, and terminate after the salt concentration distributions reaching a dynamic equilibrium state, i.e., the tolerance of the maximum concentration variation is satisfied when doubling the computation periods. For

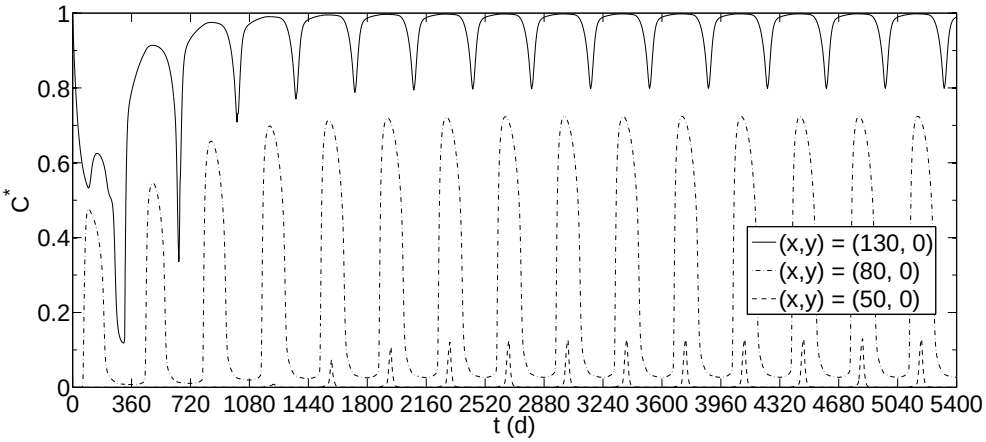

Figure 4.2. Breakthrough curves for three locations of (50, 0), (80, 0) and (130, 0).

simplicity, we use three normalized salt concentration contour lines, 0.1, 0.5 and 0.9, to describe the movement and distribution of the mixing zone.

Simulations in this study are computationally intensive tasks. Hence, all simulations start from steady-state conditions generated by assuming the mean freshwater level. Freshwater level fluctuations accompanying mass transfer effects are then introduced. The simulation time is required to be long enough to obtain a dynamic equilibrium state for the flow filed, where the dynamic equilibrium state is reached when the variation of the concentration profile with evolution time no longer change in following periods. Figure 4.2 shows the breakthrough curves for three locations of (50, 0), (80, 0) and (130, 0). These locations are selected since their normalized concentrations represents low, medium and high values in the mixing zone under the dynamic equilibrium state. It is found that the higher concentration contour reaches dynamic equilibrium state more quickly than lower one does. After 2520 d, namely 7 periods, the whole system approaches the dynamic equilibrium state. Here, the simulation results after 10 periods are employed for later analysis of the base model.

4.3 Results and Discussion

Mixing of freshwater and seawater is enhanced primarily due to the unsynchronized behavior of concentrations in the mobile and immobile domain. Two mixing zones may be defined in a dual-domain medium: one in the mobile domain, and the other in the immobile domain. There is an overlap between these two mixing zones, but they do not exactly coincide. The non-equilibrium concentrations in the mobile and immobile

domain create the driving force for mass transfer and enhance mixing.

Figure 4.3 illustrates this process within one period (see the period in Figure 4.1) by analyzing the temporal profiles of concentrations at six points at different elevation, (120, 15), (130, 15), (140,15), (70, 0), (90, 0), and (110, 0), in which the first three are approximately located at the middle depth of the water level, and the remaining points are located at the bottom of the aquifer where the mixing enhancement is the most significant (see Figure 4.1). At the beginning of the period, non-equilibrium concentrations in the mobile and immobile domains drive mass transfer from the immobile domain to the mobile domain, causing slowly increasing mobile concentrations and slowly decreasing immobile concentrations. With the decrease of the freshwater level, significant landward movement of the mixing zone causes a fast increasing concentration in the mobile domain, which results in a fast increasing concentration in the immobile domain due to enhanced mass transfer driving forces. Maximum concentrations in the mobile domain occur in the second quarter. After that, the mobile concentration gradually decreases as a result of mass transfer, while the immobile concentration keeps rising until these two become equal. When the hydraulic gradient is reversed as a result of the rise of the freshwater level, seaward movement of the mixing zone causes significant dilution and a fast decreasing mobile concentration. The immobile concentration then decreases due to the reversed mass transfer process. The point at (110, 0), the closest point to the seaward boundary, has the longest period for salt transferred from the mobile domain to the immobile domain because it is the first to receive intruded saltwater with the landward movement of the mixing zone and the

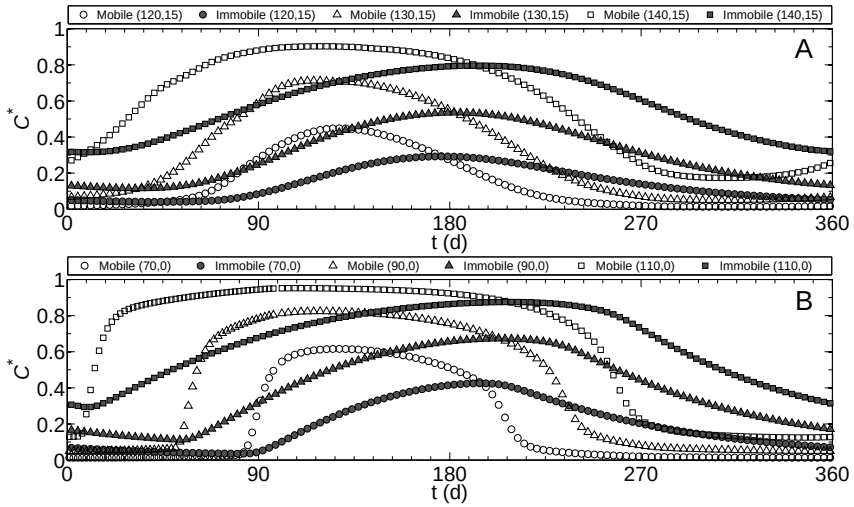

Figure 4.3 Temporal profiles of concentrations in the mobile and immobile domain at six observation points for the case with kinetic mass transfer and periodic freshwater fluctuations. The starting point of the period is at the moment of falling water level. A: (120, 15), (130, 15), and (140, 15). B: (70,0), (90,0), and (110,0). Units for these points are in meters.

last to be diluted as the mixing zone retreats seaward. By contrast, points closer to the freshwater boundary have shorter periods of mass transfer from the mobile domain to the immobile domain because they receive saltwater later as seawater intrusion progresses, and are diluted earlier by the freshwater with the seaward movement of the mixing zone. Furthermore, the profiles at different depth show similar temporal patterns, but at the shallower depth the concentrations in the mobile domain change relatively more gently than those at the bottom, indicating variable movement range of the mixing zone and different degree of mixing enhancement at different depth.

Figure 4.4 illustrates the impacts of hydrogeologic conditions on the dynamics of the mixing-zone development by the temporal and spatial distributions of three concentration contour lines, 0.1, 0.5 and 0.9.

Panel A shows the base model results: (1) the movement of different contour lines in response to freshwater fluctuations is unsynchronized due to kinetic mass transfer, resulting in significantly varying moving ranges for different contour lines, by a factor of 4; and (2) a time lag exists between freshwater level fluctuations and the movement of the mixing zone.

Panel B shows that the mixing zone in the case with larger dispersivities (B2) is thicker than that with smaller dispersivities (B1) in the absence of kinetic mass transfer. However, the enhanced thickness of the mixing zone is nearly uniform within a period for both cases without mass transfer. This indicates synchronized behavior for different contour lines in response to freshwater fluctuations, resulting in similar moving ranges

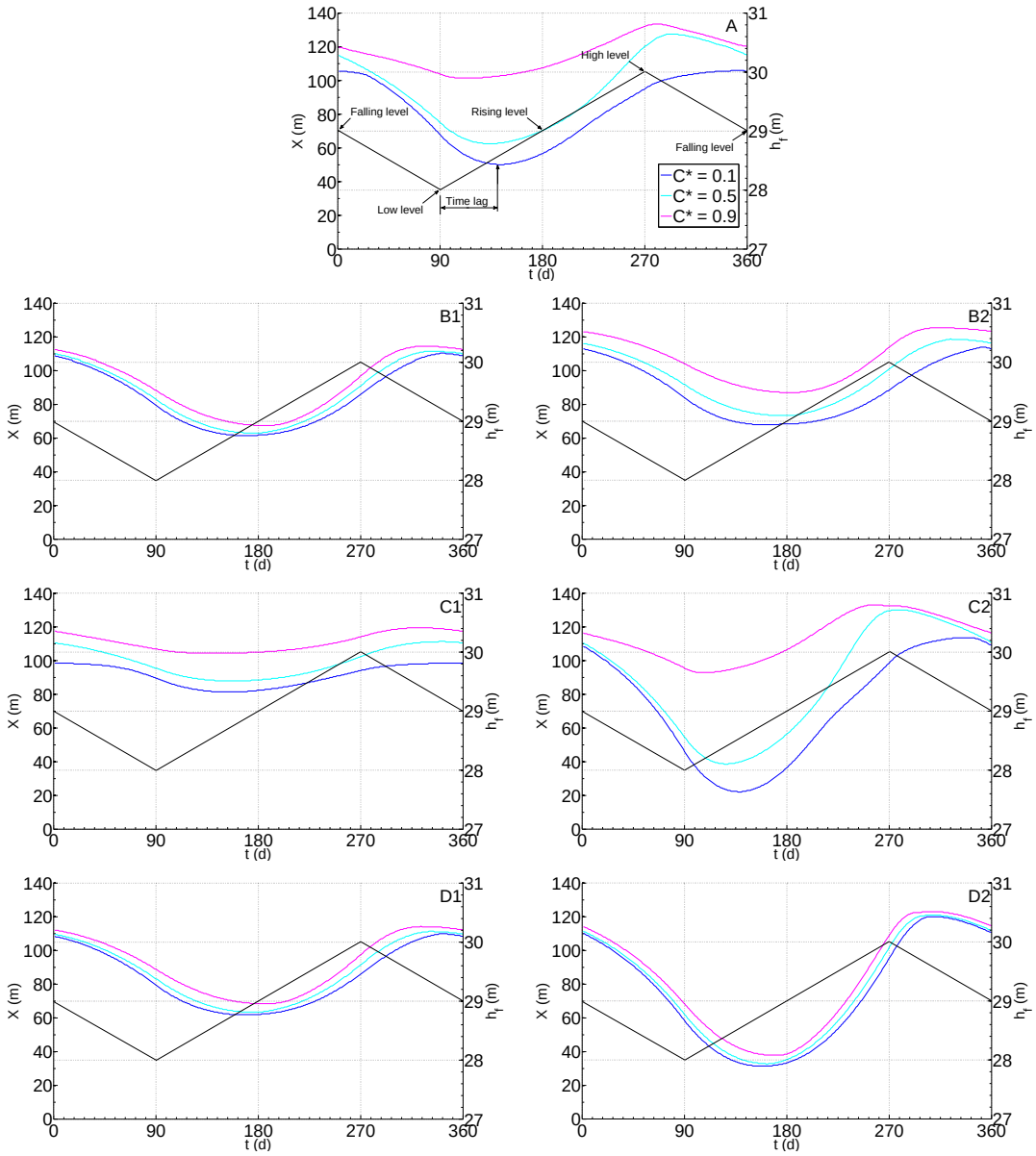

Figure 4.4 The dynamics of mixing-zone development influenced by hydrogeologic conditions, including dispersion, hydraulic conductivity, and mass transfer rate coefficient. Temporal and spatial evolution of the mixing zone distribution is characterized by three normalized concentration contour lines at the aquifer bottom (left y-axis) corresponding to periodic freshwater fluctuations (right y-axis). Panel A is the base model with defined parameters: hydraulic conductivity 30 m/d, first-order mass transfer rate coefficient 0.0028 d^{-1}, which corresponds to a unitary time scale ratio between the retention in the immobile domain and the period of freshwater fluctuations, and longitudinal and transverse dispersivities 0.5 m and 0.05 m, respectively. Panel B shows the impact of dispersion, in which B1 is the base model without kinetic mass transfer and B2 is the base model with larger dispersivities (2.5 m and 0.25 m) and

without kinetic mass transfer. Panel C shows the impact of hydraulic conductivity, in which C1 is the base model with hydraulic conductivity 10 m/d and C2 50 m/d. Panel D shows the impact of mass transfer rate coefficient, in which D1 has a time scale ratio of 0.01 and D2 100.

for different contour lines. Specifically, the 0.5 contour line remains almost at the middle of the mixing zone for the cases without mass transfer, but approaches the 0.1 contour line when the mixing zone expands and the 0.9 contour line when the mixing zone shrinks for the case with mass transfer. Because the freshwater level drops from the mean level at the beginning of a period, one may expect that the maximum landward movement of the mixing zone occurs at the end of the second quarter when the freshwater level rises to the mean level from the lowest level, which implies a three-month time lag between the freshwater level variation and the mixing zone movement. With the consideration of mass transfer, this time lag becomes shorter than a quarter, i.e., the maximum landward movement of the mixing zone occurs within the second quarter. Michael et al. [2005] identified a time lag between the seasonal freshwater level fluctuations and the submarine groundwater discharge rate in the absence of mass transfer. Our analysis indicates that the kinetic mass transfer may alter such time lags. In addition, the cases without mass transfer show almost synchronized time lags for different contour lines, while the case with mass transfer shows significant discrepancies in time lags for different concentration contour lines: the 0.9 contour line has the shortest time lag while the 0.1 contour line the longest, resulting in the expansion of the mixing zone. Likewise, similar time lag behavior and movement discrepancies of contour lines are found in the fourth quarter for the seaward movement of the mixing zone, resulting in the contraction of the mixing zone.

Panel C in Figure 4.4 shows the mixing zone distributions for different hydraulic conductivities: 10 m/d, 30 m/d (base model), and 50 m/d. It is shown that higher

hydraulic conductivity causes larger maximum and smaller minimum mixing zone thickness and more unsynchronized responses of various concentration contour lines. Mixing enhanced by mass transfer causes more significantly non-equilibrium concentrations between the mobile and immobile domain for faster flow due to enhanced time scale discrepancies between mass transfer and advection. In addition, higher hydraulic conductivities lead to larger landward and seaward movement. The impact of the amplitude of freshwater level fluctuation is similar to that of the hydraulic conductivity because variations of the amplitude essentially change the hydraulic gradient and the flow velocity. Furthermore, given a constant total porosity, altering capacity ratio, the ratio between the immobile and mobile porosity, yields different effective mobile porosities and different flow velocities. Thus, the impact of the capacity ratio is also similar to that of hydraulic conductivity and amplitude of freshwater fluctuations.

Panel D in Figure 4.4 shows the impacts of the first-order mass transfer coefficient. The mass transfer rate coefficient controls how quickly mass is exchanged between the mobile and immobile domain. Our previous study found that when the retention time scale and the period of freshwater level fluctuations become comparable, the mixing-zone thickness is maximized [Lu et al., 2009]. Three time scale ratios are considered: 0.01, 1(base model) and 100. It is shown that narrower mixing zones are developed for the ratios 0.01 and 100, compared with the ratio 1, and their unsynchronized time-lag behavior of the contour lines is similar to the case without kinetic mass transfer. Actually, mass transfer models with very small and large mass transfer rate coefficients

may be simplified to a classical advective-dispersive transport problem. For a small time scale ratio, i.e., the mass transfer is approximately equilibrium, the transport equation may be simplified by including a retardation factor. Thus, D1 also shows smaller displacements of the landward and seaward movement of the mixing zone. By contrast, for a large time scale ratio, i.e., the mass transfer is slow, the mass transfer between the mobile and immobile domains may be negligible and the entire system behaves approximately like a single-domain system with the effective porosity approaching the mobile porosity. As a consequence, the decreased porosity effectively speeds up the flow, resulting in a larger moving range of the mixing zone (see D2).

4.4 Conclusion

Our numerical experiments show that mixing enhancement in a dual-domain coastal aquifer is mainly controlled by the unsynchronized behavior of concentration distributions in the mobile and immobile domain. Such behavior is maximized at the aquifer bottom when the retention time scale in the immobile domain is comparable to the period of freshwater level fluctuations, resulting in nonuniform moving ranges of different concentration contour lines, nonuniform mixing enhancement, and significantly varying mixing zone thickness during a period. A time lag exists between the freshwater fluctuations and the movement of the mixing zone. This time lag may be altered by kinetic mass transfer. By contrast, large dispersion coefficients may create thicker mixing zones, but may not cause the unsynchronized behavior and alter the time lags of different concentration contour lines, i.e., the mixing enhancement is rather uniform in the mixing zone. The dynamics of mixing-zone development is sensitive to the flow

velocity, which is influenced by the hydraulic conductivity, amplitude of the freshwater level fluctuations, and the capacity ratio of mass transfer. These findings provide useful insights for understanding the mechanisms responsible for thick mixing zones and identifying key transport processes in coastal aquifers. Field data collection and analysis is underway for verifying these numerical results

CHAPTER 5

EFFECTS OF AQUIFER STRATIFICATION ON FRESHWATER-SEAWATER MIXING-ZONE DEVELOPMENT

5.1 Introduction

In coastal water resources management, seawater intrusion has become one of the most concerned issues. Seawater intrusion occurs in coastal aquifers when saline groundwater intrudes and contaminates a freshwater aquifer, and can be characterized in terms of the wedge penetration, shape and extent of the mixing zone between freshwater and seawater. The development of a mixing zone in coastal aquifers is a complex result of various effects such as hydrogeologic characteristics of the aquifer and hydrodynamic fluctuations of the groundwater and seawater heads. This mixing zone is one of most important features in coastal aquifers that controls regional groundwater flow dynamics and reactive transport processes. A wide mixing zone may bring significant effects on saltwater upconing processes of a pumping well and also can lead to the variation of the components of SGD. Studies have shown that the freshwater-seawater mixing zones serve as potential reaction sites for dolomitization and dissolution of carbonate rocks [e.g., Wigley and Plummer, 1976; Plummer, 1977; Rezaei et al., 2005].

Under steady state conditions, the width of the mixing zone depends basically on local dispersion with longitudinal and transverse dispersion controlling mixing between freshwater and seawater bodies [Abarca et al., 2007]. Local longitudinal dispersion on macroscopic transport in heterogeneous domains is of minor importance. Local

transverse dispersion, by contrast, significantly contributes to solute mixing and has now widely been recognized as a leading factor in explaining the width of a steady mixing zone [Dagan, 2006]. An increasing transverse dispersivity would have a shear effect, bringing the steady mixing zone seaward at the bottom and landward at the top and finally creating a broader mixing zone. However, pore-scale transverse dispersion only cause the presence of a thin mixing zone, as already visualized by laboratory and field experiments [Fiori and Dagan, 1999; Lebbe 1999; Zhang et al., 2002; Goswami and Clement, 2007; Abarca and Clement, 2009]. Wide mixing zones, ranging from hundreds of feet to miles, have been detected in many coastal aquifers all over the world [Kohout and Klein, 1967; Wu et al., 1993; Xue et al., 1993; Price et al., 2003; Barlow, 2003; Dausman and Langevin, 2005]. For example, the width of the mixing zone in the surficial Biscayne aquifer of the Miami area, Florida, US, reaches several hundreds of miles, and is still increasing [Dausman and Langevin, 2005]. In practice, many investigators present numerical solutions by assuming a large, perhaps unwarranted, value of transverse dispersivity. In other words, a large value of transverse dispersivity only provides a convenient way to reproduce the wide transition zone in reality, but sometimes seems to be unreasonable and holds a poor physical meaning [Dagan, 2006]. The theoretical analyses by Held et al. [2005] indicated that use of macroscopic dispersion coefficient is inappropriate and the effective dispersion coefficients are more close to the local-scale coefficients. Therefore, there are supposed to be some undetected mechanisms which could lead to wide mixing zones in coastal regions.

In past decades, a number of numerical studies targeted at simulating the mixing

zone have been conducted in an attempt to gain better understanding of the mechanisms response for the mixing-zone development [e.g., Volker and Rushton, 1982; Ataie-Ashtiani et al., 1999, Cartwright et al., 2003; Chen et al., 2004; Abarca et al., 2006; Karasaki et al., 2006; Xia et al., 2007; Lu et al., 2009]. In addition to dispersion/diffusion, factors affecting flow and mixing in the mixing zone mainly include: (1) transient tidal activity; (2) inland water table fluctuations; (3) kinetic mass transfer; and (4) hydraulic heterogeneity. Ataie-Ashtiani et al. [1999] and Chen et al. [2004] showed that tidal activity forces the seawater to intrude further inland and also creates a thicker interface. Field observations on an unconfined coastal aquifer in Australia suggested that the wave-induced groundwater pulse can cause the significant oscillations in the mixing zone of the order of several meters in the horizontal direction [Cartwright et al., 2003]. By contrast, tidal fluctuations are unlikely to cause large interface fluctuations because damping of the tidal signal is much higher than that of the pulse signal [Cartwright et al., 2003; Li et al., 2004]. On the other hand, it is now becoming increasingly evident that inland water table fluctuations in response to pumpage, rainfall, and upstream canal stage would lead to monthly, yearly or decadal oscillations of the mixing zone. This long-term movement of the mixing zone, combined with kinetic mass transfer effects, can significantly enhance the width of the mixing zone [Lu et al., 2009].

Heterogeneity in hydraulic conductivity of the formation perturbs flow over various length scales and is expected to play a very significant role in the behavior of density-dependent systems [Schincariol and Schwartz, 1990; Simmons, 2001]. Most of previous

studies regarding the effect of heterogeneity on density dependent flow focused on unstable configurations, i.e., the presence of higher density fluid over lower density fluid [e.g., Mcdibbin and O'Sullivan, 1980; Mckibbin and Tyvand 1982 and 1983; Schincariol and Schwartz, 1990; Schincariol and Mendoza, 1997, Schincariol, 1998; Prasad and Simmons, 2003]. However, the effect of heterogeneity on stable configurations, namely, seawater intrusion problems, has little been studied [Schwarz, 1999; Held et al., 2005; Abarca et al., 2006; Kerrou and Renard, 2010]. A study conducted by Abarca et al. [2006] showed that the effects of moderate heterogeneity with random distribution on increasing the steady state mixing-zone width are small. In particular, there is very limited research regarding the effects of stratified heterogeneity on the mixing-zone development [Mualem and Bear, 1974; Nakagawa et al., 2000]. Indeed, the role of aquifer stratification on the mixing-zone development is expected to be especially important, particularly when the inland water level fluctuation induced mixing zone movement occurs.

In this chapter, we carry out both numerical and experimental investigations of aquifer stratification effects on the mixing-zone development. Both steady state and transient conditions are respectively simulated to examine aquifer stratification effect on the shape, location, and width of the mixing zone. For the simulations of transient processes, hydrodynamic fluctuations from both landward and seaward boundaries are considered. The main objective of this study is to compare and contrast mixing-zone development in homogeneous and stratified formations and therefore to assess the importance of aquifer stratification with various geologic settings on the mixing-zone

development pattern. Most importantly, we expect to provide an alternative explanation for wide mixing zones found in many field conditions.

5.2 Numerical Simulations

The density-dependent groundwater flow code, SEAWAT-2000, is employed to simulate the cases in this study.

5.2.1 Mathematical Description

The governing equations used by SEWAT-2000 have been detailed in section 3.2.1.

5.2.2 Conceptual Model, Boundary Conditions and Model Parameters

A schematic of the conceptual model is shown in Figure 5.1. The model represents a vertical section through a coastal aquifer with a total length $L = L_L + L_s$. The x-z co-ordinate origin is located at the bottom-left corner of the simulation domain. L_s is the horizontal length of aquifer beneath the seabed, which is also equivalent to the horizontal length of free seawater zone at the mean seawater level in the simulation domain. L_L is horizontal aquifer distance between the mean coastline and the inland boundaries. To reduce the computation effort, L_s and L_L are set to be 100 m and 300 m, respectively. The height of the model domain H is 42 m. The mean freshwater level at the landward boundary h_f and the mean sea level h_s are 40.2 m and 39 m, respectively. The beach slope equals 0.1 in the nearshore region.

The aquifer is assumed to be isotropic with porosity $n_e = 0.4$, longitudinal dispersivity α_L = 0.5 m and transverse dispersivity α_T = 0.05 m. The magnitude of the dispersivities used in this study is the same as those adopted by previous numerical studies [Robinson et al., 2006 and 2007, Lu et al., 2009]. A horizontal layer of the darker zone is presented with a different hydraulic conductivity, representing a simple aquifer stratification in coastal regions. The height of the layer is d, and the distance between the layer bottom and aquifer bottom is D. The values of hydraulic conductivity for this layer and the remaining region within the aquifer equal to K_2 and K_1, respectively. Parameters d, D, K_1 and K_2 vary in the simulations in order to examine their respective effects on the mixing-zone development. The assumed values for hydrogeologic parameters are listed in Tables 5.1.

To reproduce real coastal environments, the whole domain is divided into two zones: a surface seawater zone (zone I) and an aquifer zone (zone II), which are separated by a sloping aquifer-ocean interface. High hydraulic conductivity (10^4 m d^{-1}), effective porosity n_e =1, and constant saltwater concentration of 35 kg m^{-3} are assigned to the cells in zone I to reproduce coastal surface water [Brovelli et al., 2007; Robinson et al., 2007; Lu et al., 2009]. To study the mixing-zone development under transient flow conditions, we consider water level oscillations from seaward and inland boundaries, respectively. Seawater level oscillations indicate the short-period tidal forcing, while inland freshwater level fluctuations are usually relatively much longer period and found to be seasonal in reality [Michael et al., 2005]. Here, a cosine function is assumed to

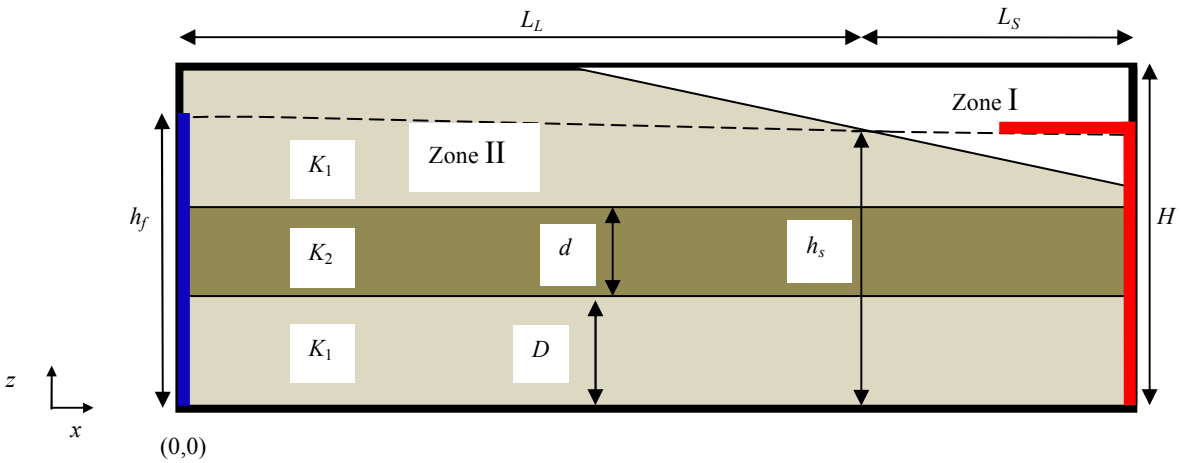

Figure 5.1 Model geometry and boundary conditions. The simulation domain is divided into two zones: a surface seawater zone (zone I, not shaded) and an aquifer zone (zone II, shaded). Left (blue) and right (red) zones representative the cells assigned inland and seaward boundaries, respectively.

Table 5.1. Model parameters

Parameter	Variable	Value
Domain length, m	$L_S + L_L$	400
Domain height, m	H	42
Beach slope	φ	0.1
Longitudinal dispersivity, m	α_L	0.5
Transverse dispersivity, m	α_T	0.05
Total effective porosity	θ	0.4
Mean seawater level, m	h_s	39
Mean freshwater level, m	h_f	40.2
Seawater density, kg m^{-3}	ρ_s	1025
Freshwater density, kg m^{-3}	ρ_f	1000
Salt concentration, kg m^{-3}	C_s	35

describe the periodic boundary water level fluctuations:

$$h = ACos\omega t + h_m \tag{5.4}$$

where h is time-varying head, A is the amplitude of water level fluctuations, ω is the angular frequency, and h_m is the mean seawater level. A is set to be 1 m for both tidal and inland water level fluctuations. ω equals 12.567 d^{-1} (period = 0.5 d) for tidal activities and 0.0174 d^{-1} (period = 360 d) for seasonal freshwater level fluctuations. Because the timescale difference between tide and seasonal freshwater level fluctuations is significant, the water level at one boundary is reasonably assumed to be constant when simulating the water level fluctuations at the other boundary.

Figure 5.1 shows the shape of the seaward boundary is an inverse L. The horizontal strip of cells are used to reproduce the flat surface of the sea since we approximate the free seawater zone using a high value of hydraulic conductivity [Brovelli et al., 2007]. When simulating tidal forcing on the sloping beach interface, constant saltwater concentration of 35 kg m^{-3} and above defined time-varying head are assigned to the right side boundary (the zone of red color in Figure 5.1). Likewise, constant saltwater concentration of 0 kg m^{-3} and defined time-varying head are assigned to the left side boundary (the zone of blue color in Figure 5.1) to simulate freshwater level fluctuations. The upper boundary is a phreatic surface with negligible groundwater recharge. The bottom of the domain is a no-flow boundary, which represents an impermeable aquifer base.

5.2.3 Model Discretization and Simulation Termination Criterion

It is well recognized that grid size is a critical factor that controls the accuracy of the variable density flow simulations [Voss and Souza, 1987; Diersch and Kolditz, 2002]. A common criterion employed to ensure an acceptable grid spacing is the grid Peclet number $P_e \approx \Delta L/\alpha_L$ [Voss and Souza, 1987], where ΔL is the grid spacing. When the value of Pe is less than 4, the grid size used represents desirable grid spacing. This grid spacing criterion has been used in many previous numerical simulations [e.g., Brovelli et al., 2007, Lu et al., 2009, Xie et al., 2010]. The grid used in our simulations is uniform with Δx = 1 m and Δz = 0.5 m, yielding 33600 cells. This grid spacing corresponds to Pe = 2 and complies with the grid discretization requirement.

To simulate the transient flow conditions, steady-state simulations are first conducted. Then, the transient boundary conditions are introduced into steady-state simulation results. As the flow field and concentration profile do not change within the double simulation period, the simulation results can be regarded under dynamic equilibrium conditions.

5.3 Mixing-Zone Development under the Steady-State Conditions

5.3.1 Simulation Results

With the neglect of both transient seaward and inland water level fluctuations, steady state cases are first simulated. Figure 5.2 shows the developed mixing zones and streamlines in one homogenous case and two stratified heterogeneous cases. For the stratified cases, the value of K in the middle layer is assumed to be one order of magnitude higher and lower than that of the remaining part of the aquifer, respectively.

It is shown that aquifer stratification can lead to significant effects on the streamline direction and mixing zone profile under steady state conditions. Recirculated seawater in the homogeneous case only comes from free surface water zone, i.e., the zone above the beach bed, while in both cases with aquifer stratification, it can be derived from the seaward boundary.

For the homogenous case, a relatively uniform and narrow mixing zone is formed due to density gradient and local dispersion. Furthermore, other homogenous cases with different magnitudes of hydraulic conductivity are also simulated. Results indicate that the magnitude of *K* does not bring significant effects on the mixing-zone development in homogenous cases, though the case with a higher *K* can lead to a little bit wider mixing zone near the coastline.

Rather than a uniform and thin mixing zone developed in the homogeneous case, a significantly wide mixing zone is constructed in the embedded lower *K* layer in the stratified case (see Figure 5.2B). Due to the difference of *K* in the upper two layers, the streamlines both from freshwater and seawater are refracted at the interface between two layers. The flow refraction here can be explained by the refraction law of streamlines in the pure freshwater aquifer (see Figure 5.3). As streamlines penetrate from the bottom layer (high *K* layer) to the middle layer (low *K* layer), the refracted streamlines approach the normal to the boundary, which is similar to the condition in Figure 5.3(a). As a result, saltwater transports along the direction of the streamlines, and the mixing zone in the middle layer is significantly widened. In contrast, when the streamlines pass from the

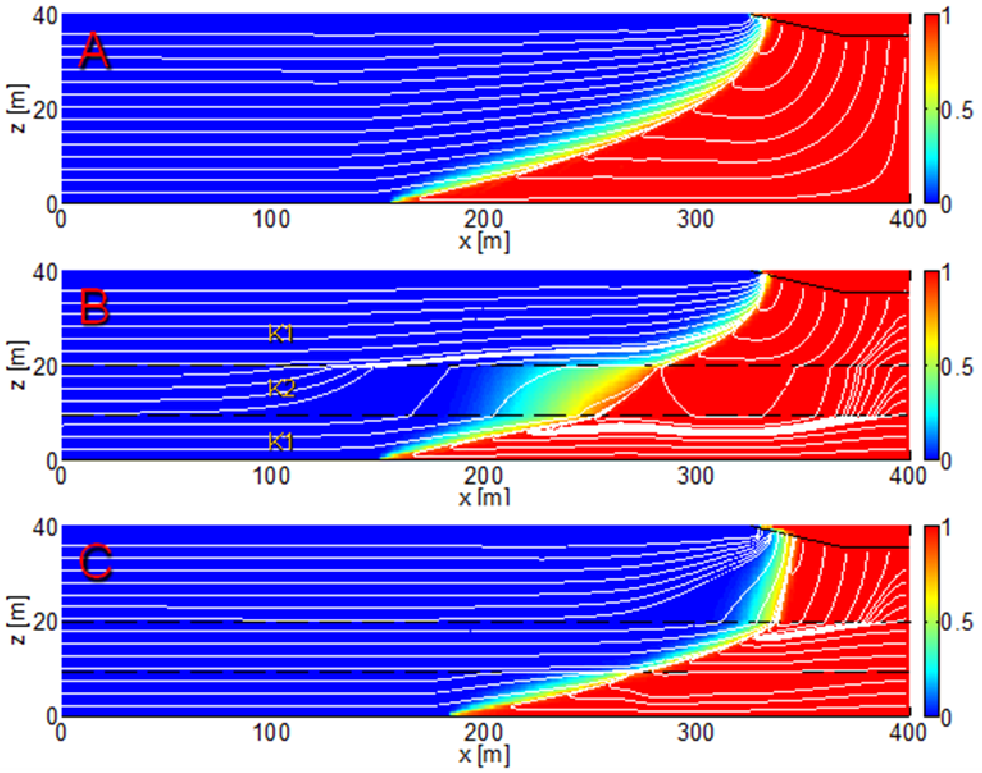

Figure 5.2 Simulation results of salt concentrations (colored contours) and streamlines for steady state conditions. A: homogenous case; B: stratified case (K_1/K_2 = 10); C: stratified case (K_1/K_2 = 0.1).

(a)

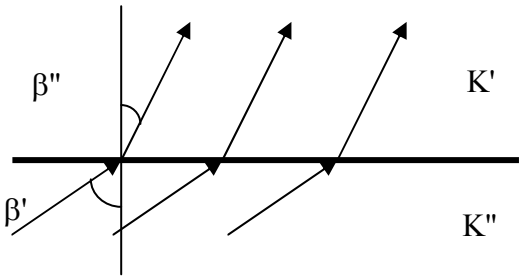

K'< K", β' < β"

(b)

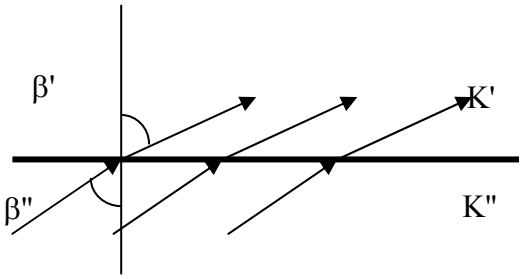

K'> K", β' > β"

Figure 5.3 Refraction Law of the streamlines at the interface between two permeabilities.

middle layer to the upper layer, the mixing zone is slightly narrowed due to the flow refracted from the low K layer to the high K layer. The flow refraction law is also applicable to the case with an embedded high K layer, which leads to a thinner mixing zone in the middle layer, and a widened mixing zone in the top layer.

5.3.2 Sensitivity of the Relative Magnitude of Heterogeneity

Figure 5.4 shows the sensitivity analysis results for the effects of relative magnitude of K on the mixing-zone development. It is shown that increasing the ratio between K_1 and K_2, for both cases, causes the mixing zones to become vertical in the region above a higher K zone due to flow refraction. As a result, the position of the toes retreats seaward. Other simulation results (not shown here) indicate the constant ratio K_1/K_2 with different magnitudes of K_1 and K_2 would lead to almost the same mixing zone profiles, although the timescales to reach the steady state may be different. In other words, the ratio between K_1 and K_2 controls the mixing zone profile under the steady state conditions.

Figure 5.5 shows the effects of the magnitude of aquifer heterogeneity on toe position, relative total mass in the low K layer, and the position of the mixing zone (2.5% to 97.5% of saltwater concentration) in the low K layer. The relative total mass is defined as the total mass in the middle layer divided by the total mass in the corresponding part in the homogeneous case. It can be seen that with the increased ratio of K_1/K_2, the toe position gradually moves seawater, which indicates that the presence of a strong heterogeneity in the coastal aquifer would lead to the alleviation of seawater

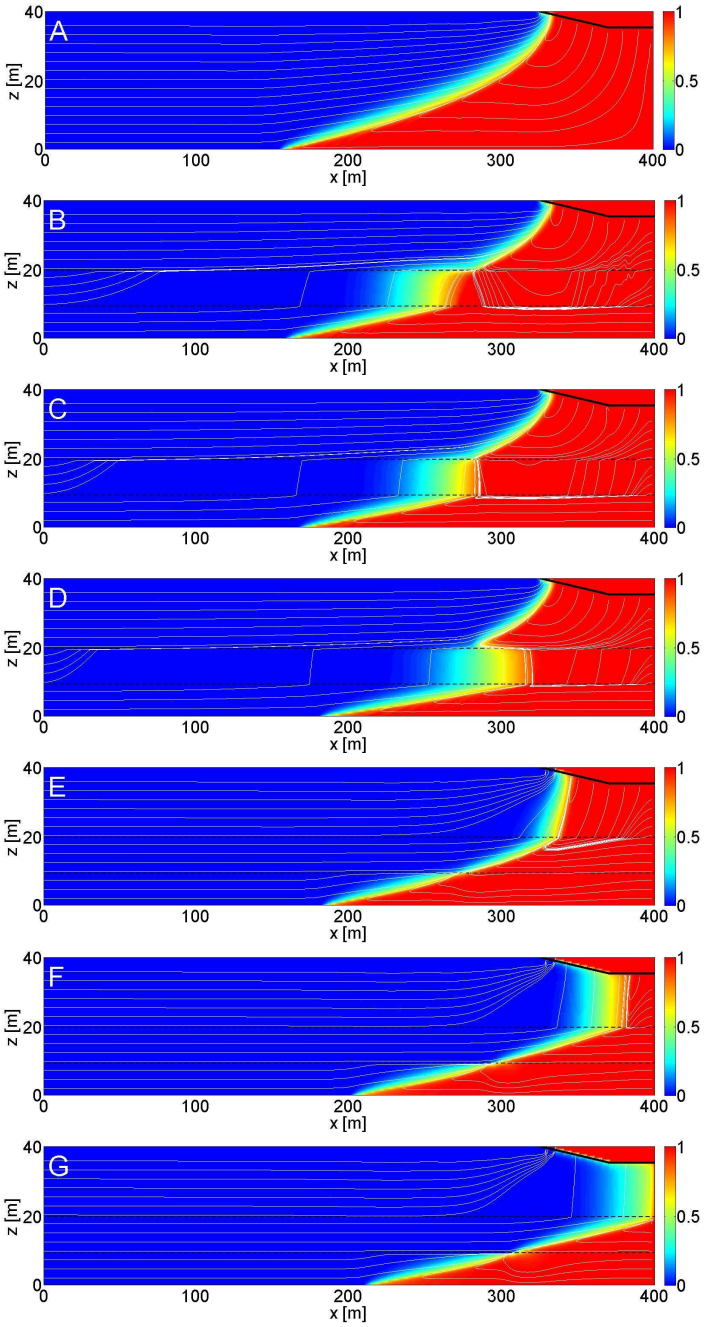

Figure 5.4 Sensitivity of the magnitude of heterogeneity. A: Homogeneous case; B: $K_1/K_2 = 10$; C: $K_1/K_2 = 100$; D: $K_1/K_2 = 200$; E: $K_1/K_2 = 0.1$; F: $K_1/K_2 = 0.02$; G: $K_1/K_2 = 0.01$.

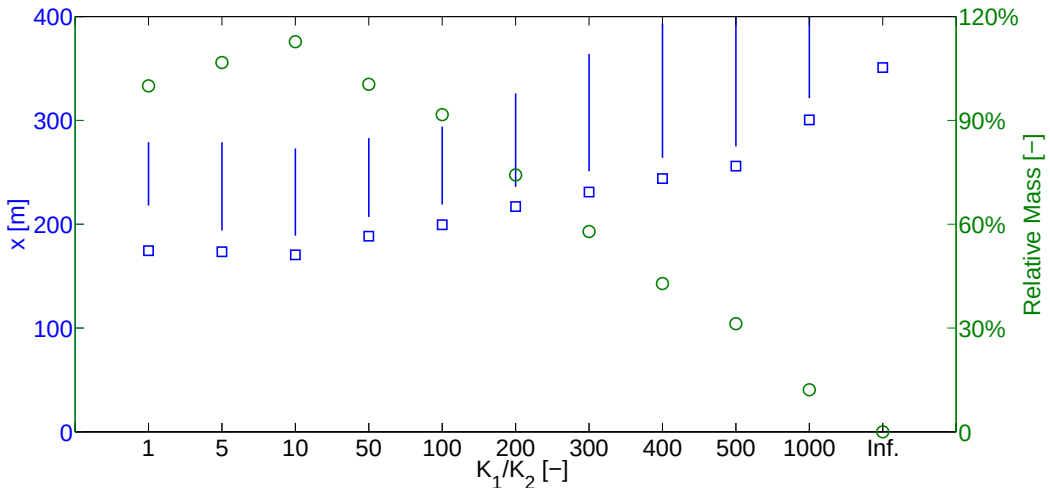

Figure 5.5 The effects of the magnitude of aquifer heterogeneity on toe position, relative total mass in the low *K* layer, and the position of the mixing zone (2.5% to 97.5% of saltwater concentration) in the low K layer. (O): relative total mass in the low *K* layer; (□): toe position; (—): the position of the mixing zone in the low *K* layer.

intrusion. On the other hand, the relative total mass is first slightly increased, then decreased after the heterogeneity is larger than one order of magnitude, resulting that the mixing zone in the middle layer first moves landward and then seaward. The mixing-zone width in the middle layer, is first increased, followed by the decrease due to the retreat of the mixing zone. Considering a limiting case that K_2 is infinitely small, the total mass and the mixing-zone width in the middle layer equal zero, i.e., no salts in the middle layer. Under such condition, the top is closest to the seaward boundary.

5.3.3 Sensitivity of the Layer Height

Figure 5.6 shows the simulation results of mixing-zone development in the two-layer cases. Similar to the three-layer cases, the mixing zone is wide in a lower *K* layer when this layer is lies above a layer with a higher *K* (See Figures 5.6B and 5.6D). However, the toe position in these two cases further retreats seaward compared to the corresponding three-layer case. Comparing Figures 5.2A with 5.6D, and 5.2C with 5.6B, it is found that a larger depth of the lower *K* layer results in a thinner mixing zone and a larger depth of the higher *K* layer a wider mixing zone. For the two-layer case with a higher *K* layer lying above a lower *K* layer (Figure 5.6A and 5.6C), however, there are no significant differences of the toe position and mixing zone width compared with those in the homogeneous case.

5.4 Mixing-Zone Development under Transient-Flow Conditions

Previous studies have demonstrated that transient flow conditions from both seaward and landward boundaries have significant effects on the mixing zone

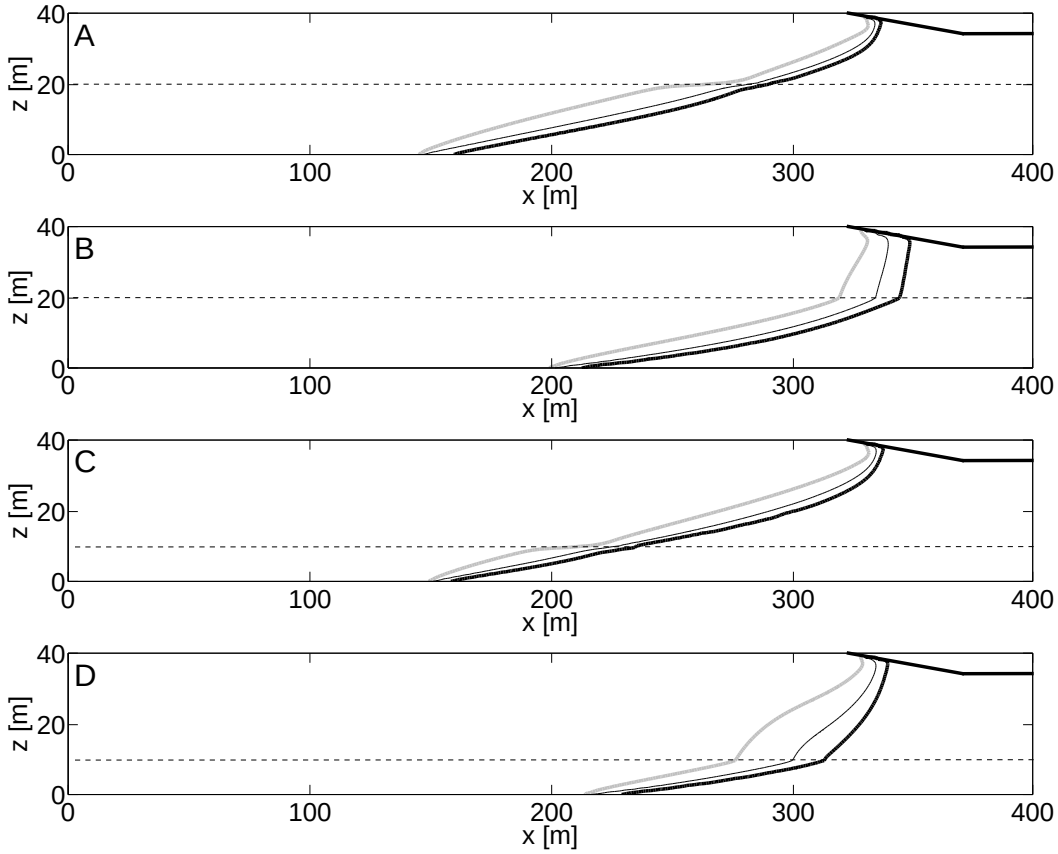

Figure 5.6 Sensitivity of aquifer layer height on the mixing-zone development.

development [e.g., Ataie-Ashtiani et al., 1999; Dausman and Langevin, 2005; Lu et al., 2009; Lu and Luo, 2010]. In this study, tidal activities and freshwater level fluctuations are considered to investigate their respective effects on the mixing-zone development in stratified aquifers. For freshwater level fluctuations, we first study an instantaneous decrease of freshwater level and then seasonal freshwater level fluctuations.

5.4.1 Effects of Tidal Activities

Figure 5.7 shows the mixing zones under the tidal conditions. The numerical results found that the profile of mixing zones do not change significantly within a tidal period. Compared with steady state conditions, the tidal activities do not have much effect on how far the seawater intrudes into the aquifer, but significantly enhance mixing in the upper region for the homogeneous case and the case with a lower K in the middle layer.

5.4.2 Effects of an Instantaneous Decrease of the Freshwater Level

Figure 5.8 shows the simulation results of transient mixing-zone development of two-layer and three-layer cases under the conditions that the freshwater level experiences an instantaneous decrease from 40.2 m to 39.2 m. After the instantaneous decrease of the freshwater level, for both cases, seawater in each layer intrudes inland but with different speeds. The different intrusion speeds of mixing zones in different layers result in detaching the toe in the higher K layer from the top of the mixing zone in the lower layer, which subsequently leads to the density gradient between these two layers and the transport of salts into the lower layer. This process is also called mixed convection, i.e., flow is driven by density difference and advection. Furthermore,

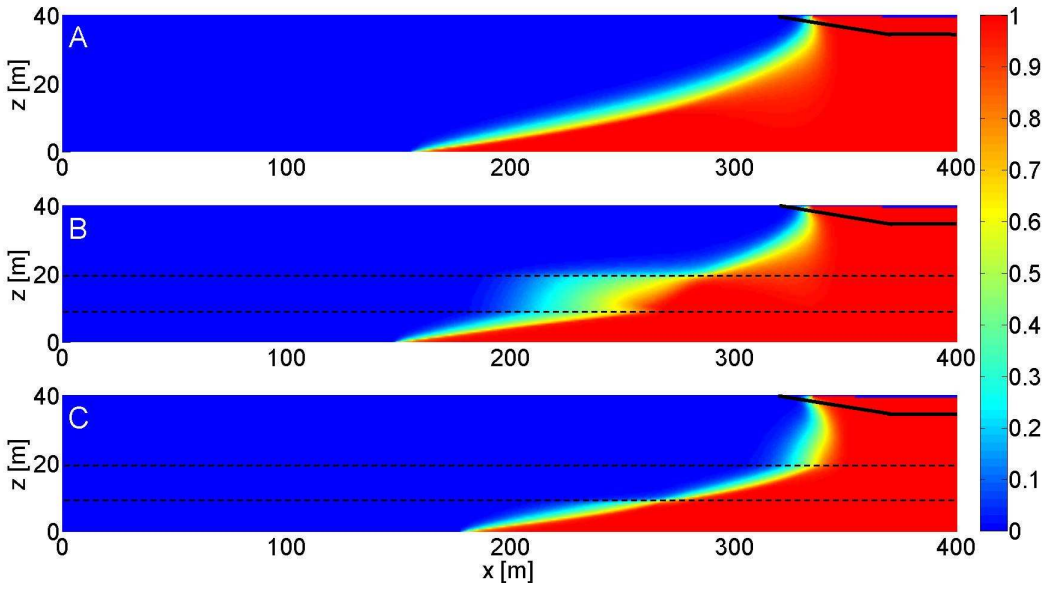

Figure 5.7 Ming-zone development under tidal activities. (A): homogeneous case; (B): $K_1/K_2 = 10$; (C) $K_1/K_2 = 0.1$.

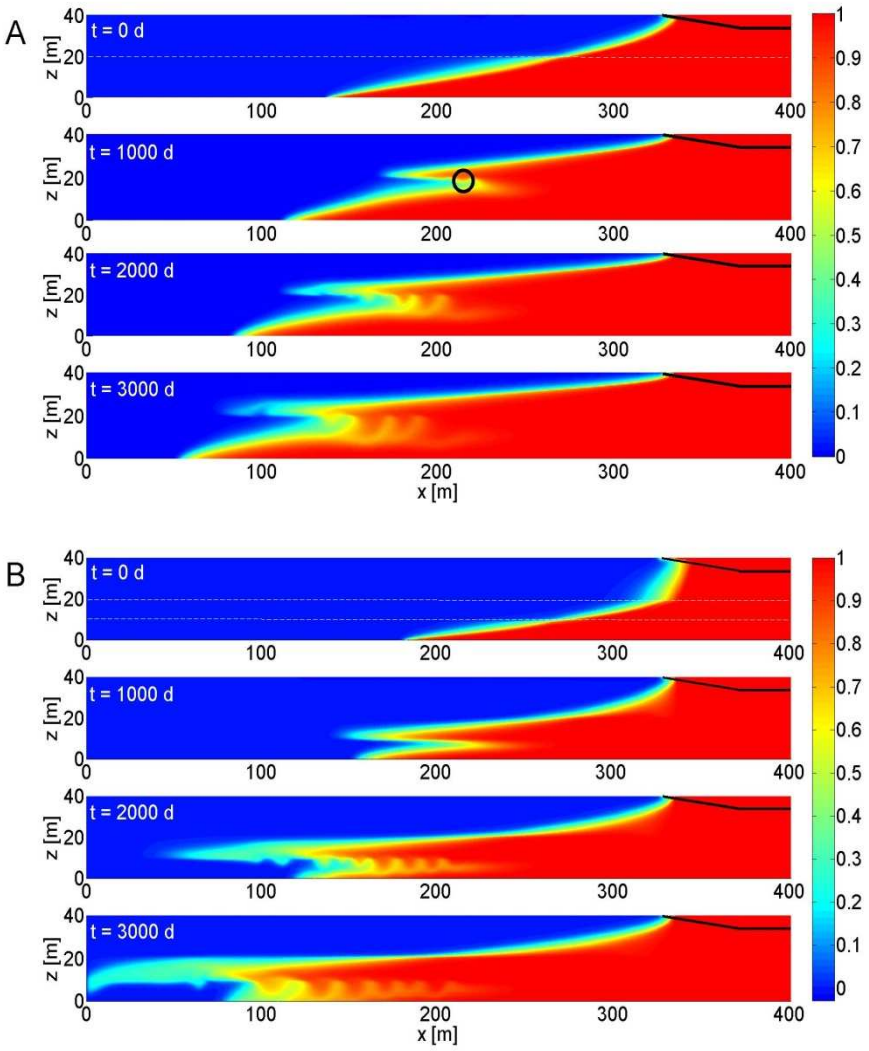

Figure 5.8 Transient mixing-zone development after an instantaneous decrease of the freshwater level. K_1 = 3 m/d, K_2 = 30 m/d. (A): two layer case; (B): three layer case.

seawater in the higher *K* layer in three-layer case intrudes much faster than that in two-layer case, and therefore, one can observe the finger earlier in two-layer case (as shown by the black circle in Figure 5.8A) than in three-layer case due to a lower mixed convection ratio (free convection driven by density gradient to the forced convection) in the three-layer case. After salts penetrate from the high *K* layer into the low *K* layer, mixing zones in both layers will be significantly widened. On the other hand, after freshwater level experiences 1 m decrease, the system will need extremely long time to reproduce the steady state condition.

5.4.3 Effects of Seasonal Freshwater Level Fluctuations

Figure 5.9 shows the transient mixing-zone development under seasonal freshwater level fluctuations. It can be seen that the mixing zone profile changes dramatically, especially in the upper two layers. The transient mixing zone profile is highly sensitive to the magnitude of the *K* in each layer, fluctuation period and the amplitude of freshwater level at the inland boundary. In this case, however, we don't observe a finger due to the short residence time.

5.5 Laboratory Experimental Visualization

In order to validate the above steady-state numerical results, a laboratory experiment is conducted. The experiments were performed in a flow tank 1800 mm long, 600 mm high and 100 mm wide. Real coastal sands were packed in the tank as the homogenous porous medium, 440 mm high at the freshwater end and 428 mm high at the sea end. Slat (NaCl) solutions were used as the seawater and the contaminant sources.

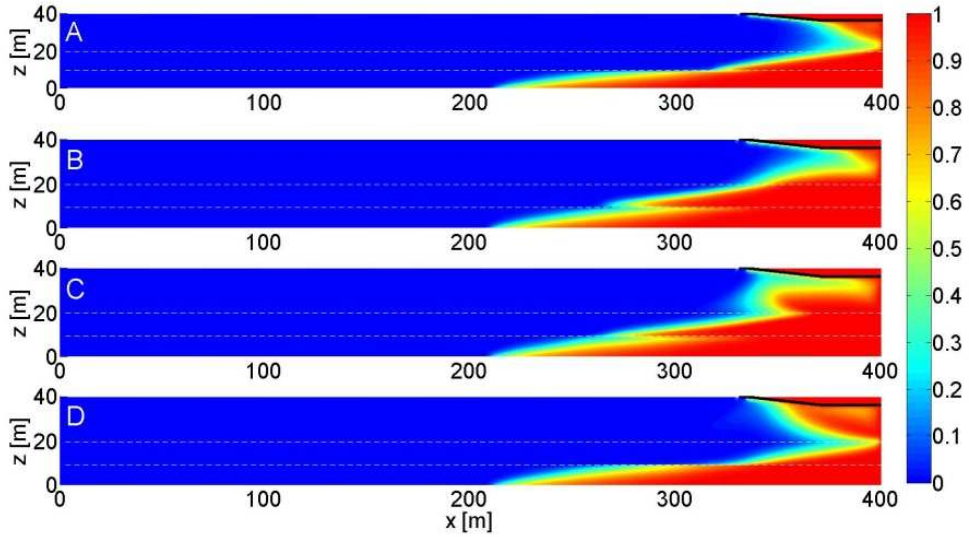

Figure 5.9 Transient mixing-zone development under seasonal freshwater level fluctuations. K_1 = 3 m/d, K_2 = 150 m/d. (A): falling level; (B) low level; (C) rising level; (D) high level.

The freshwater head was maintained constant through a constant-head cell. The tank walls are made of transparent acrylic material so that the dyed seawater can be visible from outside the tank and could be photographed. The photographs are then processed to convert the color intensity into solute contours.

Figures 5.10 and 5.11 show the laboratory experiment results and corresponding numerical results, respectively. One can observe that the numerical results can exactly reproduce the experiment results. In addition, a wide mixing zone can be found in the low *K* layer in the case B because of streamline refraction. However, almost no saltwater is in the top layer in the case C, which is different from the previous simulation results. The reason is that there is not a slope considered in the current case.

5.6 Conclusion

Aquifer stratification is a common phenomenon in natural conditions, which is usually neglected in the study of coastal hydrogeologic systems. However, aquifer stratification may bring significant effects on freshwater-seawater mixing-zone development. This study employs both numerical and experimental methods to investigate the aquifer stratification on mixing-zone development under steady-state and transient flow conditions. The specific finding of the present study include:

Under steady-state conditions:

(1) When a low *K* layer lies above a layer with a higher *K*, the mixing zone in the low *K* layer would be widened due to streamline refraction, and vice versa;

(2) The steady-state mixing zone profile in stratified aquifers is only determined by the relative magnitude of *K* in different layers;

(3) Increasing the magnitude of heterogeneity would lead to the retreat of the toe, first increase and then decrease of the mixing-zone width;

(4) When the height of the aquifer is constant and a low K layer lies above a high K layer, increasing the height of low K will lead to shrink of the mixing zone;

Under transient tidal conditions:

(1) The mixing zone in the top layer can be slightly widened by tidal fluctuations;

Under the conditions of an instantaneous decrease of freshwater level :

(2) The mixing zone in high K layer in the three layer model moves inland faster than in two layer model because of the faster advective flow.

(3) The finger is first developed in two *K* layer model because of the higher mixed convection ratio.

(4) The system after an instantaneous decrease of freshwater level need extremely long time to reformulate the steady state condition, and therefore transient condition should be considered in later theoretical studies as well as field studies.

Under seasonal freshwater level fluctuations:

(1) The mixing zone profile changes dramatically. Transient mixing zone profile is highly sensitive to the magnitude of the K in each layer, fluctuation period and the amplitude of freshwater level at the inland boundary.

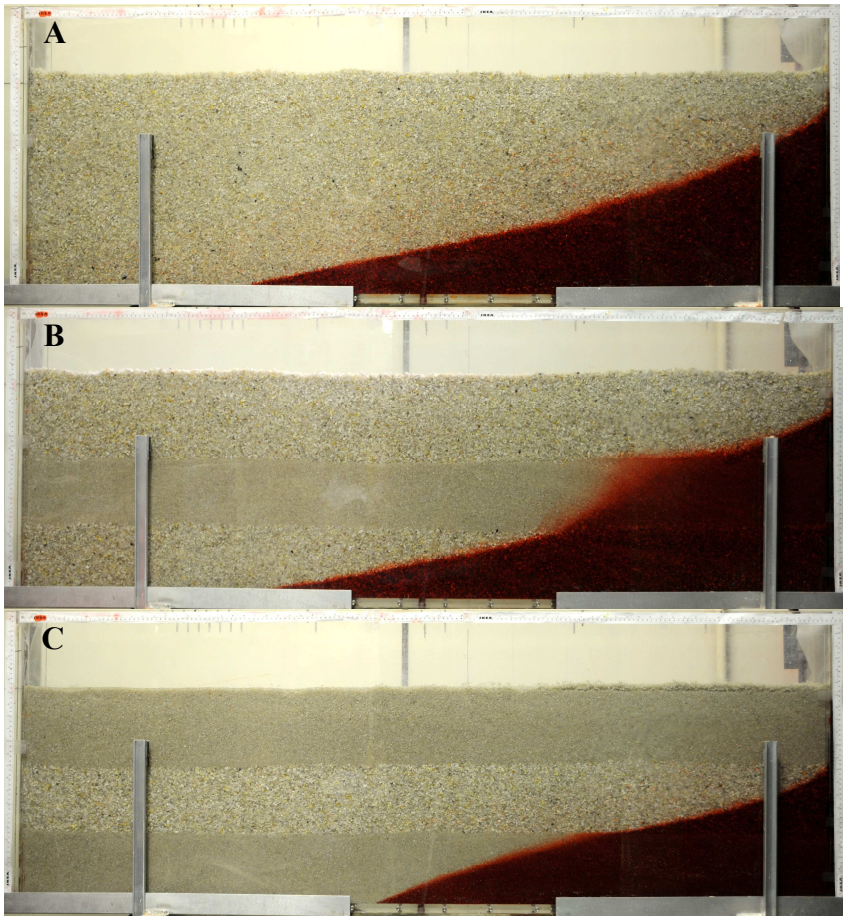

Figure 5. 10 Laboratory experiment results.

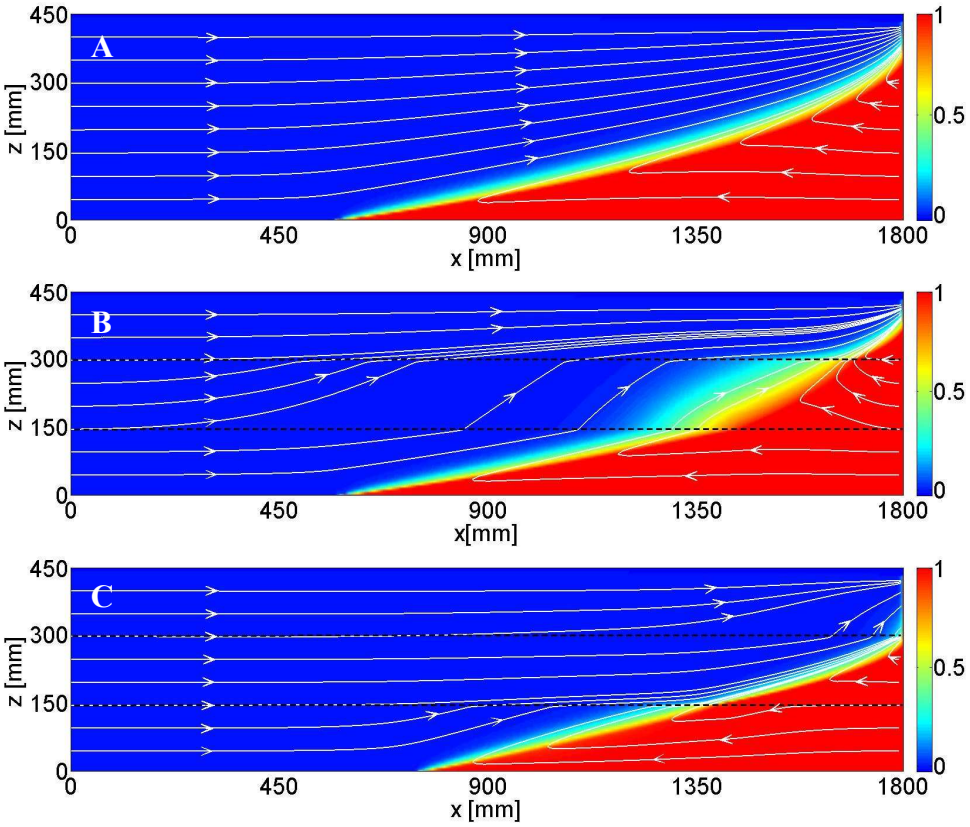

Figure 5. 11 Numerical results of the laboratory-scale cases.

.

CHAPTER 6

RECOVERY EFFICIENCY OF AQUIFER STORAGE AND RECOVERY (ASR) WITH MASS TRANSFER LIMITATIONS

6.1 Introduction

Aquifer storage and recovery (ASR) is an effective strategy for optimal management of groundwater resources. ASR involves injecting freshwater into aquifers through a well (or a cluster of wells) when excessive water is available (storage), and pumping water out from the same or adjacent wells when needed (recovery). The injection, storage and recovery process forms one cycle of ASR (see Figure 6.1). Interest in ASR has been growing in the face of declining groundwater levels due to excessive exploitation, increasing vulnerability of surface water supplies to contamination, and salinization of groundwater resources in coastal and offshore environments [e.g., Eastwood and Stanfield, 2001; Almulla et al., 2005; Pyne, 2005; Lowry and Anderson, 2006; Culkin et al., 2008; Vandenbohede et al., 2008]. Specifically, ASR avoids the construction of large and expensive reservoirs, prevents easy loss of freshwater resources, and provides a cost-effective solution to water resources management. In addition, the development of environmentally friendly ASR systems can alleviate land subsidence and act as a hydraulic barrier against saltwater intrusion in coastal regions [e.g., Shammas, 2008].

The performance of an ASR system is generally quantified by the recovery efficiency (RE), defined as the quantity of stored water that can be recovered without

further treatment divided by the total quantity injected [Kimbler et al., 1975]. It is not uncommon that RE may be significantly lower than 100% for ASR systems installed in an initially non-potable aquifer due to the mixing between the injected freshwater and originally-contaminated groundwater. Primary mechanisms that may influence the RE of an ASR system are those that can introduce or enhance mixing in the subsurface, including density gradient driven convection, dispersion and diffusion, heterogeneity of the aquifers, kinetic mass transfer and others [e.g., Kuman and Kimbler, 1970; Moulder, 1970; Merritt, 1986; Maliva et al., 2006; Ward et al., 2007, 2008, 2009; Lu et al., 2009]. For example, numerical studies of three ASR field sites in Wisconsin, USA showed that dispersive mixing was an important process affecting the RE and a larger longitudinal dispersivity would lead to a much lower RE due to enhanced mixing [Lowry, 2004; Lowry and Anderson, 2006]. Among all these mechanisms, kinetic mass transfer was recognized as a potential key factor that may control the RE of ASR system [Eastwood and Stanfield, 2001; Culkin et al., 2008]. In geologic formation exhibiting dual-domain behavior, e.g., mobile-immobile domains such as media consisting of factures and matrices, preferential flow paths and stagnant and dead pores, or in an aquifer containing strongly sorbing contaminants, injection of potable water may break the local geochemical equilibrium in the subsurface and cause dissolution and desorption of chemical constituents from matrices and rocks, which may contaminate the injected potable water and potentially release more toxic compounds. Culkin et al. [2008] observed significant salinity rebounds during the storage phase in ASR field experiments in Charleston, South Carolina, USA, which was successfully characterized by a dual-

domain mass transfer model. Thus, prior to significant depletion of the immobile domain or solid phase, one would always expect a low RE.

Although the prevalent existence of mass transfer behavior in natural aquifers has been recognized [e.g., Coats and Smith, 1964; van Genuchten and Wierenga, 1976] and many numerical and analytical solutions have been developed to simulate divergent and convergent dispersion with mass transfer limitations [e.g., Chen, C.-S., 1985, 1986; Coltz and Oxley, 1991; Moench, 1995], the effectiveness and efficiency of ASR subject to mass transfer limitations remains unknown. In particular, there is no guidelines to determine the likelihood of ASR being successful and to optimize ASR operational parameters with mass transfer limitations. The present study numerically and analytically investigates the efficiency of an ASR system in dual-domain aquifers with mass transfer limitations under various hydrogeologic and operational conditions. Simple and effective relationships between transport parameters and ASR operational parameters are derived to quantify the effectiveness and ascertain the potential of ASR systems with mass transfer limitations. Specific questions to be answered by the present research are as follows: (1) How can we determine whether a site is appropriate or not for ASR operational parameters on ASR performance; and (3) How many cycles are needed for an ASR system to perform well?

6.2 Numerical Model

Figure 6.1 shows the conceptual model of a typical ASR system with a fully-penetrated pumping well installed in a confined, homogeneous, and isotropic aquifer.

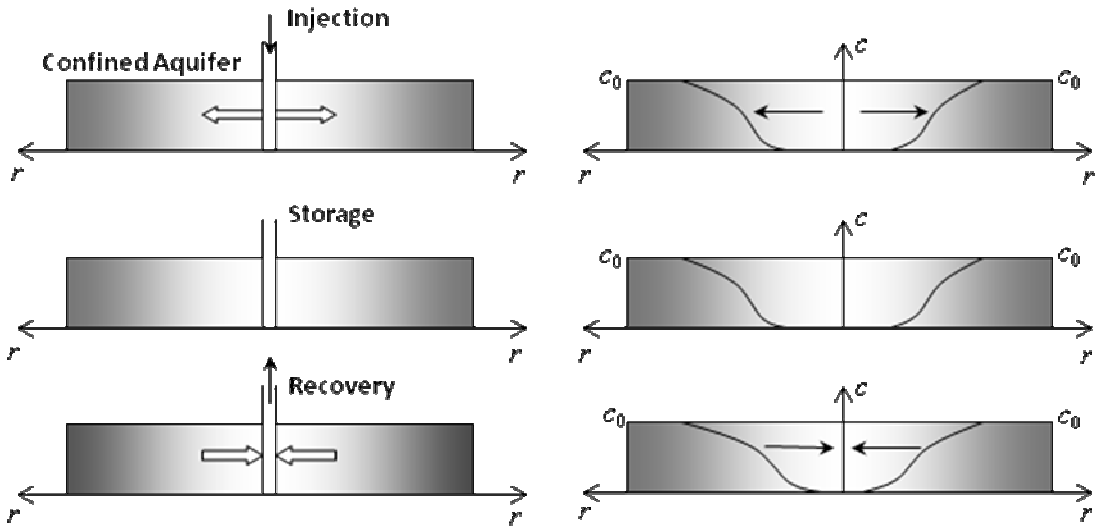

Figure 6.1 Schematic conceptual model or an ASR system with a fully-penetrating well in a confined aquifer in an axisymmetric coordinate system.

The three dimensional domain is modelled by a two-dimensional axisymmetric cross-section. The vertical axis of rotation is located at the pumping well. The medium consists of overlapped mobile and immobile domains, which have a uniform initial contaminant concentration of c_0. The mass transfer process between the mobile and immobile domain is described by a first-order mass transfer model. An ASR cycle consists of an injection, resting (storage) and extraction (recovery) phase. The groundwater velocity is assumed to be steady state at each phase and the transition period between the two phases is neglected [Harvey et al., 1994]. During the injection phase, freshwater is injected into the aquifer and a concentration front moves away from the pumping well. During the storage phase, no flow occurs but the concentration profile may be altered by mass transfer between the mobile and immobile domain. During the recovery phase, stored water is expected via the same pumping well and the concentration front moves toward the pumping well. For simplicity, we assume that the injection flow rate and the recovery rate are the same and the flow field is static during the storage phase. These assumptions are reasonable in practice and have been adopted in many other studies [e.g., Ward et al., 2007, 2008; 2009]. The RE is evaluated by setting a criterion of the average concentration of extracted water at the pumping well, such as the U.S. potable-water standard. In the absence of dispersion and mass transfer, i.e., advection is the only process, the ASR system is completely reversible and the RE is 1. With dispersion and mass transfer, the injection and extraction phase are not identically reversed and the RE is less than 1 because mixing enhancement due to dispersion and mass transfer is not reversible.

6.2.1 Governing Equations

In radial coordinates, the conceptual model can be described by one-dimensional dual domain advective-dispersive transport and a first-order mass transfer model [e.g., Bear, 1979; Chen, 1985]:

Mobile domain:

Injection and recovery phase:

$$\theta_m \frac{\partial c_m}{\partial t} + \theta_{im} \frac{\partial c_{im}}{\partial t} = \frac{1}{r} \frac{\partial}{\partial r} (\theta_m r \alpha_L |v| \frac{\partial c_m}{\partial r}) - \theta_m v \frac{\partial c_m}{\partial r} \qquad r > r_w \qquad (6.1)$$

Storage phase:

$$\theta_m \frac{\partial c_m}{\partial t} + \theta_{im} \frac{\partial c_{im}}{\partial t} = 0 \qquad r > r_w \qquad (6.2)$$

Immobile domain:

$$\theta_{im} \frac{\partial c_{im}}{\partial t} = \xi (c_m - c_{im}) \qquad r > r_w \qquad (6.3)$$

where t [T] is the time; r [L] is the radial distance from the well center; r_w [L] is the well radius; θ_m [-] and θ_{im} [-] are porosities of the mobile and immobile domain, respectively; c_m [M/L^3] and c_{im} [M/L^3] are dissolved solute concentrations in the mobile and immobile domain, respectively; α_L [L] is the longitudinal dispersivity; v [L/T] is the pore fluid velocity; ξ [$1/T$] is the first-order mass transfer rate coefficient.

The steady-state velocity is given by:

Injection and recovery phase: $v = \pm \frac{q}{2\pi\theta_m r}, \qquad r > r_w$ (6.4)

Storage phase: $v = 0$

where q [L^2/L] is the specific pumping rate (positive sign for injection and negative for extraction), defined as the flow rate per unit length of aquifer thickness. Substituting Eq. (6.4) into Eqs. (6.1) yields:

Injection phase: $\theta_m \frac{\partial c_m}{\partial t} + \theta_{im} \frac{\partial c_{im}}{\partial t} = -\frac{q}{2\pi r} \frac{\partial c_m}{\partial r} + \frac{q\alpha_L}{2\pi r} \frac{\partial^2 c_m}{\partial r}, \qquad r > r_w$ (6.5)

Recovery phase: $\theta_m \frac{\partial c_m}{\partial t} + \theta_{im} \frac{\partial c_{im}}{\partial t} = \frac{q}{2\pi r} \frac{\partial c_m}{\partial r} + \frac{q\alpha_L}{2\pi r} \frac{\partial^2 c_m}{\partial r}, \qquad r > r_w$ (6.6)

The boundary conditions are given by:

Injection phase: $c_m(r \to \infty, t) = c_{im}(r \to \infty, t) = c_0, \ (vc_m - \alpha_L v \frac{\partial c_m}{\partial r})\Big|_{r=r_w} = 0$

Extraction phase: $c_m(r \to \infty, t) = c_{im}(r \to \infty, t) = c_0, \ \frac{\partial c_m}{\partial r}\Big|_{r=r_w} = 0$ (6.7)

where c_0 [M/L^3] is the initial background concentration. Note that the boundary conditions for the extraction phase are different from the previous radial pumping problems [e.g., Chen and Woodside, 1998; Harvey et al., 1994], in which the concentrations at the infinite distance are 0, representing a finite contaminant plume length. This is because such problems only involved extraction phases with or without storage phase, which resulted in a trivial solution of concentration c_0 for an infinite plume. However, for ASR systems, such a problem does not occur because the

extraction phase always follow the injection and storage phases, which result in nonuniform concentration distributions at the beginning of extraction phases.

The initial conditions at the beginning of each ASR phase are defined as a function of the radial distance of the pumping well for both mobile and immobile domain:

$$c_m(r, t=0) = c_{m0}(r), \quad c_{im}(r, t=0) = c_{im0}(r), \tag{6.8}$$

where the time is reset for each ASR cycle. $c_{m0}(r)$ and $c_{im0}(r)$ are not constant functions and vary for different phases and different ASR cycles. For the first injection phase, $c_{m0}(r)$ and $c_{im0}(r)$ are equal to c_0.

6.2.2 Dimensional Analysis

We introduce the following dimensionless groups:

Concentration: $$c_m^* = \frac{c_m}{c_0}, \quad c_{im}^* = \frac{c_{im}}{c_0} \tag{6.9}$$

Spatial distance: $$R = \frac{r}{\alpha_L}, \; R_0 = \frac{r_w}{\alpha_L} \tag{6.10}$$

Mass transfer coefficients:

$$\text{Capacity ratio: } \beta = \frac{\theta_{im}}{\theta_m} \tag{6.11}$$

$$\text{Mass transfer timescale: } \tau_{im} = \frac{\theta_{im}}{\xi} \tag{6.12}$$

where $\tau_{im}\,[T]$ is a dimensional parameter.

ASR operational parameters:

$$\text{Time:}\quad \tau = \frac{t}{t_{im}} \tag{6.13}$$

$$\text{Pumping rate:}\quad \phi = \frac{\beta q}{\pi \alpha_L^2 \xi} \tag{6.14}$$

$$\text{Injection duration:}\quad T_i = \frac{t_i}{\tau_{im}} \tag{6.15}$$

$$\text{Storage duration:}\quad T_s = \frac{t_s}{\tau_{im}} \tag{6.16}$$

$$\text{Recovery duration:}\quad T_e = \frac{t_e}{\tau_{im}} \tag{6.17}$$

where t_i, t_s and t_e are the actual time periods of the injection, storage and extraction phase. All these time periods are normalized by the mass transfer timescale.

By substituting the velocity field given by Eq. (6.4) and the defined dimensionless groups into Eqs. (6.1) and (6.2), the governing equations for an ASR system can be transformed into:

Model domain:

$$\text{Injection phase:}\quad \frac{\partial c_m^*}{\partial \tau} + \beta \frac{\partial c_{im}^*}{\partial \tau} = \frac{\phi}{2R}\left(-\frac{\partial c_m^*}{\partial R} + \frac{\partial^2 c_m^*}{\partial R^2}\right),\ R > R_0\ \&\ 0 < \tau < \tau_i \tag{6.18}$$

$$\text{Storage phase:}\quad \frac{\partial c_m^*}{\partial \tau} + \beta \frac{\partial c_{im}^*}{\partial \tau} = 0,\qquad R > R_0\ \&\ T_i < \tau < T_i + T_e \tag{6.19}$$

$$\text{Recovery phase:}\quad \frac{\partial c_m^*}{\partial \tau} + \beta \frac{\partial c_{im}^*}{\partial \tau} = \frac{\phi}{2R}\left(\frac{\partial c_m^*}{\partial R} + \frac{\partial^2 c_m^*}{\partial R^2}\right),$$

$$R > R_0 \ \& \ T_i + T_s < \tau < T_i + T_s + T_e \qquad (6.20)$$

Immobile domain:

$$\frac{\partial c_{im}^*}{\partial \tau} = c_m^* - c_{im}^*, \qquad R > R_0 \qquad (6.21)$$

Correspondingly, the boundary and initial conditions become:

Injection phase: $c_m^*(R \to \infty, \tau) = c_{im}^*(R \to \infty, \tau) = 1$, $(c_m^* - \frac{\partial c_m^*}{\partial R})\Big|_{R=R_0} = 0$ (6.22)

Recovery phase: $c_m^*(R \to \infty, \tau) = c_{im}^*(R \to \infty, \tau) = 1$, $\frac{\partial c_m^*}{\partial R}\Big|_{R=R_0} = 0$

and

$$c_m^* = \frac{c_{m0}(r)}{c_0}, \ c_{im0}^* = \frac{c_{im0}(r)}{c_0} \qquad (6.23)$$

Our definition of dimensionless groups follows the previous study for intermittent extraction of contaminant plumes [Harvey et al., 1994]. Other dimensionless systems are also available for mass transfer models [e.g., van Genuchten and Wierenga, 1976; Goltz and Oxley, 1991]. The advantage of the defined dimensionless parameters is that the time is normalized by the mass transfer timescale, which is particularly useful for studying the storage phase. In addition, Eqs. (6.18)-(6.21) are also valid for linear rate-limited sorption processes by modifying dimensionless groups accordingly [Harvey et al., 1994].

6.2.3 Numerical Solution

Analytical solutions in the Laplace domain have been derived for radial injection and extraction problems [e.g., Chen, 1985, 1986, 1987; Chen and Woodside, 1998; Moench, 1989, 1995; Goltz and Oxley, 1991; Huang and Goltz, 2006; Huang et al., 2010]. Such analytical solutions have been used to analyze tracer tests in convergent and divergent radial flow fields [Novakowski, 1992; Moench, 1995; Becker and Charbeneau, 2000], decontamination by pumping with rate-limited sorption or mass transfer [e.g., Goltz and Oxley, 1991; Harvey et al., 1994], and single-well push-pull tracer tests [Huang et al., 2010]. For the injection and recovery phase, the proposed ASR model is a combination of radial dispersion in convergent and divergent flow fields and rate-limited mass transfer, which can be readily solved by modifying the available solution. For the storage phase, analytical solutions in time domain are given by [Harvey et al., 1994]:

$$c_m^*(\tau) = -\frac{\beta}{\beta+1}\left(c_{im0}^* - c_{m0}^*\right)\exp\left(-(\beta+1)\tau\right) + \frac{\beta c_{im0}^* + c_{m0}^*}{1+\beta} \tag{6.24}$$

$$c_{im}^*(\tau) = -\frac{\beta}{\beta+1}\left(c_{im0}^* - c_{m0}^*\right)\exp\left(-(\beta+1)\tau\right) + \frac{\beta c_{im0}^* + c_{m0}^*}{1+\beta} \tag{6.25}$$

where c_{m0}^* and c_{im0}^* are the initial concentrations at the beginning of the storage phase. In addition, numerical codes, such as MT3DMS and SUTRA, are also available for modeling axisymmertic solute transport by adjusting transport parameters to account for cylindrical geometry [Langevin, 2008]. In the present research, we use Matlab built-in *pde* and *ode* solvers to solve Eqs. (6.18-6.21), which yield satisfactory results comparing with analytical solutions.

6.3 Evaluation of ASR Performance

The performance of an ASR system is evaluated by the RE, which is defined as [Kimbler et al., 1975]:

$$\mathrm{RE} = \frac{V_r(c_m^*(R_0) < c_{crit}^*)}{V_i} \tag{6.26}$$

where V_r is the volume of recovered water through the pumping well that satisfies the predefined standard, i.e., the concentration of the extracted water is less than the critical concentration c_{crit}^*, and V_i is the total volume of injected freshwater. Certainly, RE increases with c_{crit}^*, i.e., more water can be recovered for lower-standard quality requirements. We here assume $c_{crit}^* = 0.1$, which represents that the initial contaminant concentration is 10 times of the criterion. During the recovery phase, if the extracted concentration becomes greater than c_{crit}^*, the pumping will be terminated because the extracted water will need further aboveground treatment.

Other than the critical concentration c_{crit}^*, which is a function of the initial contaminant concentration and the predefined criterion, RE is affected by both transport parameters, including dispersion and mass transfer coefficients, and ASR operational parameters, including durations of injection, storage and extraction phase and well flow rates. At a selected site, i.e., transport parameters are fixed, the optimization of ASR operational parameters is the major problem. Furthermore, due to rather stable seasonal fluctuations in freshwater resources availability, i.e., the durations of injection, storage and extraction phases are pretty constant, well pumping rates are the most flexible

parameters to control. For simplicity, we assume $t_i = t_i = t_e$, i.e., equal durations of injection, storage and extraction phase, representing a 4 month time period for each phase for a yearly-based ASR cycle. To analyze the ASR performance at different sites, we vary three dimensional parameters: β, T_i, and ϕ, in which β is controlled by the mass transfer capacity or the size of the immobile domain, T_i is influenced by the mass transfer timescale. i.e., the first-order mass transfer rate coefficient and the immobile porosity, given constant pumping periods, and ϕ is influenced by the well pumping rate, mass transfer coefficients and dispersivity.

6.4 Results and Discussion

6.4.1 Single ASR Cycle

Figure 6.2 shows the RE of a single ASR cycle at different β, T_i and ϕ. The tested parameter ranges are: $\beta \sim 10^{-1}$ - 10^{1} and $\phi \sim 10^{0}$ - 10^{5}, in which $\beta = 0.1$ represents a small portion of the immobile domain (~9%) and $\beta = 10$ a large portion of immobile domain (~91%) and $T_i = 0.1$ represents a large mass transfer timescale comparing with pumping periods and a small transfer rate coefficient and $T_i = 10$ represents a small mass transfer timescale and a large mass transfer rate coefficient. The major information summarized by Figure 6.2 is summarized in the following:

1. The RE increase with the well pumping rate given β and T_i for cases with non-zero RE because higher pumping rates imply more freshwater injected into the contaminated aquifer within a same injection period and the plum will be diluted.

2. In many combination of β and T_i, the RE remains zero, i.e., no recovered water satisfies the predefined standard, c^*_{crit} = 0.1, within the wide tested range of ϕ. However, no clear pattern of β and T_i can be observed for zero RE from Figure 6.2.

3. At a small β, e.g., β = 0.1, the RE increases with T_i at the same ϕ, implying a faster mass transfer rate yields a higher RE for a small immobile domain. However, such behavior is not consistent with the increase of β. For example, at β = 0.5, the RE of T_i = 0.1 is greater than that of T_i = 1.

4. At a large T_i. e.g., T_i = 10, the RE decreases with β, implying a larger immobile domain yields a lower RE for a fast mass transfer rate coefficient. At low T_is, the cases of zero RE do not show a consistent pattern.

6.4.1.1 Zero and non-zero RE

Understanding the pattern of cases with zero RE is an essential problem for ASR design because it identifies specific conditions inappropriate for ASR. According to the zero-gradient boundary condition at the well during the extraction phase, the concentration of extracted water is identical to the concentrations at adjacent locations. RE = 0 implies that after the storage phase the concentration at such adjacent locations are greater than c^*_{crit} so than no freshwater can be extracted. Consider such an adjacent point, R_0^+, with an infinitesimally small distance to the well boundary. During the injection phase, we assume that the concentration at this point will quickly change to

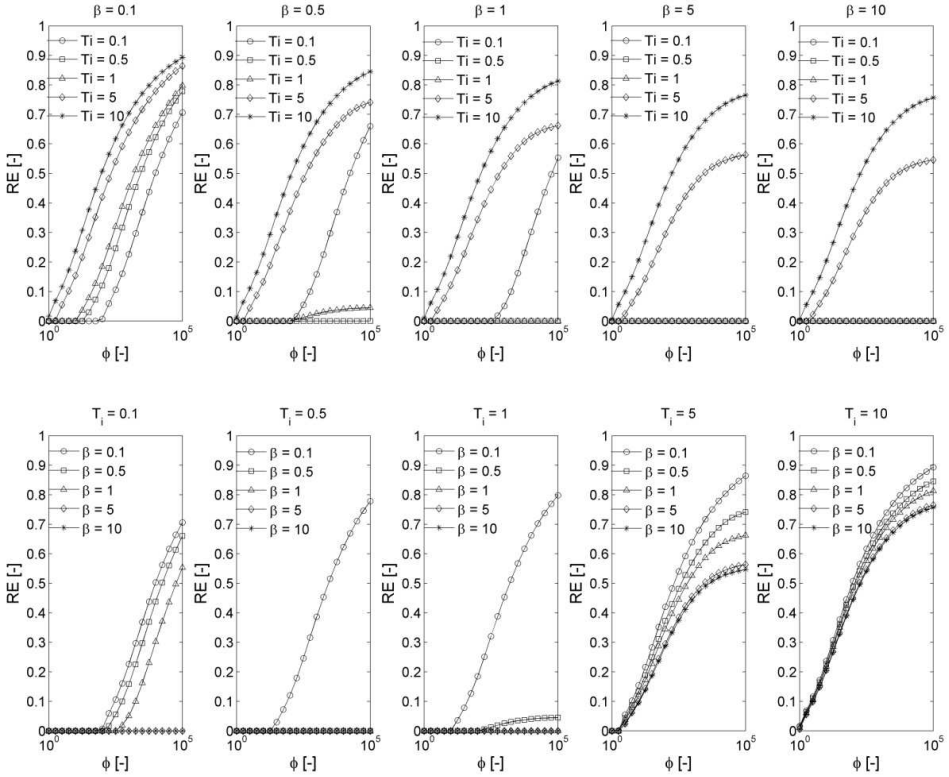

Figure 6.2 Recovery efficiency (RE) for a single ASR cycle at various mass transfer parameters and pumping operational parameters.

zero as a result of freshwater flushing at a large flow rate. Thus, the immobile concentration history at this point during the injection phase is governed by the following equation:

$$\frac{\partial c_{im}^{*}(R_0^{+})}{\partial \tau} = -c_{im}^{*} \tag{6.27}$$

which yields

$$c_{im}^{*}(R_0^{+}) = \exp(-\tau) \tag{6.28}$$

and the initial condition for the subsequent storage phase is:

$$c_{m0}^{*} = 0 \tag{6.29}$$

$$c_{im0}^{*} = \exp(-T_i) \tag{6.30}$$

Substituting Eqs. (6.29) and (6.30 into (6.24) yields the concentration at the end of the storage phase:

$$c_{m}^{*}(R_0^{+}, T_i + T_s) = \frac{\beta}{1+\beta}\exp(-T_i)\{1 - \exp[-(1+\beta)T_s]\} \tag{6.31}$$

Thus, for a non-zero RE, the ASR system must satisfy

$$\frac{\beta}{1+\beta}\exp(-T_i)\{1 - \exp[-(1+\beta)T_s]\} < c_{crit}^{*} \tag{6.32}$$

This is a simple relationship that can be applied to evaluate the applicability for a single ASR cycle. For the proposed case, $T_i = T_s$ and $c^*_{crit} = 0.1$, we have:

$$c^*_m(R_0^+, T_i + T_s) = \frac{\beta}{1+\beta}\exp(-T_i)\{1-\exp[-(1+\beta)T_s]\} < 0.1 \tag{6.33}$$

Figure 6.3 shows the contour lines of $c^*_m(T_s)$ as a function of β and T_i. The area contained by thick contour line of 0.1 indicates the regions of β and T_i that will yield zero RE. All simulated cases in Figure 6.2 are shown by " + ". There is no exception that all the cases with zero RE fall into area contained by 0.1 contourline and all the cases with no-zero RE are located outside of this area. Thus, the simple Inequality (6.32) provides an efficient approach for determining the likelihood of single ASR cycle being successful. Furthermore, Inequality (6.32) gives operational guidance for ASR systems: (1) Inequality (32) does not involve the well pumping rate, indicating that increasing the well pumping rate is not an effective way for improving the RE within a single ASR cycle at aquifers falling into the zero-RE area shown in Figure 6.3; and (2) there are two ways to convert a zero-RE cases to a non-zero RE case by increasing the injection period, which yields a longer mass transfer duration to deplete contaminant in the immobile domain, and by decreasing the storage period, which yields a shorter mass transfer duration for the higher concentration in the immobile domain entering the low-concentration mobile domain. Essentially, the effective ways are to move the points inside the zero-RE are in Figure 6.3 vertically. In addition, if the concentration at the end of the injection phase is greater than c^*_m, decreasing the storage period is not effective.

Finally, Figure 6.3 also shows that a lower c_m^* yields a larger zero-RE area. An aquifer with a fast mass transfer rate coefficient, i.e., a larger T_i, or a small immobile domain, i.e., a small β, is generally appropriate for ASR. Thus, for aquifers without mass transfer or with equilibrium (i.e., instantaneous) mass transfer, we can always have a positive RE.

6.4.1.2 Effects of Mass Transfer Parameters

Given the same ASR operational strategies, i.e., constant well flow rate q and phase durations (t_i, t_s and t_e), the RE is controlled by the mass transfer parameters, including capacity ratio β and mass transfer timescale τ_{im}, and the dispersivity α_L. According to the dimensionless groups, the effect of dispersivity is opposite to the well flow rate: a larger dispersivity yields a lower RE because more freshwater is contaminated due to enhanced mixing. In the following, we consider constant ASR operational parameters and dispersivity and examine the transferability of an ASR strategy to aquifers with different mass transfer parameters by varying β and T_i (Note T_i is controlled by τ_{im} for constant t_i).

With the same flow rate and dispersivity, the RE is ultimately controlled by the mobile concentration at the adjacent points to the well boundary at the end of the storage phase, described by Eq. (6.31). That is, a lower c_m^* (T_i + T_s) yields a higher RE and a higher c_m^* (T_i +T_s) a lower RE. Taking derivatives of Eq. (6.33) with respect to β and T_i (We assume T_i= T_s), we have:

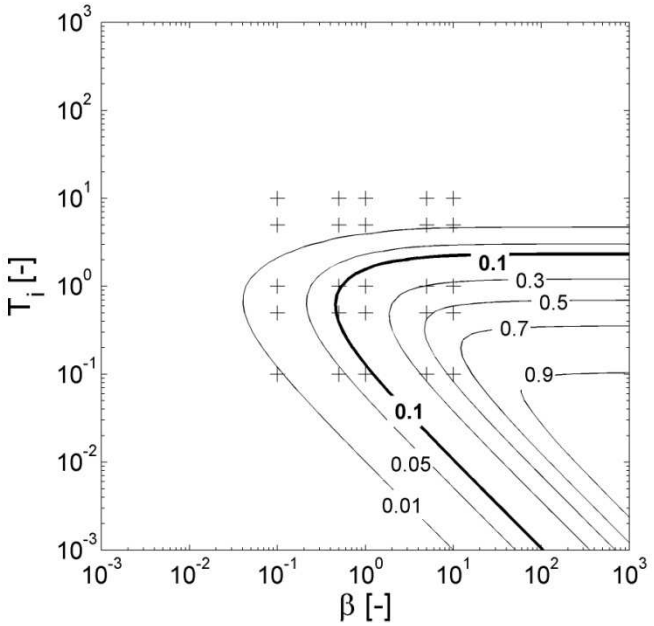

Figure 6.3 Concentration in the mobile domain after the storage phase for a single ASR cycle. Contour lines represent predefined concentration criteria. "+" indicates the numerical case evaluated.

$$\frac{\partial c_m^*(R_0^+, T_i + T_s)}{\partial \beta} = \frac{1}{(1+\beta)^2}\exp(-T_i)\{1-\exp[-(1+\beta)T_i]\}$$

$$+\frac{\beta T_i}{1+\beta}\exp(-T_i)\exp[-(1+\beta)T_i] > 0 \tag{6.34}$$

$$\frac{\partial c_m^*(R_0^+, T_i + T_s)}{\partial \beta} = \frac{\beta}{1+\beta}\{(2+\beta)\exp[-(2+\beta)T_i] - \exp(-T_i)\} \tag{6.35}$$

Thus, for constant mass transfer timescale, $c_m^*(R_0^+, T_i + T_s)$ always increases with β, resulting in a decreasing RE as shown by Figure 6.2. For a constant β, let $\frac{\partial c_m^*(R_0^+, T_s)}{\partial \beta} = 0$. We obtain a critical T_i,

$$T_{crit} = \frac{\ln(2+\beta)}{1+\beta} \tag{6.36}$$

and

$$\frac{\partial c_m^*(R_0^+, T_i + T_s)}{\partial \beta} > 0, \text{ if } T_i < T_{crit} \tag{6.37}$$

$$\frac{\partial c_m^*(R_0^+, T_i + T_s)}{\partial \beta} < 0, \text{ if } T_i < T_{crit} \tag{6.38}$$

Thus, the changing pattern of $c_m^*(R_0^+, T_i + T_s)$ with the mass transfer timescale or mass transfer rate coefficient is not monotonic.

Figure 6.4 shows that T_{crit} decreases with β and the concentration gradient nonmonotonically changes with T_i. Figure 6.4a identifies the specific cases shown in Figure 6.2. For β = 0.5, T_{crit} = 0.61. Thus, Figure 6.2 shows a decrease of RE from T_i = 10 to T_i = 1 (negative concentration gradient in Figure 6.4b) and then an increase to T_i = 0.1 (positive concentration gradient in Figure 6.4b). In fact, this non-monotonic behavior always occurs in the presence of mass transfer. Consider two limiting cases: one with an extremely high T_i and the other nearly 0. The high T_i represents a small mass transfer timescale or a very large mass transfer rate coefficient. Thus, the kinetic mass transfer process becomes equilibrium and the transport problem may be described by an advection-dispersion equation with a retardation factor. On the other hand, the low T_i case implies a large mass transfer timescale or a very small transfer rate coefficient. In such cases, mass transfer may be neglected and the transport problem may be simplified into an advection-dispersion equation. Both limiting cases will yield high RE and T_{crit} is the turning point between them.

Figure 6.5 shows the concentration profiles for the cases with β = 0.5 and different T_i at the same well flow rate and pumping durations. During the injection phase, the immobile domain serves as a contaminant source for all cases. However, immobile concentrations drop significantly for T_i = 10 due to fast mass transfer and remain high levels for T_i = 0.1due to slow mass transfer. During the storage phase, the mobile concentration rebounds as a result of mass transfer from the immobile domain with higher concentrations. By the end of the storage phase, mobile and immobile

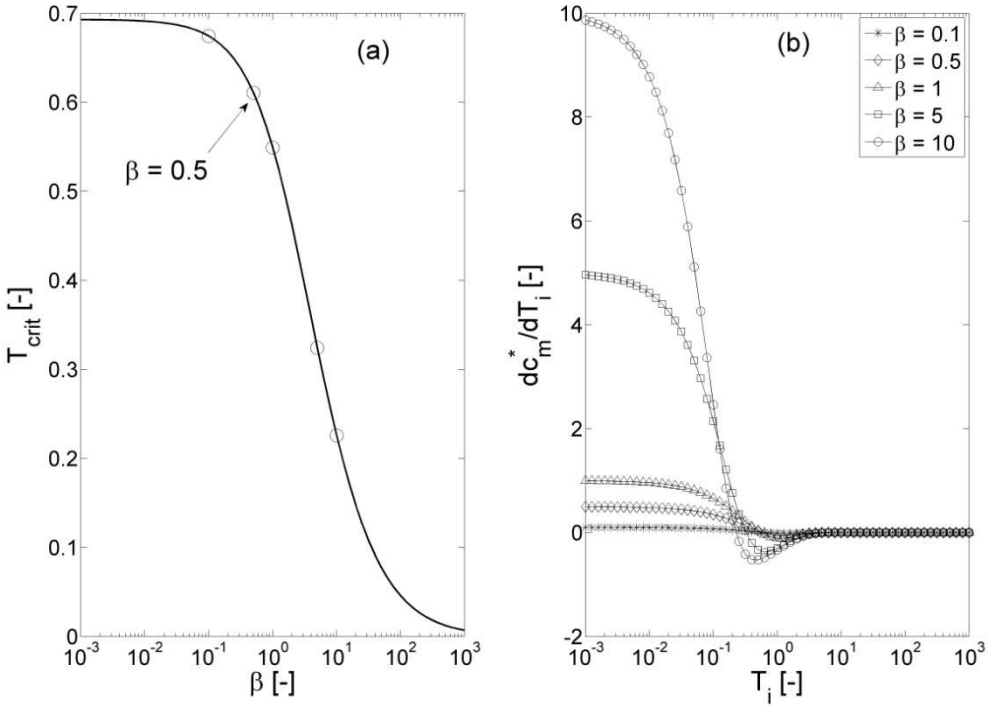

Figure 6.4 Critical timescale at different capacity ratio and sensitivity of concentration at the pumping well to the dimensionless timescale.

concentrations reach equilibrium for T_i = 10, while there remain small and significant concentration differences for T_i = 1 and T_i = 0.1, respectively. As a result of the equilibrium concentrations, the immobile domain always serves as a sink during the recovery phase for T_i = 10, which has positive impact on the RE. For T_i = 1, the immobile domain initially as a contaminant source and then as a sink after the plume front in the mobile domain passes. By contrast, the immobile domain mostly serves as a contaminant source near the pumping well for T_i = 0.1. However, such negative impact on the RE may not be significant because of slow mass transfer rates. That is, the overall effect on the RE is an integral result of both immobile domain functions and mass transfer rates. With the increase of T_i, the immobile domain transforms from a contaminant source to a sink, but the increased mass transfer rate may enhance the negative impact from the function as a contaminant sink. The critical value of T_{crit} reflects a turning point when the immobile domain functions and mass transfer rate reach a certain balanced state.

Inequalities (6.37) and (6.38) also provide very useful operational guidance for ASR systems. At a selected site with $T_i > T_{crit}$, one may need to increase the injection duration significantly in order to achieve an improved RE. A slight increase may even result in a lower RE. Furthermore, Eq. (6.36) yields the range (0, ln 2) for T_{crit}, which implies that if the injection duration satisfies $t_i > \ln 2\,\tau_{im}$ (or $t_i > 0.6931\,\tau_{im}$), increasing pumping duration is an effective approach for improving RE. $\ln 2\,\tau_{im}$ is known as the half life of mass transfer, i.e., the time period for the concentration to decay to one half

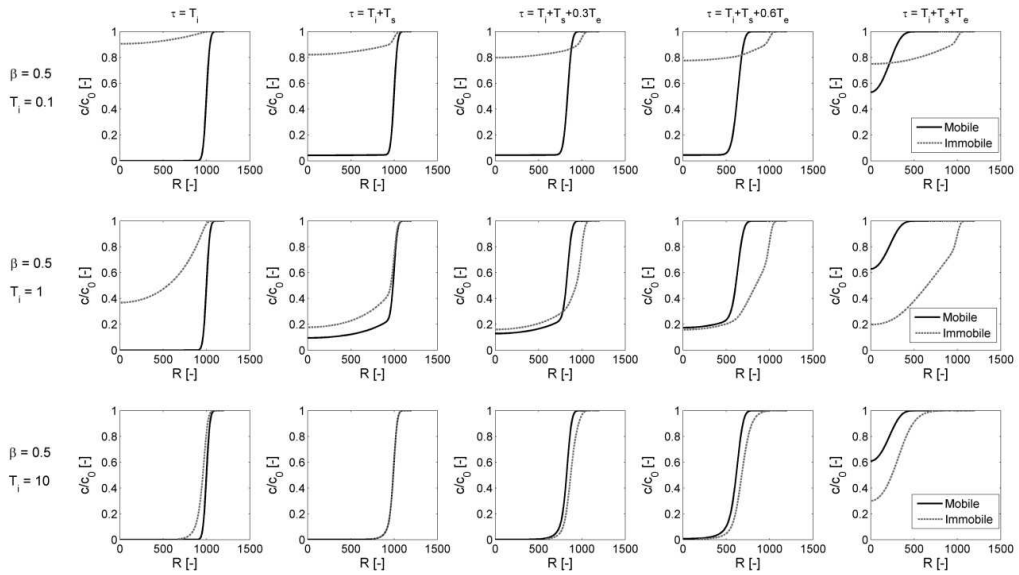

Figure 6.5 Concentration profiles during a single ASR cycle at different mass transfer timescale or injection duration.

of its initial value by assuming first-order decay. Thus, increasing pumping period is effective when the period is greater than the half life of mass transfer.

6.4.2 Multiple ASR Cycles

Figure 6.6 shows a typical concentration history at the pumping well during multiple ASR cycles for specified parameters. For injection phases, the concentration remains zero as a result of freshwater flushing. During the first three ASR cycles, no water can be recovered because at the end of the storage phase the concentration is greater than the predefined standard due to mass transfer from the immobile domain. Thus, recovery phases during the first three cycles actually function as storage phases. From the fourth cycle, the mobile concentration drops below the standard at the end of the storage phase so that freshwater can be withdrawed from the pumping well until the concentration rises to the standard. The withdrawal period during the recovery phase increases with the ASR cycle, representing that the RE increases with the ASR cycle. The immobile domain functions as a contaminant source at the early ASR cycles, and gradually transforms into a contaminant sink during the recovery phase. In general, the RE of an ASR system improves with ASR cycles and a zero-RE ASR because multiple ASR cycles essentially increase the injection duration and total injected freshwater. Here, we are particularly interested in how many ASR cycles are necessary for such a transformation.

To determine the number of needed ASR cycles for a system to transform from a zero RE to a non-zero RE, we still focus on the adjacent points to the well boundary.

Because no water can be extracted for an ASR system with a zero RE, the actual storage duration is actually the sum of the designed storage phase and recovery phase. By the end of such a cycle, the mobile and immobile concentration are:

$$c^*_{m,n-1}(R_0^+, T_i + T_s + T_e) = c^*_{im0,n-1} \exp(-T_i) \frac{\beta}{1+\beta} \{1 - \exp[-(1+\beta)(T_s + T_e)]\} \tag{6.39}$$

$$c^*_{im,n-1}(R_0^+, T_i + T_s + T_e) = c^*_{im0,n-1} \exp(-T_i) \frac{1}{1+\beta} \{\beta - \exp[-(1+\beta)(T_s + T_e)]\} \tag{6.40}$$

where $c^*_{m,n-1}$ and $c^*_{im,n-1}$ are the mobile and immobile concentration during the (n - 1)th ASR cycle, and $c^*_{im0,n-1}$ is the initial immobile concentration of the nth cycle. Thus, at the end of the storage phase of the nth cycle, we have:

$$c^*_{m,n}(R_0^+, T_i + T_s) = \exp(-T_i) \frac{\beta}{1+\beta} \{1 - \exp[-(1+\beta)T_s)]\}$$

$$\left\{ \exp(-T_i) \frac{\beta}{1+\beta} \{\beta + \exp[-(1+\beta)(T_s + T_e)]\} \right\}^{n-1} \tag{6.41}$$

A non-zero RE for the nth cycle requires:

$$c^*_{m,n}(R_0^+, T_i + T_s) < c^*_{crit} \tag{6.42}$$

By assuming $T_i = T_s = T_e$, we have:

$$c^*_{m,n}(R_0^+, T_i + T_s) = \exp(-T_i) \frac{\beta}{1+\beta} \{1 - \exp[-(1+\beta)T_i]\}$$

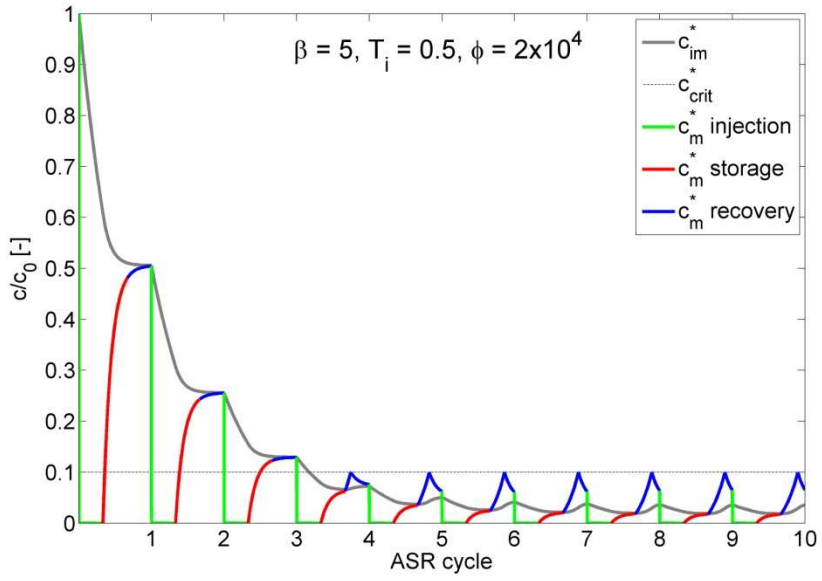

Figure 6.6 Concentration history at the pumping well for multiple ASR cycles.

$$\left\{\exp(-T_i)\frac{1}{1+\beta}\{\beta+\exp[-2(1+\beta)T_i]\}\right\}^{n-1} \tag{6.43}$$

which yields

$$n > 1+\left\{-T_i+\ln\left[\frac{1}{1+\beta}\{\beta+\exp[-2(1+\beta)T_i]\}\right]\right\}^{-1}\ln\left\{\frac{1+\beta}{\beta}\frac{\exp(T_i)}{1-\exp[-(1+\beta)T_i]}c^*_{crit}\right\} \tag{6.44}$$

Figure 6.7 shows the areas with zero RE and non-zero RE delineated by the contourlines of the mobile concentration at the end of the storage phase of the *n*th cycle. The subplot of cycle 1 is identical to Figure 6.3. With the increase of ASR cycles, the area with zero RE, i.e., the area contained by the contourline of 0.1becomes smaller and more tested cases, "+" symbols, all outside of the area. At cycle 7, all the tested cases, expect the one with $\beta = 10$ and T_i = 0.1, should have non-zero RE at a large pumping rate. In addition, the area with zero RE shrinks with ASR cycles, but the shape of the contourlines remains similar, indicating that the effects of mass transfer and operational parameters on multiple ASR cycles may be similar to those identified in the single ASR cycle. Actually, taking derivatives of Eq. (6.43) with respect to n, β , and T_i, respectively, we can also obtain $\frac{\partial c^*_m(R_0^+, T_i+T_s)}{\partial n} < 0$ for $n \geq 2$, $\frac{\partial c^*_m(R_0^+, T_i+T_s)}{\partial \beta} > 0$, and a critical value, $T_{crit}(n,\beta)$, by setting $\frac{\partial c^*_m(R_0^+, T_i+T_s)}{\partial T_i} = 0$. Thus, the RE improves with ASR cycles, decreases with capacity ratio, and exhibits non-monotonic behavior in

terms of mass transfer timescale and injection duration. Figure 6.8 shows that the critical timescale decreases with ASR cycle and all cases with different β approach a low value of 0.0405 according to our numerical solution. In addition, T_{crit} is a monotonic, decreasing function of β at first cycle, a non-monotonic function at intermediate cycles, and a monotonic, increasing function at late cycles.

Figure 6.9 shows the contoured areas for the required cycles to achieve a non-zero RE. For $\beta \le 1$, all the tested cases should expect a non-zero RE within two ASR cycles. For a large capacity ratio, i.e., $\beta = 5$ and 10, more ASR cycles are required for slow mass transfer cases. In particular, the case with $\beta = 10$ and T_i = 0.1 requires more than 10 cycles.

Figure 6.10 shows the numerically-simulated RE for $\beta = 5$ at a constant ϕ. For large mass transfer rate coefficients, i.e., T_i = 5 and 10, the first ASR cycle has a non-zero RE. For T_i = 1, 0.5, and 0.1, it requires 2, 4, and 7 ASR cycles, respectively. The result is consistent to that shown by Figures 6.6, 6.7 and 6.9.

6.5 Summary and Conclusion

ASR is an effective strategy for sustainable management of water resources, but its efficiency may be limited by kinetic mass transfer caused by contaminant sorption and dual-domain behavior of subsurface media. A numerical model is developed for simulating ASR performance by combining the convergent and divergent dispersion models with a first-order mass transfer model. More importantly, by analyzing the

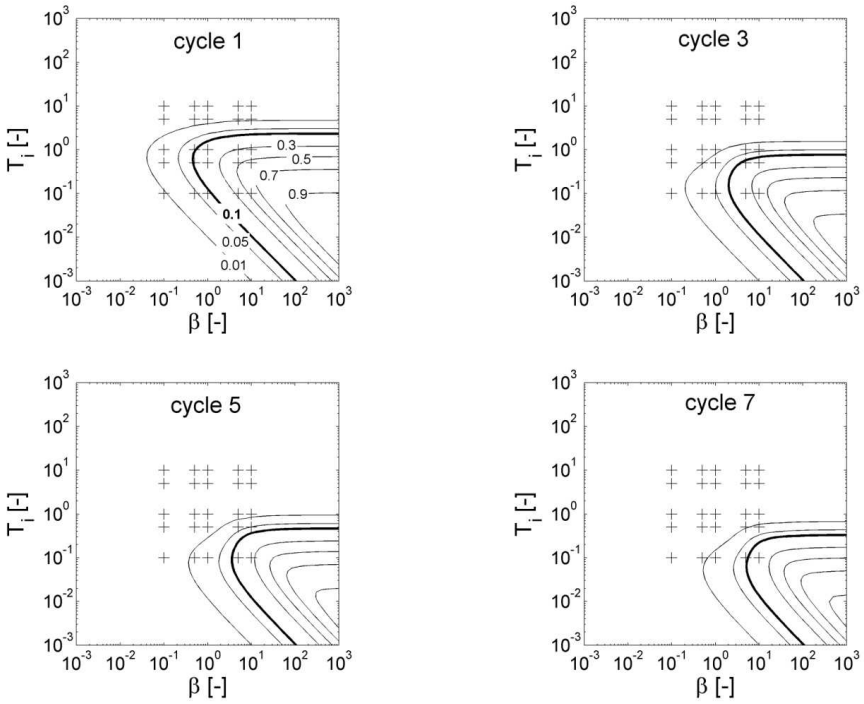

Figure 6.7 Evolution of zero-RE cases with ASR cycles as a function of mass transfer parameters.

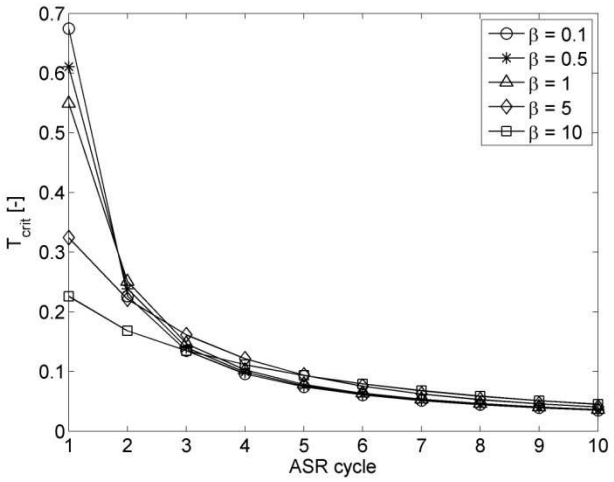

Figure 6.8 Critical timescale at multiple ASR cycles.

concentration history at the pumping well, simple relationships between mass transfer parameters and ASR operational parameters are derived for understanding ASR performance and improving its efficiency. Several practical and useful contour figures are generated based on such relationships for delineating the ranges of mass transfer parameters and the necessary ASR cycles that may yield effective and efficient ASR performance. The developed numerical model and analyzed results provide very useful and practical guidance for determining a potential ASR site with mass transfer limitations and optimizing ASR operations. The main conclusions that can drawn from the analysis are follows:

1. Increasing well pumping rates may yield higher RE for a single ASR cycle. but usually does not transform an ASR system from zero RE to non-zero RE.

2. RE decreases with the mass transfer capacity ratio, i.e., a large immobile domain or sorption capacity often undermines the ASR efficiency.

3. The effect of mass transfer rate coefficients and the injection period on the ASR efficiency is not monotonic. A critical value, T_i, may be defined for both single and multiple ASR cases. When the injection period is greater than such a critical value, increasing injection period results in a higher RE. Contrarily, when the injection period is less than the critical value, increasing the injection period may even yield a lower RE.

4. ASR efficiency improves with multiple ASR cycles and the required cycles for a zero-RE ASR in a single cycle to transform into a non-zero RE is derived as a function of mass transfer parameters and the durations of injection, storage and recovery phases.

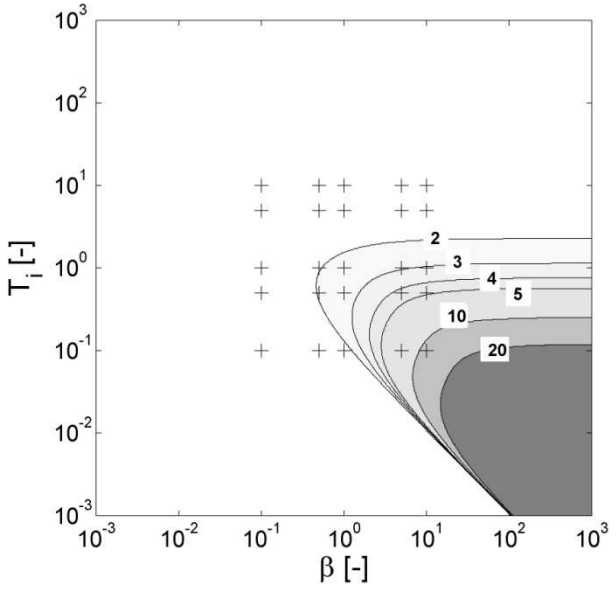

Figure 6.9 Required number of ASR cycles for achieving a non-zero RE.

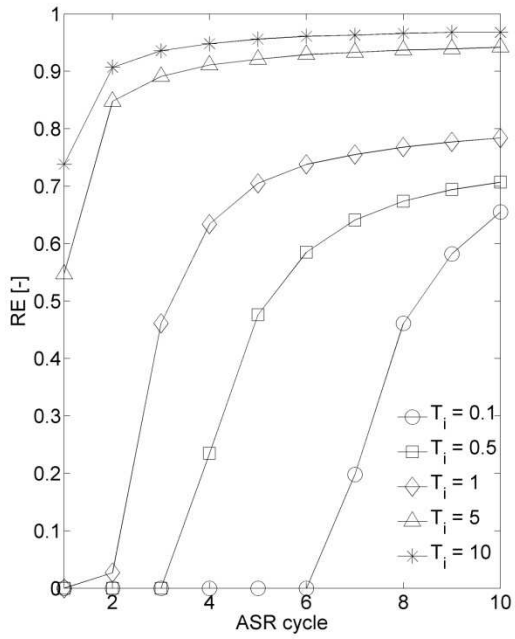

Figure 6.10 RE improvement with ASR cycles for β=5 and $\phi = 1x10^5$.

5. The immobile domain may function as a contaminant source or sink or both during the recovery phase. In aquifers with large capacity ratio and slow mass transfer, the immobile domain may serve as a long-term contaminant source that causes negative impacts on ASR efficiency. By contrast, in aquifers with small capacity ratio and fast mass transfer, concentrations in the mobile and immobile domain may quickly reach equilibrium at the end of storage phase so that the immobile domain mostly serves as a contaminant sink, which improves the RE. With the increase of ASR cycles, the immobile domain will eventually transform from a contaminant source to a sink.

Our primary analyses rely on the concentration history at the pumping well, which are based on the following assumptions: (1) steady-state flow in each phase and no transitional period between them; and (2) relative fast flow so that the concentration at the pumping well quickly drops to zero. Thus, although the proposed numerical model require homogeneous aquifers, the analyzed results, such as Figure 6.3, 6.7 and 6.9, may also be valid for heterogeneous aquifers.

CHARPTER 7

CONCLUSIONS

This thesis investigated the effects of kinetic mass transfer and aquifer stratification on mixing-zone development, respectively. In addition, recovery efficiency of aquifer storage and recovery in aquifers with kinetic mass transfer limitation has been studied. The main conclusions are given below:

(1) Both the scaled-tank model and the field model show that the combination of the moving mixing zone and kinetic mass transfer may significantly enhance the extent of mixing and create a wider mixing zone than the models without kinetic mass transfer. In addition, sensitivity analyses indicate that a larger capacity ratio (immobile porosity/mobile porosity) of mass transfer leads to a wider mixing zone, and the maximum width of the mixing zone may be reached for a given capacity ratio when the mean retention timescale in the immobile domain (the reciprocal of mass transfer rate) and the period of water-level fluctuations are comparable

(2) Mixing zone enhancement is mainly controlled by the unsynchronized behavior of concentration distributions in the mobile and immobile domain. Such behavior is maximized at the aquifer bottom when the retention time scale in the immobile domain is comparable to the period of freshwater level fluctuations, resulting in a thicker mixing zone. Kinetic mass transfer may alter the time lag between periodic freshwater level fluctuations and the movement of the mixing zone, causing the expansion and

contraction of the mixing zone. That is, the effect of mixing enhancement by kinetic mass transfer may be nonuniform in the mixing zone, and the mixing zone thickness may vary significantly within a period. By contrast, large dispersion coefficients may create thicker mixing zones, but may not cause such unsynchronized behavior and alter the time lags of different concentration contour lines. As a result, the mixing enhancement is rather uniform in the mixing zone. The dynamics of mixing-zone development is sensitive to the flow velocity, which is influenced by the hydraulic conductivity, amplitude of the freshwater level fluctuations, and the capacity ratio of kinetic mass transfer.

(3) Both numerical and laboratory experiment results showed that under steady-state conditions, mixing is significantly enhanced in a layer with a lower hydraulic conductivity when it lies above a layer with a higher hydraulic conductivity. The increased mixing-zone width is primarily the result of refraction of recirculated saltwater and recharged fresh groundwater. Under transient conditions created by tidal activities, the mixing zone only slightly changes compared with the steady-sate case. However, mixing-zone development is significantly influenced by long-term freshwater level fluctuations, which may create the movement of the mixing zone. Furthermore, aquifer stratification may lead to unsynchronized movement of the mixing zone in different layers. In cases where a preferential-flow lies above a low-permeable layer, the unsynchronized movement may result in density gradient and enhanced mixing between layers.

(4) By analyzing the concentration history at the pumping well, we obtain simple and effective relationships for investigating ASR efficiency under various mass transfer parameters, including capacity ratio and mass transfer timescale, and operational parameters, including injection durations and well pumping rates. Based on such relationships, one can conveniently determine whether a site with mass transfer limitations is appropriate or not for ASR and how many ASR cycles are required for achieving a positive RE. Results indicate that the immobile domain may function as a contaminant source or sink or both during the recovery phase, and RE usually improves with well flow rate, the decrease of capacity ratio, and the ASR cycles. However, RE is a non-monotonic function of the mass transfer timescale and the injection duration. A critical timescale is given for quantifying this non-monotonic behavior. When the injection period is greater than such a critical value, increasing the injection period results in a higher RE. By contrast, when the injection period is less than the critical value, increasing the injection period may even yield a lower RE.

CHARPTER 8

LIMITATIONS AND IMPLICATIONS

8.1 Limitations of the Studies

When studying the coupled effects of kinetic mass transfer and seasonal freshwater level fluctuations on the mixing-zone development, a first-order dual domain mass transfer model is used to describe mass transport behavior. The main reason for us to choose this model is due to its simplicity. In fact, there are several other mass transfer models available such as multi-rate mass transfer model, which accounts for heterogeneous mass transfer processes. It is more likely that a variety of rate-limited mass transfer processes occur in heterogeneous media due to both diffusion and slow advection. On the other hand, the model presented in this topic did not consider heterogeneities of hydraulic properties. Later studies have shown that layered heterogeneity may bring significant impacts on the profile of the mixing zone. Furthermore, a triangular, periodic function is defined to describe seasonal freshwater level fluctuations. In reality, fluctuations of freshwater level may be more complicated than a single function. Finally, when considering seasonal freshwater level fluctuations, tidal and wave activities are neglected in our study, which may bring some slight effects on the mixing-zone development.

When investigating aquifer stratification effects on the mixing-zone development, we only assumed a simple and perfect stratified aquifer. In field conditions, stratified

aquifer may be more complex than those assumed. Moreover, when we study aquifer stratification, other effects such as mass transfer are not considered.

There are also some limitations in the topic of ASR. Firstly, regional groundwater gradient is not considered in the study, which may result in an asymmetric freshwater cone and affect the recovery efficient of an ASR system [Ward et al., 2009]. Secondly, fluctuations of the freshwater level are neglected. Furthermore, density effects are not considered in the study. The coupled effects of density and kinetic mass transfer will be investigated in the future research. Finally, as indicated above, only a simple first order dual-domain mass transfer model is employed due to simplicity.

8.2 Implications of the Studies

Our studies have shown that kinetic mass transfer may widen a moving mixing zone. This finding expands our understanding of wide mixing zones found in coastal aquifers. Wide mixing zone may affect the impact area during seawater intrusion and also saltwater upcoming process of a pumping well. Furthermore, wide mixing zone reflects the variation of components of submarine groundwater discharge. Most importantly, a wide mixing zone may have significant impacts on coastal geochemical transport processes. On the other hand, a time lag is found between freshwater level fluctuations and mixing zone fluctuations. This time lag is found to be three months for no mass transfer case, which is exactly the same as the time lag between freshwater recharge and the fluctuations of SGD components. However, mass transfer effects may alter the time lag between freshwater level fluctuations and mixing zone fluctuations.

Therefore, it is expected that mass transfer effects may change the time lag between freshwater recharge and the fluctuations of SGD components.

Our studies also have indicated that aquifer stratification may lead to a wide mixing zone under both steady state and transient flow conditions. Specifically, the results have demonstrated that wide steady-state mixing zone can be resulted by flow refraction from a lower K layer into a higher K. However, the refraction law equation can not be applied to the variable density systems. The topic of flow refraction in coastal aquifers is worthy of further study. The presence of aquifer stratification would alter the timescales of both freshwater discharge and salt recirculation, and thus SGD components. Furthermore, aquifer stratification may significantly change the land-induced contaminant transport processes in coastal aquifers. On the other hand, a wide mixing zone can be developed in a stratified aquifer under transient flow conditions due to unsynchronized movement of mixing zones in different layers. In addition, even if the system is affected by an instantaneous fluctuation of freshwater level, it will need a long period to reproduce the steady state condition. Therefore, transient flow conditions may not be easily neglected in the future studies.

The study results of ASR have demonstrated that mass transfer may have significant impacts on the RE. Some parameter combination will yield a zero RE and other a non-zero RE. Therefore, when an ASR system is installed in an aquifer with significant mass transfer effects, our results can be used to first evaluate zero or non-zero RE of the ASR system. Also, the results can be employed to find the number of the ASR cycle in which water can be pumped out for the first time.

CHARPTER 9

FUTURE RESEARCH DIRECTIONS

Mixing in coastal subsurface environments has significant impacts on various flow and transport processes. Despite substantial past studies, many specific problems related to mixing in coastal hydrogeologic systems still remain unresolved. In the future, further investigations are needed to address mixing problems including both physical and geochemical aspects by using analytical, numerical and experimental methods.

The mixing problems existing in coastal aquifer systems are involved in various problems, such as mixing-zone development, submarine groundwater discharge, aquifer storage and recovery, saltwater upcoming, and contaminant transport. These practical problems are affected by site-specific hydrogeologic parameters and anthropogenic activities. Seasonal freshwater level fluctuations, aquifer stratification and kinetic mass transfer effects, among others, are worthy of further study in the future research, as they have been found to be significantly affect the flow and transport in coastal aquifers. The specific future research topics are detailed below:

9.1 Mixing-Zone Development

a. The mechanisms response for wide mixing zones in coastal aquifers are complex, which are still worthy further study. We have used numerical simulations to show the effects of kinetic mass transfer on a moving mixing zone. The subsequent work is to use the laboratory experimental method to visualize this effect on the mixing zone. To

produce the kinetic mass transfer effects, dye with some sorption on the sands will be chosen. So far, we have conducted a preliminary experiment for the mixing zone under coupled effects of mass transfer and transient flow condition (See Figure 9.1).

b. We also have shown by numerical methods that transient flow may have significant effects on a mixing zone in a stratified aquifer due to unsynchronized movement of the mixing zones in different layers. Therefore, the laboratory experimental method will also be used to visualize the mixing zone in a stratified aquifer under transient flow conditions. In addition, I will study how the magnitude of stratified heterogeneity affects the transport processes.

c. Previous studies have shown that random heterogeneity only develop an irregular steady-state mixing zone. I will investigate effects of random heterogeneity on a moving mixing zone. It is expected that the mixing zone can also be widened. Particularly, connected field of high or low hydraulic conductivity is of great interest in the future studies.

9.2 SGD

SGD has been recently regarded as an important process that controls coastal subsurface biological and ecological environments. Our studies have shown that mass transfer, aquifer stratification, and long-term freshwater level fluctuations would bring significant effects on the mixing-zone development. Therefore, these factors may further bring some effects on SGD. The specific research topics will include:

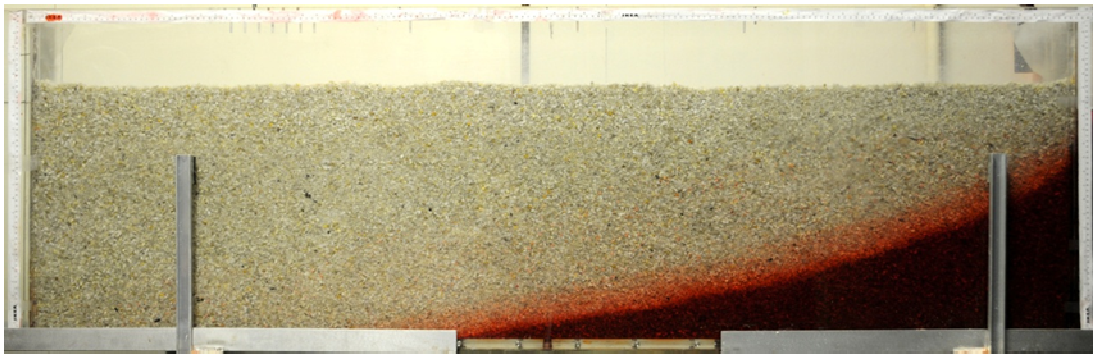

Figure 9.1 The mixing zone under coupled effects of mass transfer and transient flow condition.

a. Numerical simulations will be conducted to investigate effects of kinetic mass transfer and transient flow conditions on the SGD. Particular interests are the time lag between freshwater level fluctuation, mixing-zone fluctuation, and SGD fluctuation.

b. Another interest topic is the effects of aquifer stratification on SGD. We have observed the significant effects of aquifer stratification on the recirculated streamlines, which indicates that aquifer stratification would affect the constituent of SGD.

c. One important constituent of SGD is freshwater discharge. I will use laboratory experimental method to visualize freshwater discharge. Particularly, I will also conduct some experiments to visualize the streamline refraction in the stratified media.

9.3 ASR

a. We have studied the effects of mass transfer on recovery efficiency of ASR. Future research will investigate the coupled effects of mass transfer and density effects on recovery efficiency of ASR.

b. To enhance recovery efficiency of ASR, I will present some strategies. For example, the injection of freshwater is considered to be in a fully penetrated well, while the recovery only occurs in a half penetrated well.

c. During the aquifer recharge, some chemical species in recharged water may react with some species in background water. The hydrogeochemical processes in the process of aquifer recharge will be investigated later.

9.4 Saltwater Upconing

The existence of fresh groundwater overlaying saltwater in groundwater systems is found in many inland aquifers as well as in most coastal aquifers. The utilization of freshwater resources in those regions is therefore highly constrained by the presence of saltwater upconing (Figure 9.2), which may occur when a pumping well is installed in freshwater zone that is underlain by layers containing saltwater. The studies of saltwater upconing, including analytical, experimental, and numerical methods, have continued for several decades.

a. To the best of my knowledge, however, there is no systematic study reported about the permeability effects on saltwater upconing. This research is proposed to explore systematic k heterogeneity effects on maximum fresh groundwater pumping duration in the presence of saltwater upconing problems. For this purpose, we will generate various permutations of two-dimensional numerical models of subsurface porous media: homogenous, random, homogeneous with an impermeable lens (Figure 9.3), and isotropically/anisotropically correlated k fields. For heterogeneous cases, we will use a sequential Gaussian simulation technique to generate ten realizations in each model permutation. One objective is to study the effects of aquifer heterogeneity (i.e. variance) on the maximum pumping duration, compared with the homogeneous case. For the aquifer with an impermeable lens below the pumping well, maximum fresh groundwater pumping duration is expected to be highly increased. For this scenario, the sensitivity study of vertical distance between the well and the lens (y) and the horizontal

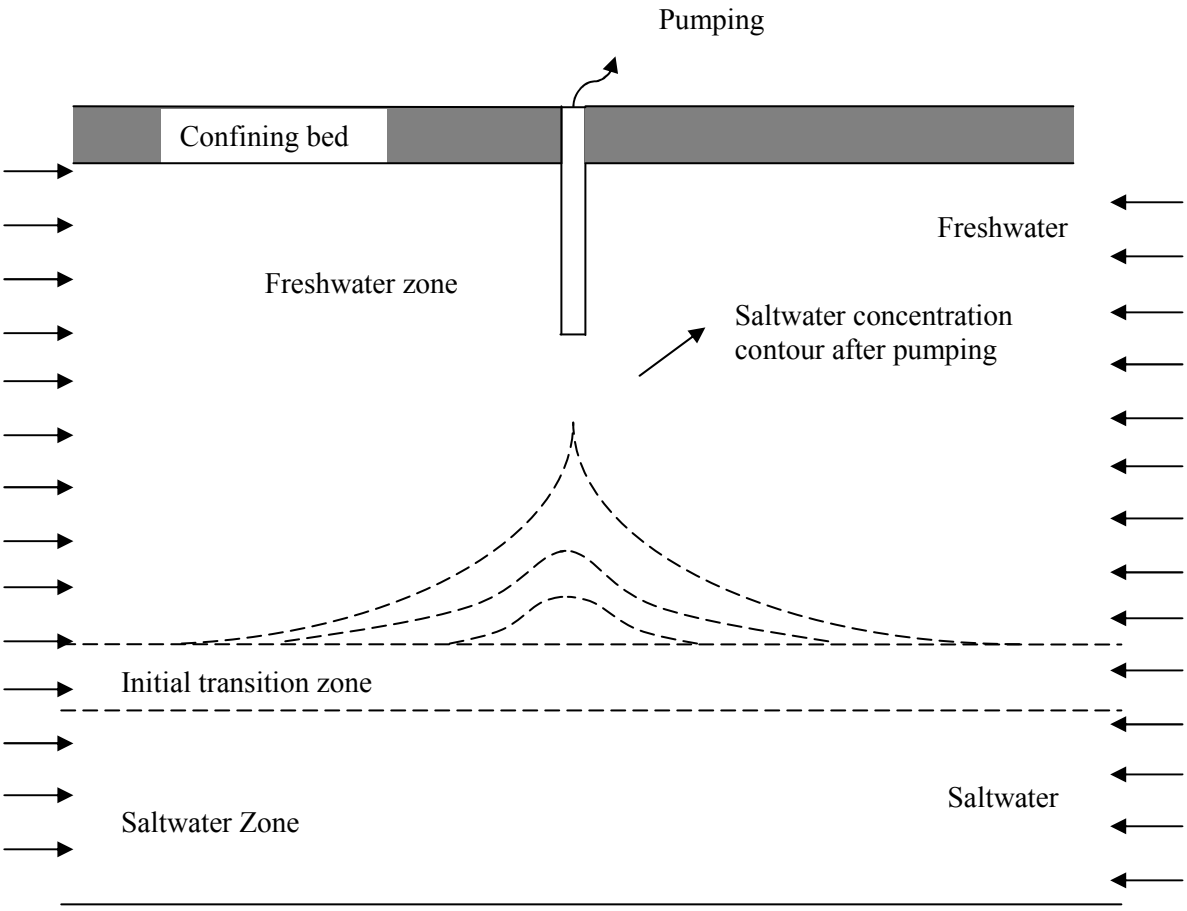

Figure 9.2 Pumping-well induced saltwater upconing.

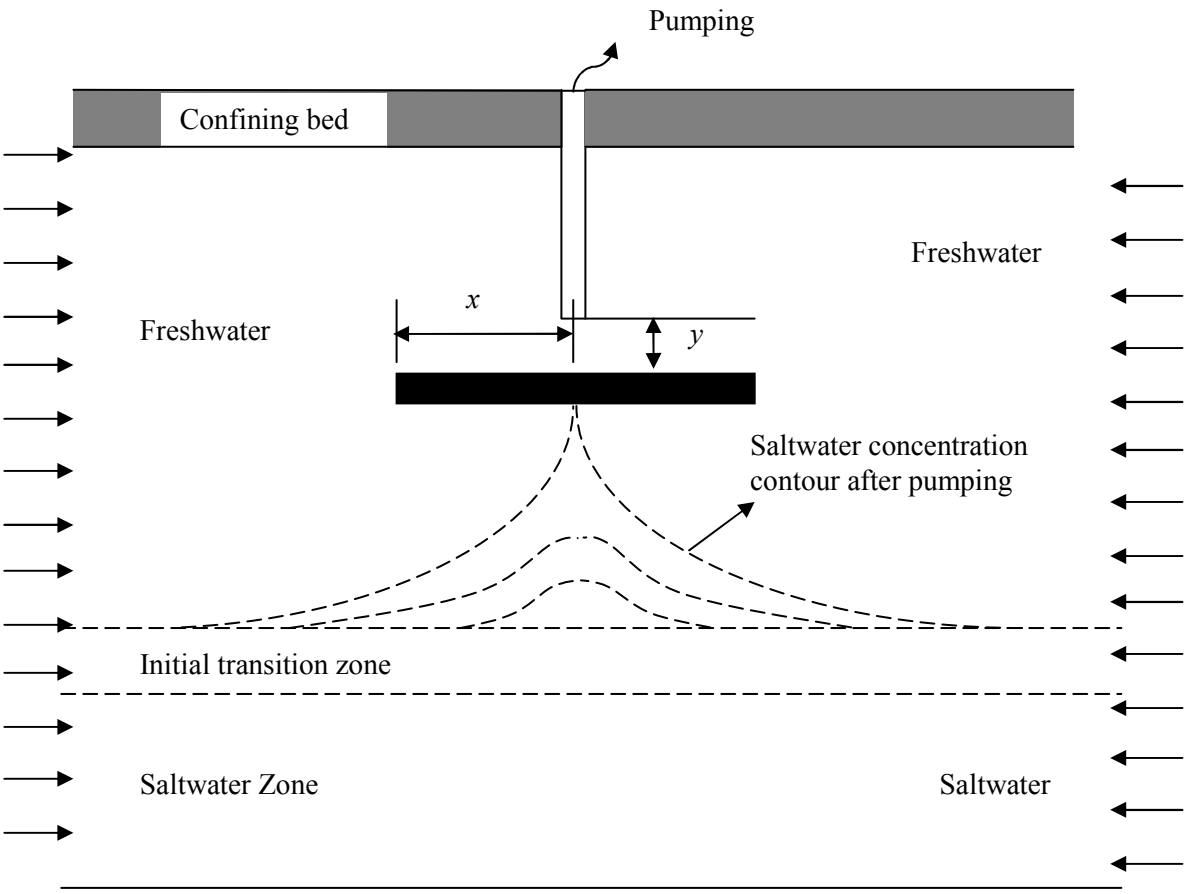

Figure 9.3 Pumping-well induced saltwater upconing in a homogeneous aquifer with an impermeable lens.

length of the lens (x) will be conducted, respectively. I am also interested in visualization of this upconing process by using a tank experiment.

b. I also plan to study the effects of kinetic mass transfer on the maximum pumping rate and saltwater upconing process, as kinetic mass transfer always occurs in subsurface environments.

9.5 Contaminant Transport in Coastal Aquifers

Land-induced contaminants may have large density and load into coastal aquifers. In coastal aquifers, the transport of contaminant may affected by various effects such as tidal activities, seasonal freshwater level fluctuations, aquifer heterogeneity, and so on.

a. I will investigate the effects of long-term freshwater level fluctuations vs. short-term tidal activities on the contaminant transport process.

b. Aquifers in reality are not homogenous. Spatial heterogeneity in hydraulic conductivity affects fluid flow and solute transport through porous media. I will use both numerical and experimental methods to show how layered heterogeneity affects the transport of dense contaminants in coastal aquifers.

c. In addition, contaminants transport in coastal aquifer may accompany some geochemical reactions. These reactive geochemical transport processes may dramatically affect coastal biological and ecological environments. In my future study, I will

investigate the transport processes of some typical contaminants and nutrition. Particularly, some field studies are expected to conduct to validate theoretical findings.

9.6 Maximum Pumping Rate for Multiwells in Coastal Aquifers

Based on the sharp interface assumption and potential theory, we have compared the analytical solutions for estimating maximum pumping rate for a well in coastal aquifer (the study is not included in this thesis). In that study, only a single well is considered. However, there may be several pumping wells located in coastal aquifers. One of the key problems of interest is that how to estimate total maximum pumping rate for these wells without seawater intrusion into any well. I will consider some optimization techniques such as genetic algorithm (GA) and artificial neural network (ANN) to solve this problem.

REFERENCES

Abarca, E. Seawater intrusion in complex geological environments. Ph.D. Thesis. Technical University of Catalonia, UPC; 2006.

Abarca, E., M. Pool, J. Carrera, and M. Dentz (2006), Can seawater intrusion modeling be simplified, Eos Trans. AGU, 87(52), Fall Meet. Suppl., Abstract H54E-05.

Abarca, E., and T.P. Clement (2009), A novel approach for characterizing the mixing zone of saltwater wedge, Geophysical Research Letter, 36, L06402, doi:10.29/2008GL036995.

Ackerer, P., A. Younes, and R. Mose (1999), Modeling variable density flow and solute transport in porous medium: 1. Numerical model and verification. Transport in Porous Media, 35, 345-373.

Almulla, A., A. Hamad, and M. Gadalla (2005), Aquifer storage and recovery (ASR): a strategic cost-effective facility to balance water production and demand for Sharjah. Desalination, 174, 193-204.

Anderson, M. P., R.J. Hunt, J, T. Krohelski, and K. Chung (2002), Using high hydraulic conductivity nodes to simulate seepage lake, Ground Water, 40(2), 117-122.

Arnell, N.W. (1998), Climate change and water resources in Britain. Climatic Change, 39, 83-110.

Ataie-Ashtiani, B., R. E.Volker, and D. A. Lockington (1999), Tidal effects on sea water intrusion in unconfined aquifers. Journal of Hydrology, 216, 17-31.

Barlow, P.M. (2003), Ground water in freshwater-seawater environments of the Atlantic coast: U.S. Geological Survey Circular 1262.

Bakker, M. (2006), Analytic solutions for interface flow in combined confined and semi-confined, coastal aquifers. Advances in Water Reources, 29, 417-425.

Bear, J. (1972), Dynamics of fluids in porous media. Elsevier, New York.

Bear, J. (1979), Hydraulics of Groundwater. New York: McGraw-Hill.

Bear, J., and G. Dagan (1964), Moving interface in coastal aquifers. Journal Hydraulics Division. ASCE, 90, 193-216.

Bear, J., and G. Dagan (1965). Some exact solutions of interface problems by means of the hodograph method. Journal Geophysical Research, 69, 1563-1572.

Bear, J., A.H.-D. Cheng, S. Sorek, D. Ouazar, and I. Herrera. Seawater intrusion in coastal aquifers concepts methods and practices. Springer, New York, 1999.

Becker, M.W., and R. J. Charbeneau (2000), First-passage-time transfer functions for groundwater tracer conducted in radially convergent flow. Journal of Contaminant Hydrology.

Benson, D. A., A.E. Carey, and S.W. Wheatcraft (1988), Numerical advective flux in highly variable velocity fields exemplified by saltwater intrusion. Journal of Contaminant Hydrology, 34, 207-233.

Berkowitz, B., and H. Scher (1997), Anomalous transport in random fracture networks, Physicial Review Letter, 69, 4038-4041.

Berkowitz, B., and H. Scher (1998), Theory of anomalous chemical transport in random facture netwooks, Physical Review E, 57, 5858-5869.

Berkowitz, B., and H. Scher, and S.E. Silliman (2000), Anomalous transport in laboratory-scale, heterogeneous porous media, Water Resources Research, 36, 149-158.

Berkowitz, B., A. Cortis, M. Dentz, H. Scher (2006), Modeling non-Fickian transport in geological formations as a continuous time random walk. Review Geophysics, 44, RG 2003.

Beuhler, M. (2003), Potential impacts of global warming on water resources in southern California. Water Science and Technology, 47, 165-168.

Bobba, A.G. (2002), Numerical modelling of salt-water intrusion due to human activities and sea-level change in the Godavari Delta, India. Hydrological Sciences Journal-Journal Des Sciences Hydrologiques, 47, 67-80.

Bond, L.D., and J.D. Bredehoeft (1987), Origins of seawater intrusion in a coastal aquifer-a case-study of the Pajaro Valley, California. Journal of Hydrology, 92, 363-388.

Bolster, D.T., D.M. Tartakovsky, and M. Dentz (2007), Analytical models of contaminant transport in coastal aquifers. Advances in Water Resources, 30, 1962-1972.

Brovelli, A., X. Mao, and D.A. Barry (2007), Numerical modeling of tidal influence on density-dependent contaminant transport. Water Resources Research, 43, W10426. doi:10.1029/2006WR005173.

Carrera, J., X. Sanchez-Vila, I. Benet, A. Medina, G. Galarza, and J. Guimera (1998), On matrox diffusion: formulations, solution methods and qualitative effects, Hydrogeology, 6, 178-190.

Cartwright, N., and P. Nielsen (2001a), Groundwater dynamics and salinity in coastal barriers. Proc. 1st Intl. Conf. on Salt Water Intrusion and Coastal Aquifers-Monitoring, Modeling and Management, Essaouira, Morocco, April 23-25, CD-ROM.

Cartwright, N., and P. Nielsen (2001b), Groundwater dynamics and salinity in beaches. Proc. Coasts and Ports 2001, 15th Australasian Coastal and Ocean Engineering Conference, Gold Coast, Australia, September 25-28, pp 441-446.

Cartwright, N., and P. Nielsen (2003), Dynamics of the salt-freshwater mixing zone in ocean beaches. 2nd Intlnational Conference on Salt Water Intrusion and Coastal Aquifers-Monitoring, Modeling and Management, Merida, Mexico, March 30- April 2.

Cartwright, N., L. Li, and P. Nielsen (2004), Response of the salt-freshwater interface in a coastal aquifer to a wave-induced groundwater pulse: field observations and modelling, Advances in Water Resources, 27, 297-303.

Chen, C.-S. (1985), Analytical and approximate solutions to radial dispersion from an injection well to a geological unit with simultaneous diffusion intio adjacent strata, Water Resources Research, 21, 1069-1076.

Chen, C.-S. (1986), Solutions for radionuclide transport from an injection well into a single fracture in a porous formation, Water Resources Research, 22, 508-518.

Chen, C.-S. (1987), Analytical solutions for radial dispersion with Cauchy boundary at injection well. Water Resources Research, 23, 1217-1224.

Chen, C.-S., and G.D. Woodside (1988), Analytical solution for aquifer decontamination by pumping, Water Resources Research, 24, 1329-1338.

Chen, W.L., and R.J. Wagenet (1995), Solute transport in porous-media with sorption-site heterogeneity. Environmental Science and Technology, 29, 2725-2734.

Cherry, G.S. (2006), U.S. Geological Survey Georgia Water Science Center and City of Brunswick-Glynn County Cooperative Water Program - Summary of Activities, July 2005 through June 2006, U.S.G.S. Open-File Report 2006-1368.

Church, T. (1996), An underground route for the water cycle, Nature, 380, 579-580.

Coats, K.H. and B.D. Smith (1964), Dead-end pore volume and dispersion in porous media. Society of Petroleum Engineers Journal, 4, 73–81.

Collins, M.A., and L.W. Gelhar (1971), Seawater intrusion in layed aquifers, Water Reources Research, 7, 971-981.

Cooper, H.H. (1959), A hypothesis concerning the dynamic balance of fresh water and salt water in a coastal aquifer. Journal of Geophysical Research 64, 461-467.

Cooper, H.H., F. A. Kohout, H.R. Henry, and R.E. Glover (1964), Sea water in coastal aquifers. U.S. Geological Water Supplu Paper, 1613-C.

Crank, J. (1975), The mathematics of diffusion, Oxford University Press, New York.

Croucher, A.E., and M.J. O'Sullivan (1995), The Henry problem for saltwater intrusion. Water Resources Research, 31, 1809-1814.

Culkin, S.L., K. Singha, and F. D. Day-Lewis (2008), Implications of rate-limited mass transfer for aquifer storage and recovery. Ground Water, 46(4), 591–605.

Dagan, G. (2006), Transverse Mixing At Fresh-Water Salt-Water Interfaces: An Unresolved Issue. First International Joint Salt Water Intrusion Conference. Tutirials.

Dagan, G., and D.G. Zeitoun (1998), Seawater-freshwater interface in a stratified aquifer of random permeability distribution. Journal of Contaminant Hydrology, 29, 185-203.

Delleur, J.W. (1999), The Handbook of Groundwater Engineering. CRC Press, New York.

Dentz, M., and B. Berkowitz (2003), Transport behavior of a passive solute in continous time random walks and multirate mass transfer, Water Resources Research, 39, 1111, doi:10.1029/2001WR001163.

Dentz, M., D.M. Tartakovsky, E. Abarca, A. Guadagnini, X. Sanchesz-Vila, and J. Carrera (2006), Variable-density flow in porous media. Journal of Fluid Mechanics, 561, 209-235.

DeWit, A., and G.M. Homsy (1997a), Viscous fingering in periodically heterogeneous porous media. 1. Formulation and linear instability. Journal of Chemical Physics, 107, 9609-9618.

DeWit, A., and G.M. Homsy (1997b), Viscous fingering in periodically heterogeneous porous media. 2. Numerical simulations. Journal of Chemical Physics, 107, 9619-9628.

Diersch, H.J.G., and O. Kolditz (2002), Variable-density flow and transport in porous media: approach and challenges. Advances in Water Resources, 25, 899-944.

Ergil, M.E. (2000), The salination problem of the Guzelyurt aquifer, Cyprus. Water Research, 34, 1201-1214.

Esatwood, J. C., and P. J. Standfield (2001), Key success factors in an ASR scheme. Quarterly Journal of Engineering Geology and Hydrogeology, 34, 399-409, doi:10.1144/qjegh.34.4.399.

Essink, G.H.P. (2003), Mathematical models and their application to salt water intrusion problems, TIAC'03: Coastal aquifers intrusion technology: Mediterranean countries, Alicante, Spain, 11-14, 57-77.

Fakir, Y., M. Mernissi, T. Kreuser, and B. Berjami (2002), Natural tracer approach to characterize groundwater in the coastal Sahel of Oualidia (Morocco). Environmental Geology, 43, 197-202.

Fan, Y., and R. Kahawita (1994), A numerical study of variable-density-flow and mixing in porous media. 30, 2707-2716.

Fiori, A., and G., Dagan (1999), Concentration fluctuations in transport by groundwater: comparison between theory and field experiments, Water Resources Research, 35, 102-112.

Foyle, A.M., V.J. Henry, and C. R.Alexander (2002), Mapping the threat of seawater intrusion in a regional coastal aquifer-aquitard system in the southeastern United States. Environmental Geology, 43, 151-159.

Galeati, G., G. Gambolati, and S.P. Neuman (1992), Coupled and partially coupled Eulerian-Lagrangian model of fresh-water-seawater mixing. Water Resources Research, 28, 149-165.

Gaus, I., P. Shand, I.N. Gale, A.T. Williams, and J.C. Wastwood (2002), Geochemical modeling of fluoride concentration changes during aquifer storage and recovery (ASR) in the Chalk aquifer in Wessex, England. Quarterly Journal of ENgineering Geology and Hydrogeology, 35, 203-208.

Gotovac, H., R. Andricevic, B. Gotovac, V. Kozulic, and M. Vranjes (2003), An improved collocation method for solving the Henry problem. Journal of Contaminant Hydrology, 64, 129-149.

Goswami, R.R., and T.P. Clement (2007), Laboratory-scale investigation of saltwater intrusion dynamics. Water Resources Research, 43, W04418.

Graf, T., and R. Therrien (2005), Variable-density groundwater flow and solute transport in porous media containing nonuniform discrete fractures. Advances in Water Resources, 28, 1351-1367.

Haggerty, R., and S.M. Gorelick (1995), Multiple-rate mass transfer for modeling diffusion and surface reactions in media with pore-scale heterogeneity, Water Resources Research, 31, 2383-2400.

Haggerty, R., and S.M. Gorelick (1998), Modeling mass transfer processes in soil columns with pore-scale heterogeneity, Soil Science Society American Journal, 62, 62-74.

Harvey, C.F., and S.M. Gorelick (1995), Temporal moment-generating equations: Modeling transport and mass transfer in heterogeneous aquifers, Water Resources Research, 31, 1895-1911.

Haggerty, R., S.A. Mckenna, and L.C. Meigs (2000), On the late-time behavior of tracer test breakthrough curves, Water Resources Research, 36, 3467-3479.

Henry, H.R. (1964), Effects of dispersion on salt encroachment in coastal aquifers, in Sea Water in Coastal Aquifers. US Geol Surv Supply Pap, 1613-C. 70-84.

Held, R., S. Attinger, and W. Kinzelbach (2005), Homogenization and effective parameters for the Henry problem in heterogeneous formations. Water Resources Research, 41, W11420. doi:10.1029/2004WR003674.

Herczeg, A., K. Rattray, P. Killon, P. Pavelic, and K. Barry (2004), Geochemical processes during five years of aquifer storage recovery. Ground Water 42(3), 438-445.

Huppert, H.E., and A. W. Woods (1995), Gravity-driven flows in porous layers. Journal Fluid Mechanics, 292, 55-69.

Huyakorn, P.S., P.F. Andersen, J.W. Mercer, and H.O. White (1987), Saltwater intrusion in aquifers: development and testing of a three-dimensional finite element model. Water Resources Research, 23(2), 293-312.

Johannes, R.E. (1980), The ecological significance of the submarine discharge of groundwater. Marine Ecology-Progress Series, 3, 365-373.

Kacimov, A.R., and Yu. V. Obnosov (2001), Analytical solution for a sharp interface problem in sea water inrtusion into a coastal aquifer. Proceedings: Mathematical, Physical and Engineering Sciences, 457, 3023-3038.

Kacimov, A.R., and M.M. Sheif (2007), Sharp interface, one-dimensional seawater intrusion into a confined aquifer with controlled pumping: Analytical solution. Water Resources Research, 42, W06501, doi:10.1029/2005WR004551.

Kafri, U., and A. Arad (1979), Current subsurface intrusion of Mediterranean seawater possible source of groundwater salinity in the rift valley system, Israel. Journal of Hydrology, 44, 267-287.

Karasaki, K., I. Kazumasa, and K. Maekawa (2006), Simulation of salt water intrusion. Proceedings, TOUGH Symposium, Lawrence Berkeley National Laboratory, Berkeley, California, May 15-17.

Kashgarian, M., and N. Tanaka (1991), Antarctic intermediate water intrusion into south-Atlantic bight shelf waters. Continental Shelf Research, 11, 197-201.

Kim, K.Y., H. Seong, T. Kim, K.H. Park, N.C. Woo, Y.S. Park, G. W. Koh, and W.B. Park (2006), Tidal effects on variations of fresh-saltwater interface and groundwater flow in a multilayered coastal aquifer on a volcanic island (Jeju Island). Journal of Hydrology, 330, 525-542.

Kimbler, O.K., Kazmann, R.G., and W.R. Whitehead (1975), Cyclic Storage of Fresh Water in Saline Aquifers. Louisiana State University, Baton Rouge, LA.

Kolditz, O., R. Ratke, H.J.G. Diersch, and W. Zielke (1998), Coupled groundwater flow and transport .1. Verification of variable density flow and transport models. Advances in Water Resources, 21, 27-46.

Kumar A., and O.K. Kimbler (1970), Effect of dispersion, gravitational segregation, and formation stratification on the recovery of freshwater stored in saline aquifers. Water Resources Research, 6 (6), 1689–1700.

Lam, R.H.F., J.P. Brown, A.M. Fan, and A. Milea (1994), Chemicals in California drinking-water-source contaminants, risk assessment, risk management, and regulatory standards. Journal of Hazardous Materials, 39, 173-192.

Langevin, C.D., W.B. Shoemaker, and W. Guo (2003), Modflow-2000, The U.S. Geological Survey modular ground-water flow model−Documentation of the Seawat-2000 version with the variable density flow process (VDF) and the integrated MT3DMS transport process (IMT), U.S. Geol. Surv. Open File Rep., 03-426, 43 p.

Langevin, C.D., and W. Guo (2006), MODFLOW/MT3DMS-based simulation of variable-density ground water flow and transport. Ground Water, 44, 339-351.

Largier, J.L., and S. Taljaard (1991), The dynamics of tidal intrusion, retention, and removal of seawater in a bar-built estuary. Estuarine Coastal and Shelf Science, 33, 325-338.

Lebbe, L. (1999), Parameter identification in fresh-saltwater flow based on borehole resistivities and freshwater head data, Adv. Water Resour. 22, 791-806.

Le Gal La Salle, C., J. Vanderzalm, J. Hutson, P. Dillon, P. Pavelic, and R. Martin (2005), Isotope evolution and contribution to geochemical investigations in aquifer storage and recovery: A case study using reclaimed water at Bolivar, South Australia. Hydrological Processes, 19, 3395-3411.

Liu, G.S., Zheng, C.M. and S.M. Gorelick (2007), Evaluation of the applicability of the dual-domain mass transfer model in porous media containing connected high-conductivity channels. Water Resour. Res., 43, W12407, doi:10.1029/2007WR005965.

Loaiciga, H.A., D.R. Maidment, and J.B. Valdes (2000), Climate-change impacts in a regional karst aquifer, Texas, USA. Journal of Hydrology, 227, 173-194.

Lowry, C. (2004), Assessment of aquifer storage recovery: defining hydraulic controls on recovery efficiency at three representative sites in Wisconsin. M.S. thesis, Department of Geology and Geophysics, University of Wisconsin at Madison, Madison, Wisconsin.

Lowry, C.S. and M.P. Anderson (2006), An assessment of aquifer storage recovery using ground water flow models. Ground Water, 44(5), 661–667.

Lu, C., P.K. Kitanidis, and J. Luo (2009), Effects of kinetic mass transfer and transient flow conditions on widening mixing zones in coastal aquifers, Water Resources Research, 45, W12402, doi:10.1029/2008WR007643.

Ma, L., and R.F. Spalding (1996), Stable isotope characterization of impacts of artificial ground water recharge. Water Resources Bulletin, 26, 1273-1282.

Maliva, R.G., W.X. Guo, and T.M. Missimer (2006), Aquifer storage and recovery: recent hydrogeological advances and system performance. Water Environmental Research, 78, 2428-2435.

Mao, X., P. Enot, D.A. Barry, L. Li, A. Binley, and D.-S. Jeng (2006), Tidal influence on behavior of a coastal aquifer adjacent to a low-relief estuary. Journal of Hydrology, 327, 110-127, doi: 10.1016/j.jhydrol.2005.11.030.

Merritt, M.L. (1986), Recovering fresh water stored in saline limestone aquifers. Ground Water 24(4), 516–529.

Mirecki, J.E., B.G. Campbell, K.J. Conlon, and M.D. Petkewich (1998), Solute changes during aquifer storage recovery testing in a limestone/clastic aquifer. Ground Water 36, 394-403.

Michael, H.A., A.E. Mulligan, and C.F. Harvey (2005), Seasonal oscillations in water exchange between aquifers and the coastal ocean. Nature, 436, 1145-1148.

Michalak, A.M., and P.K. Kitanidis (2000), Macroscopic behavior and random-walk particle tracking of kinetically sorbing solutes. Water Resources Research, 36(8), 2133–2146.

Moulder, E.A. (1970), Freshwater bubbles: a possibility for using saline aquifers to store water. Water Resoures Research, 6(5), 1528–1531.

Moench, A.F. (1989), Convergent radial dispersion: A Laplace transform solution for aquifer tracer testing, Water Resources Research, 25, 439-447.

Monch, A.F. (1995), Convergent radial dispersion in a double-porosity aquifer with fracture sink: Analytical solution and application to a field experiment in fractured chalk, Water Resources Research, 31, 1823-1835.

Moore, W.S. (1996), Large groundwater inputs to coastal waters revealed by ^{226}Ra enrichments. Nature, 380, 612-614.

Naji, A., A.H.-D. Cheng, and D. Ouazar (1998), Analytical stochastic solutions of saltwater/freshwater interface in coastal aquifers. Stochastic Hydrology and Hydraulics, 12, 413-430.

Neilson-Welch, L., and L. Smith (2001), Saline water intrusion adjacent to the Fraser River, Richmond, British Columbia. Canadian Geotechnical Journal, 38, 67-82.

Neville, C.J. (2006), Modeling dual-domain transport with MT3D. S.S. Papadpulos & Associates, Inc.

Novakowski, K.S. (1992), The analysis of tracer experiments conducted in divergent radial flow fields, Water Resources Research, 28, 3215-3225.

OTA (1984), Office of Technology Assesment, Protection the nation's groundwater from contamination, Washington D.C. OTA-o-233, 224.

Ozturk, Y.F. (1970), Seawater intrusion length in stratified estuaries. Water Research, 7, 477-487.

Pauc, H. (1989), Salt intrusion and suspended material dynamics at a river seawater interface-floos-water and low -water stages in the Oued Mazafran (west of Algiers). Marine Geology, 87, 95-102.

Plimmer, L.N. (1977), Defining reactions and mass-transfer in part of Floridan aquifer, Water Resources Research, 13, 5, 801-812.

Paniconi, C., I. Khlaifi, G. Lecca, A. Giacomelli, and J. Tarhouni (2001), Modeling and

analysis of seawater intrusion in the coastal aquifer of eastern Cap-Bon, Tunisia. Transport Porous in Media 43, 3-28.

Parkurst, D.L., and M.D. Petkewich (2001), Geochemical modeling of an aquifer storage recovery experiment, Charleston, South Carolina. USGS Open-File Report 02-89. Reston, Virginia: USGS.

Paster A., G. Dagan, and J. Guttman (2006), The salt-water body in the Northern part of Yarkon-Taninim aquifer: field data analysis, conceptual model and prediction. Journal of Hydrology, 323, 154-167, doi: 10.1016/j.jhydrol.2005.08.018.

Petkewich, M.D., D.L. Parkurst, K.J. Conlon, B.G. Campbell, and J.E. Mirecki (2004), Hydrologic and geochemical evalution of aquifer strage recovery in the Santee Limestone Black Mingo Aquifer, Charleston, South Carolina, 1998-2002. USGS Scientific Investigations Report 2004-5046. Reston, Virginia: USGS.

Price, R.M., Z. Top, J.D. Happell, and P.K. Swart (2003), Use of tritium and helium to define groundwater flow conditions in Everglades National Park. Water Resources Research, 39(9), 1267. doi:10.1029/2002WR001929.

Pyne, R.D.C. (2005). Aquifer Storage and Recovery Issues and Concepts, St. Johns River Water Management District Special Publication SJ2005-SP12; St. Johns River Water Mnagement District: Jacksonville, Florida.

Qahman, K., and A. Larabi (2006), Evaluation and numerical modeling of seawater intrusion in the Gaza aquifer (Palestine). Hydrogeology Journal, 14, 713-728.

Ramesh, R., K.S. Kumar, S. Eswaramoorthi, and G.R. Purvaja (1995), Migration and contamination of major and trace-elments in groundwater of Madras City, India. Environmental Geology, 25, 126-136.

Reinelt, P. (2005), Seawater intrusion policy analysis with a numerical spatially heterogeneous dynamic optimization model. Water Resources Research, 41, W05006, doi:10.1029/2004WR003111.

Rezaei, M, E. Sanz, E, Raeisi, C, Ayora, E, Vazquez-Sune ,and J, Carrera (2005). Reactive transport modeling of calcite dissolution in the fresh salt water mixing zone. Journal of Hydrology, 311(1-4), 282-298.

Robinson, C., L. Li, and D.A. Barry (2006), Effect of tidal forcing on a subterranean estuary. Advances in Water Research, 30, 851-865.

Robinson, C., B. Gibbes, and L. Li (2006), Driving mechanism for groundwater flow and salt transport in a subterranean estuary, Geophysical Research Letter, 33, L03402, doi:10.1029/2005GL025247.

Robinson, C., B. Gibbes, H. Garey, and L. Li (2007a), Salt-freshwater gynamics in subterranean estuary over a spring-neap tidal cycle. Journal of Geophysical Research, 112, C09007, doi:10.1029/2006JC003888.

Robinson, C., L. Li, and H. Prommer (2007b), Tide-induced recirculation across the aquifer-ocean interface, Water Resources Research, 43:W07428. doi:10.1029/2006WR005679.

Salamon, P., D. Fernandez-Garcia, , J.J. Gomez-Hernandez (2006), Modeling mass transfer processes using random walk particle tracking. Water Resources Research, 42, W11417, doi:10.1029/2006WR004927.

Santiago, A. E. (1991), Turbidity and seawater intrusion Laguna-de-Bay. Environmental Monitoring and Assessment, 16, 85-95.

Sakr, S. A. (1999), Validity of a sharp-interface model in a confined coastal aquifer. Hydrogeology Journal, 7, 155-160.

Schincariol, R.A., and F.W. Schwartz (1990), An experimental investigation of variable density flow and mixing in homogeneous and heterogenous media. Water Resources Research, 26, 2317-2329.

Schincariol, R.A., F.W. Schwartz, and C.A. Mendoza (1994), On the generation of instabilities in variable density flow. Water Resources Research, 30, 913-927.

Segovia-Zavala, J.A., F. Delgadillo-Hinojosa, and S. Alvarez-Borrego (1998), Cadmium in the coastal upwelling area adjacent to the California-Mexico border. Estuarine Coastal and Shelf Science, 46, 475-481.

Shammas, M.I. (2008), The effectiveness of artifical recharge in combating seawater intrusion in Salalah coastal aquifer, Oman. Environmental Geology, 55, 191-204.

Sherif, M.M., and V.P. Singh (1999), Effect of climate change on sea water intrusion in coastal aquifers. Hydrological Processes, 13, 1277-1287.

Simmons, G. M. (1992), Importance of submarine groundwater discharge (SGWD) and seawater cycling to material flux across the sediment/water interfaces in marine environments. Marine Ecology-Progress Series, 84, 173-184.

Simmons, C.T., and K.A. Narayan (1996), Modelling density-dependent flow and solute transport at the Lake Tutchewop saline disposal complex, Victoria. 206, 219-236.

Strack, O.D.L. (1976), A single-potential solution for regional interface problems in coastal aquifers. Water Resources Research, 12, 1165-1174.

Simmons, C.T., M.L. Pierini, and J.L. Hutson (2002), Laboratory investigation of variable-density flow and solute transport in unsaturated-saturated porous media. Transport in Porous Media, 47, 215-244.

Simpson, M.J., and T.P. Clement (2003), Theoretical analysis of the worthinese of Henry and Elder problems as bechmarks of density-dependent groundwater flow models. Advances in Water Reosurces, 26, 17-31.

Simmons, C.T. (2005), Variable density groundwater flow: from current challenges to future. Hydrogeology Journal, 13, 116-119.

Smith, A.J. (2004), Mixed convection and density-dependent seawater circulation in coastal aquifers. Water Resources Research, 40, W08309, doi:10.1029/2003WR002977.

Vandenbohede, A., E. Van Houtte, and L. Lebbe (2008). Study of the feasibility of an aquifer storage and recovery system in a deep aquifer in Belgiu. Hydrological Science Journal, 53, 844-856.

Vanderzalm, J.L., C. Le Gal La Salle, J. L. Hutson, and P.J. Dillon (2002), Water quality changes during aquifer storage and recovery at Bolivar, South Australia. In Management of Aquifer Recharge for Sustainability, ed. P. J. Dillon, 265-268. Lisse, The Netherlands: Swets & Zeitlinger.

van Genuchten, M.T., and P.J. Wierenga (1976), Mass-transfer studies in sorbing porous-media: 1. Analytical solution, Soil Science Society American Journal, 40, 473–480, 1976.

van Genuchten, M.T. and F.N. Dalton (1986), Models for simulating salt movement in aggregated filed soils. Geoderma, 38, 165–183.

Volker, R.E., and K.R. Rushton (1982), An assessment of the importance of some parameters for seawater intrusion in aquifers and a comparison of dispersive and sharp-interface modelling approaches. Journal of Hydrology, 56:239-50.

Voss, C.I., and W.R. Souza (1987), Variable density flow and solute transport simulation of regional aquifers containing a narrow freshwater-seawater mixing zone, Water Resources Research, 23, 1851-1866.

Welty, C., and L.W. Gelhar (1991), Stochastic-analysis of the effects of fluid density and viscosity on macrodispersion in heterogenous porous-media. Water Resources Research, 27, 2061-2075.

Welty, C., A.C. Kane, and L.J. Kauffman (2003), Stochastic analysis of transverse dispersion in density-coupled transport in aquifers. Water Resources Research, 39, 1105.

Wigley, T.M.L., and L.N. Plummer (1976), Mixing of carbonate waters, Geochimica Et Cosmochimica Acta, 40, 9, 989-995.

Winter, T.C. (1976), Numerical simulation analysis of the interaction of lakes and groundwater. U. S. Geol. Surv. Prof., 1001.

Ward J.D., Simmons, C.T. and P.J. Dillon (2007), A theoretical analysis of mixed convection in aquifer storage and recovery: How important are density effects? Journal of Hydrology, 343, 169–186.

Ward J.D., Simmons, C.T., and P.J. Dillon (2008), Variable-density modelling of multiple-cycle aquifer storage and recovery (ASR): importance of anisotropy and layered heterogeneity in brackish aquifers. Journal of Hydrology, 356, 93–105.

Ward J.D., Simmons, C.T., Dillon, P.J. and P. Pavelic (2009), Integrated assessment of lateral flow, density effects and dispersion in aquifer storage and recovery. Journal of Hydrology, 370, 83–99.

Wu, J.C., Y.Q. Xue, P.M. Liu, J.J. Wang, Q.B., Jiang, and H.W. Shi (1993), Sea-water intrusion in the coastal area of LaiZhou Bay, China. 2. Sea-water intrusion monitoring. Ground Water, 31, 740-745.

Xue, Y.Q., J.C. Wu, P.M. Liu, J.J. Wang, Q.B. Jiang, and H.W. Shi (1993), Sea-water intrusion in the coastal area of LaiZhou Bay, China.1. Distribution of Sea-water Intrusion and its hydrochemical characteristics. Ground Water, 31, 532-537.

Zhang Q., R.E. Volker, and D.A. Lockington (2001), Influence of seaward boundary condition on cotaminat transport in unconfined coastal aquifer. Journal of Contaminant Hydrology, 49(3-4), 201-215.

Zhang Q., R.E. Volker, and D.A. Lockington (2002), Experimental investigation of contaminant transport in coastal groundwater. Advances in Environmental Research, 6, 229-237.

Zinn, B. L.C. Meigs, C.F. Harvey, R. Haggerty, W.J. Peplinski, C.F. Von Schwerin (2004), Experimental visualization of solute transport and mass transfer processes in two-dimensional conductivity fields with connected regions of high conductivity. Environmental Science and Technology, 38, 14, 3916-3926.

Zubari, W.K., I.M. Madany, S.S. Aljunaid, and S. Almanaii (1994), Trends in the quality of groundwater in Bahrain with respect to salinity, 1941-1992. Environment International.